Title
Photoaffinity Labeling Studies on a Promoter of Dendritic Spine Formation

Permalink
https://escholarship.org/uc/item/64f2v53z

Author
Sibucao, Kevin

Publication Date
2017

Peer reviewed|Thesis/dissertation

UNIVERSITY OF CALIFORNIA, SAN DIEGO

Photoaffinity Labeling Studies on a Promoter of Dendritic Spine Formation

A dissertation submitted in partial satisfaction of the requirements for the degree
Doctor in Philosophy

in

Chemistry

by

Kevin Carlo Abril Sibucao

Committee in charge:

      Professor Jerry Yang, Chair
      Professor Rommie Amaro
      Professor Tadeusz Molinski
      Professor Gentry Patrick
      Professor Charles Perrin

2017

This Dissertation of Kevin Carlo Abril Sibucao is approved, and it is acceptable in quality and form for publication on microfilm and electronically:

_____

_____

_____

_____

_____
Chair

University of California, San Diego

2017

DEDICATION

This dissertation is dedicated to Mom, Papa, and Camille.

EPIGRAPH

Hope springs eternal

—Alexander Pope, *An Essay on Man* (1734)

TABLE OF CONTENTS

LIST OF FIGURES

LIST OF TABLES

LIST OF ABBREVIATIONS

Aβ	Beta-amyloid
AD	Alzheimer's Disease
AMPA	α-Amino-3-hydroxy-5-methyl-4-isoxazolepropionic acid
Amp-100	Ampicillin (100 µg/mL)
ApoE	Apolipoprotein E
APP	Amyloid precursor protein
ATP	Adenosine triphosphate
BCA	Bicinchoninic acid
BSA	Bovine serum albumin
Boc_2O	Di-tert-butyl dicarbonate
BTA	6-Methylbenzothiazole
CIAP	Calf intestinal alkaline phosphate
DCC	Dicyclohexylcarbodiimide
DCM	Dichloromethane
DIPEA	Diisopropylethylamine
DMF	Dimethylformamide
DMP	Dess-Martin periodinane
dppf	1,1'-Bis(diphenylphosphino)ferrocene
DTT	Dithiothreitol
ECL	Enhanced chemiluminescence
EDTA	Ethylenediaminetetraacetic acid
EG	Ethylene glycol
Et_2O	Diethyl ether

Et$_3$N	Triethylamine
EtOAc	Ethyl acetate
FRET	Förster Resonance Energy Transfer
GAP	GTPase activating protein
GEF	Guanine exchange factor
GST	Glutathione *S*-transferase
GDP	Guanine diphosphate
GTP	Guanine triphosphate
HATU	1-[Bis(dimethylamino)methylene]-1*H*-1,2,3-triazolo[4,5-*b*]pyridinium 3-oxid hexafluorophosphate
HRP	Horseradish peroxidase
iPrOH	Isopropanol
IPTG	Isopropyl β-D-thiogalactoside
ITC	Isothermal titration calorimetry
kb	Kilobase
kDa	Kilodalton
LB	Lysogeny broth
LIMK	LIM kinase
LDS	Lithium dodecyl sulfate
Mcpba	*meta*-Chloroperbenzoic acid
MeOH	Methanol
NMDA	*N*-methyl-D-aspartic acid
NHS	*N*-hydroxysuccinimide
PAGE	Polyacrylamide gel electrophoresis
PBS	Phosphate buffered saline

PBST	Phosphate buffered saline with Tween 20
PKC	Protein Kinase C
PPh$_3$	Triphenylphosphine
SDS	Sodium dodecyl sulfate
TAE	Tris-acetate-EDTA
TBAF	*tert*-Butylammonium fluoride
t-BuLi	*tert*-Butyllithium
TBS	Tris buffered saline
TBST	Tris buffered saline with Tween 20
TFA	Trifluoroacetic acid
TFAA	Trifluoroacetic anhydride
TFMD	Trifluoromethyl diazirine
TFMK	Trifluoromethyl ketone
THF	Tetrahydrofuran
TMS	Trimethylsilyl
Tris	Tris(hydroxymethyl)aminomethane
TsCl	Tosyl chloride

ACKNOWLEDGEMENTS

I am indebted to everyone who made this dissertation possible. I would like to thank my advisor, Professor Jerry Yang, for giving me the opportunity to work in his lab. I am grateful for the support and mentorship that he provided. The project that he gave me was truly a challenging one, and I value the confidence that he had in my ability to conduct independent research. I would also like to thank the other members of my committee: Professor Rommie Amaro, Professor Tadeusz Molinksi, Professor Charles Perrin, and Professor Gentry Patrick. I appreciate all the feedback they provided during my departmental exam, qualifying exam, and defense.

I am grateful for the staff at the various department research facilities who were invaluable when it came to acquiring data. I would like to thank Dr. Anthony Mrse for his assistance with NMR as well as Dr. Yongxuan Su and Joshua Lee for their help with mass spectrometry. Without them, I would not have been able to characterize the compounds I synthesized. I would also like to thank Dr. Majid Ghassemian at the Biomolecular and Proteomics Mass Spectrometry Facility. The protein identification data that he helped me obtain was part of this dissertation's key finding.

My labmates provided invaluable support and advice. I am thankful for those who started before me and welcomed me into the lab. Dr. Alice Luong and Dr. Yuchen Cao worked with me in 6114 when I first joined the lab. Even though Alice was occupied with her post-doctoral work and Yuchen was focused on graduating, both helped get me started with synthesis. We often talked about animals and pets—namely, Alice and her dogs and Yuchen and her rabbit. Leibniz Hang and

Kevin Cao were two of the first friends I made in graduate school. I am grateful to Leibniz for all the times we went to Ralph's to find late night manager's specials and for all nicknames he coined for me (namely "K2," which sticks to this very day). Kevin Cao and I shared many things in common—including a first name and three letters of our last names. I am indebted to him for all the car rides he gave me during our time in lab together. (If you ever need a ride to airport early in the morning, just call me up. I'll even get you a McGriddle!) I would also like to acknowledge Dr. Dan Sheik, Dr. Tim Chung, and Kate Veccharelli for all the encouragement and assistance they provided me during their time in the Yang lab.

As I became a more senior graduate student, new people joined the lab, and they, too, were important to my graduate school journey. I will remember all the BJ's trips that I made with Jamie Do for pazookies and all the jokes and quips I made at her expense during these trips (all of which I hope she took well). John Kim always was willing to help me troubleshoot any issues I had with biochemical experiments—especially Western blots. The pet-assisted therapy (in the form of his pet cat) he provided proved to be a great stress and anxiety reliever. I also am grateful for the contributions that Young-Hun Kim, Dr. Geoffray Leriche, Tak Koyanagi, Venus Tong, Elissa Min, Alvin Yep, and Fanny Fu made to my graduate school experience.

During my time in the Yang lab, I had the honor of mentoring two undergraduates: Andy Nguyen and Henry Lee. Each assisted me with different parts of my project. Andy aided me with synthesis. He synthesized grams of the early stage intermediates needed for the numerous synthetic routes that I attempted. He produced prodigiously and earned the nickname "The Lean, Mean EG_4-Amine

Making Machine." Henry, on the other hand, helped with me out with the fascin portion of this work. The amount of fascin he expressed for me and the number of gels he ran proved to be invaluable. Also, he was a good caretaker of the cells we grew; he never contaminated a culture. The progress that both Andy and Henry made in the Yang lab as scientists made me proud to be their mentor.

Serving as a teaching assistant was one of best experiences I had as a graduate student. I thank Professor Charles Perrin and Professor Jerry Yang for nominating me for the Teaching Assistant Excellence Award. I am grateful to Professor Jerry Yang for providing me the opportunity to lecture for his Chemistry 140A and Chemistry 256 classes when needed. Finally, I would like to thank my students—especially those who followed me through the whole 140 series. I enjoyed teaching all of you. I hope that I made (organic) chemistry a little more enjoyable than you thought it would be.

I would also like to acknowledge the Newman Center Catholic Community at UCSD and the San Diego Humane Society. I have been a member of UCSD's Newman Center since I moved to San Diego in 2011, and I have volunteered in the Education department at the San Diego Humane Society since 2013. It has been a privilege to be a part of both communities.

Lastly, I would like to thank my family for all their love and support. Although I mention my immediate family in the dedication, this thesis is really dedicated to my whole family—extended family included. There are too many people to list, and I did not want to forget anyone. They are a big part of my life, and they always made time to visit me during my trips back to the Bay Area.

VITA

2011   Bachelor of Arts in Molecular and Cell Biology, University of California, Berkeley

2013   Master of Science in Chemistry, University of California, San Diego

2017   Doctor of Philosophy in Chemistry, University of California, San Diego

ABSTRACT OF THE DISSERATION

Photoaffinity Labeling Studies on a Promoter of Dendritic Spine Formation

by

Kevin Carlo Abril Sibucao

Doctor of Philosophy in Chemistry

University of California, San Diego, 2017

Professor Jerry Yang, Chair

The small molecule BTA-EG$_4$ has been shown to be a promoter of dendritic spine formation. The mechanism behind this phenomenon, however, is not well understood. The work in this dissertation is motivated by this gap in knowledge.

The first part of this dissertation focuses on photoaffinity labeling studies to identify the cellular targets of BTA-EG$_4$. Chapter 1 provides a summary of Alzheimer's disease, the rational design of BTA-EG$_4$, and methods to determine targets of small molecules. In Chapter 2, the synthesis of a BTA-EG$_4$-based photoaffinity labeling probe and photodegradation studies are presented. Kinetic studies demonstrate that the probe photolyzes rapidly under UV light. In Chapter 3, photoaffinity labeling studies and subsequent protein identification experiments are reported. Competition experiments with the photoaffinity labeling probe and BTA-

EG_4 demonstrate that the probe labels a 55-kDa protein specifically. Tandem mass spectrometry revealed that the 55-kDa protein is the actin binding protein fascin 1.

The second part of this dissertation focuses on the major protein identified from photoaffinity labeling studies, fascin 1. Chapter 4 provides a brief survey of the structure and function of fascin 1. In Chapter 5, characterizations of the interaction between $BTA-EG_4$ and fascin 1 are reported. Isothermal titration calorimetry confirms the physical binding between fascin 1 and $BTA-EG_6$, a $BTA-EG_4$ analog. Slow speed sedimentation assays reveal that $BTA-EG_4$ does not affect the actin-bundling activity of fascin 1. However, GST pull-down experiments show that $BTA-EG_4$ inhibits the binding of fascin 1 with the GTPase Rab35. In addition, this work demonstrates that $BTA-EG_4$ may be mechanistically distinct from the known fascin inhibitor G2.

PART 1

Identifying the Target of BTA-EG$_4$

Chapter 1

Introduction: Alzheimer's Disease and its Therapies; A Spinogeneic Molecule

1.1 Alzheimer's Disease: An Overview

Alzheimer's disease (AD) is a neurodegenerative disease marked by a decline in memory and cognitive ability and is the most common form of dementia.[1] Symptoms of the disease are mild at the onset but become more severe over time. Initially, the most common symptom is a worsening of memory.[1] Patients in the advanced stages of the disease are unable to perform basic tasks such as communication and are usually bed-ridden. Patients typically succumb to complications of the disease. The most common immediate causes of death are pneumonia and heart failure.[2] Unfortunately, there is no cure for AD.
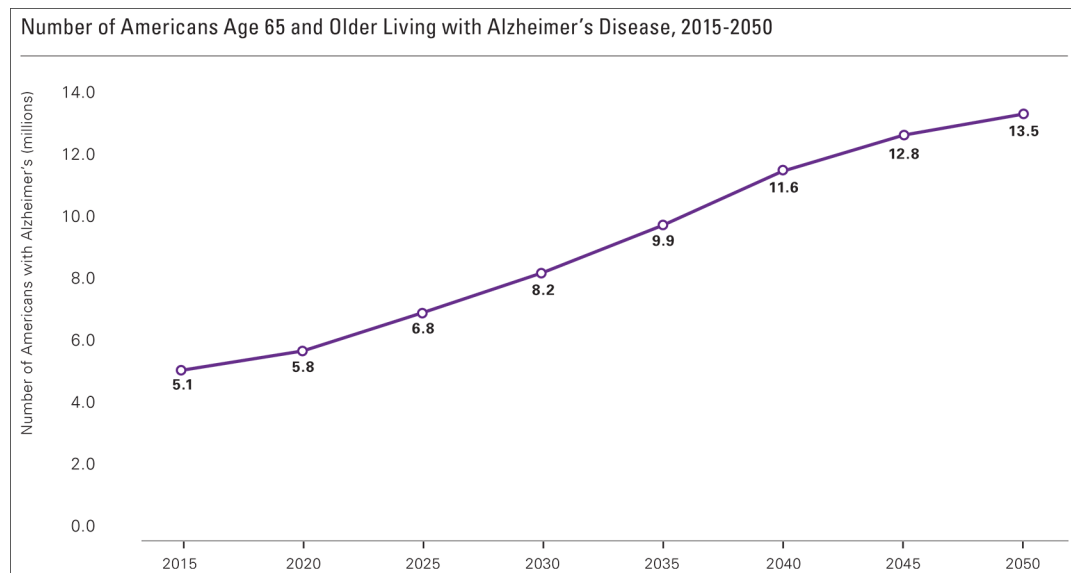
Figure 1.1. **Current Trajectory of the Number of Americans Age of 65 and Older Living with Alzheimer's Disease.** Graph courtesy of The Alzheimer's Association (Creative Common License).[3]

AD afflicts the elderly. Presently, it is estimated that about 13% of Americans over the age of 65 have the disease.[4] Furthermore, the prevalence of AD doubles for every five years past 65.[4] Economically, AD is on track to have an increasingly

large impact. As people live longer, the frequency of AD in the general population and the cost of care for these patients are expected to rise. Currently, over five million American have AD, and it is estimated that the cost of care for these patients amounts to over two-hundred billion dollars.[3] In 2050 if the current trajectory holds, it is projected that the number of Americans with AD will nearly triple and that the cost of care will top one trillion dollars (Figure 1.1).[3]

Clearly, the impacts of AD are far-reaching. The disease's effects can be seen on the small scale—individuals and families—as well as on much larger scales—governments and economies. This motivates the research to better understand the disease and to find therapeutics that can slow, stop, or reverse its progression.

1.2 Current Therapeutic Strategies for the Treatment of Alzheimer's Disease

Currently, there are two classes of FDA approved drugs for the treatment of AD: acetylcholinesterase inhibitors and NMDA receptor antagonists.[5] Both of these classes of drugs target abnormalities related to neurotransmitters.

The neurotransmitter acetylcholine has been shown to be critical for learning and the formation of memories.[6] In the brains of AD patients, dysfunctions in "cholinergic" pathways, molecular pathways that are associated with acetylcholine, have been observed. Specifically, it has been hypothesized that deficiencies in acetylcholine synthesis results in decreased activation of cholinergic neurons.[7] From these observations, it was reasoned that a potential therapeutic strategy against AD

is to increase the amount of acetylcholine in synapses. Acetylcholinesterase is an enzyme that reduces the concentration of acetylcholine by cleaving the neurotransmitter into choline and acetate;[8] thus, inhibition of this enzyme should increase acetylcholine levels and promote cholinergic function.[7] Examples of FDA approved acetylcholinesterase inhibitors include galantamine,[9] rivastigmine,[10] and donepezil (Figure 1.2).[11]

Glutamate, another neurotransmitter, targets NMDA receptors.[12] Upon binding to glutamate, NMDA receptors open and allow an influx of ions, such as calcium into the neuron.[12] Overstimulation of these receptors by glutamate is toxic to neurons; this phenomenon is known as excitotoxicity.[13] In the brains of AD patients, there is an increase of glutamate in synapses caused by abnormalities in glutamate processing such as glutamate-glutamine cycling[14] or glutamate reuptake.[15] Antagonists of the NMDA receptors have been developed to combat this pathology.[16] Currently, the only NMDA receptor antagonist on the market is mementine.[17]

| Galantamine | Rivastigamine | Donepezil | Mementine |
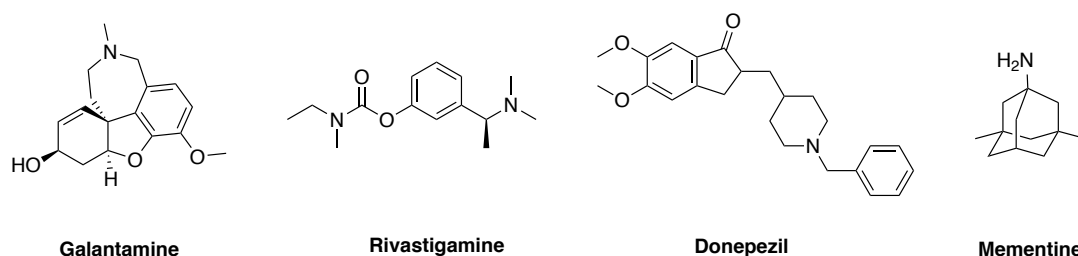
Figure 1.2. **Chemical Structures of Current AD Drugs.**

Both classes of drugs do not cure AD; they may, however, mitigate some of the symptoms of AD.[18] In addition, the evidence regarding the effectiveness of these

drugs have been mixed.[17,18] Clearly, there is a need for the development of new therapies for AD.

1.3 Alzheimer's Disease and the Amyloid Cascade Hypothesis

Even though over a century has passed since Alois Alzheimer first described AD,[19] the exact cause of the disease is not completely understood. Aside from those previously mentioned, there are many other pathologies that define the disease and give clues to a cause. One of the major pathologies of AD that has motivated a great deal of research is the presence of β-amyloid (Aβ) plaques, deposits of Aβ peptides that are universally seen in the brains of AD patients post-mortem.[20]
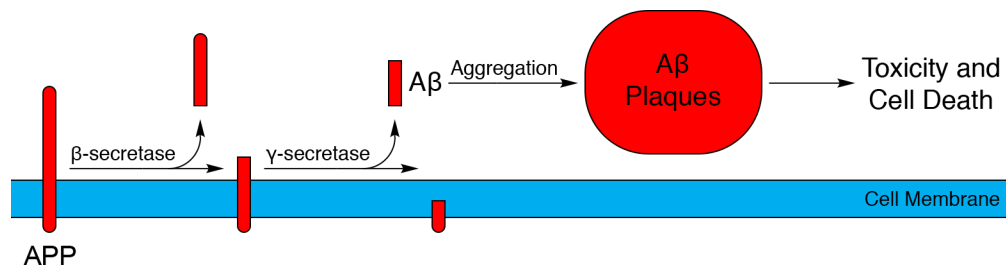
Figure 1.3. **The Amyloid Cascade Hypothesis.** APP can be cleaved by β-secretase and subsequently by γ-secretase to yield Aβ. Aβ can aggregate into plaques which are toxic and can cause cell death.

The Aβ peptide is a cleavage product of the amyloid precursor protein (APP).[21] APP is a membrane-bound protein that is the substrate of the secretases, a class of proteolytic enzymes.[21] Cleavage of the extracellular domain by β-secretase and γ-secretase generates the Aβ peptide (Figure 1.3).[21] A forty residue peptide (Aβ$_{1-40}$) and a forty-two residue peptide (Aβ$_{1-42}$) are the two major products of this

process. These Aβ peptides can form oligomers, which can further aggregate into plaques. Of the two major peptides, $Aβ_{1-42}$,[22] the more hydrophobic of the two, has been found to aggregate faster[23].

Several mechanisms have been proposed that account for the accumulation of Aβ peptides in the brain. In familial AD, mutations in APP have been shown to increase the production of Aβ dramatically.[24] In non-familial AD, these mutations are not observed, which indicates that dysfunctional Aβ degradation and clearance pathways may be the cause.[25] These pathways include degradation by the proteases such as neprilysin[26] and cathepsin D[27] as well as transport of Aβ from the brain to the blood stream by the receptor protein LRP1.[28] In addition, the lipoprotein apolipoprotein E (ApoE) interacts with LRP1 and has been implicated as a protein involved in the clearance of Aβ.[29] Findings regarding the mechanism of ApoE-mediated clearance have been mixed. Mechanistically, it has been hypothesized that Aβ binds ApoE and that ApoE carries Aβ to target proteins such as LRP1 for clearance.[30] It has been shown that the ApoE isotype ε4 retards clearance of Aβ when compared to the ε2 and ε3 isotypes.[31] Interestingly, the ε4 allele is the greatest genetic risk factor for AD.[30] Other studies, however, suggest that ApoE interacts minimally Aβ.[32] ApoE may exert its effect on clearance by competing with Aβ for its shared binding partners, especially those involved in Aβ clearance such as LRP1.[32]

Cell culture experiments demonstrate that Aβ is toxic to neurons;[33] however, it is not clear exactly how these Aβ oligomers and plaques are toxic to neurons. One hypothesis is that the plaques increase oxidative stress for cells.[34] Oxidative stress damages proteins and DNA, and this damage can cause cell death. In the post-

mortem brains of AD patients, many markers for oxidative stress are observed such as low ratios of reduced glutathione, elevated 4-hydroxynonenal, and decreased levels of superoxide dismutase and catalase.[35] Aβ may play a role in increasing the oxidative stress in the neuron. Aβ can participate in redox chemistry that produces reactive intermediates that can damage other molecules in the cell.[36,37] For example, Aβ can reduce Cu^{2+} into Cu^{+}; subsequent reaction of Cu^{+} with molecular oxygen yields H_2O_2.[36] In addition, it has been proposed that Aβ, when present in the cell membrane, can oxidize lipids.[37] This can lead to the formation of harmful electrophilic species such as 4-hydroxynonenal.[37]

1.4 Targeting Amyloid Plaques as a Therapeutic Strategy

Although acetylcholinesterase inhibitors and NMDA receptor antagonists may provide some relief to AD patients, their palliative effects are modest at best. Clearly, there is a need for additional AD therapeutics that can slow the disease further, halt its progression, or even reverse its effects.

Over the past decade, the Yang lab has developed small molecules that target amyloid plaques. The major hypothesis behind this strategy is that Aβ toxicity may be caused by deleterious interactions between plaques and cellular proteins. Specifically, Aβ may interfere with proteins that are responsible for regulating reactive oxidative species levels in the cell. Disrupting these Aβ-protein interactions may reduce Aβ toxicity.

Thioflavin-T is a small molecule commonly used to detect and stain amyloids.[38] Initial studies by Dr. Petra Inbar in the Yang lab demonstrated that this molecule inhibits the binding of an Aβ antibody with Aβ fibrils—although not completely.[39] In subsequent studies, Inbar and other Yang lab members synthetized new uncharged derivatives of thioflavin-T. The methyl group was removed from the nitrogen to eliminate the positive charge, and an oligoethylene glycol tail was added to improve water solubility (Figure 1.4).[40] Two of these compounds were synthesized and tested: BTA-EG$_4$ and BTA-EG$_6$ (for the purposes of this thesis, I will focus mainly on BTA-EG$_4$). These compounds inhibited the IgG-fibril interaction more effectively than thioflavin-T and also are more biocompatible due to increased cell membrane permeability.[40,41]
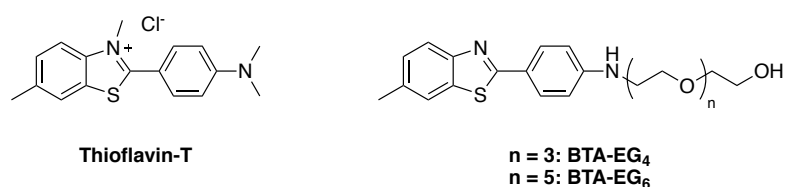
Figure 1.4. **Chemical Structures of Thioflavin-T, BTA-EG$_4$, and BTA-EG$_6$.**

Later work by Dr. Lila Habib in the Yang lab investigated the effect of BTA-EG$_4$ on SH-SY5Y cells treated with Aβ. It was demonstrated that BTA-EG$_4$ can rescue these cells from some of the toxicity associated with Aβ.[42] This observation was attributed to BTA-EG$_4$'s ability to interfere with interactions between catalase and Aβ that inhibits catalase and increases oxidative stress in the cell.[42]

1.5 BTA-EG$_4$: A Spinogenic Molecule

Cell culture experiments supported the idea that interfering with the interaction between Aβ fibrils and associated proteins such as catalase could decrease the toxicity of Aβ plaques. In collaboration with the Hoe lab at Georgetown University, BTA-EG$_4$ was tested in mice to see if the observed activity of BTA-EG$_4$ in vitro would translate in vivo.

BTA-EG$_4$ appeared to improve memory and learning in an AD mouse model.[43] When the neurons of these mice were imaged, an increase in dendritic spine density was observed.[43] This phenomenon is known as spinogenesis. Perhaps even more striking is that both effects were also seen in wild-type mice.[44] Since wild-type mice brains do not have amyloid plaques, this suggests that this phenomenon is independent of Aβ.

Dendritic spines are small protrusions that are present on the surface of dendrites. Morphologically, many dendritic spines are mushroom-like; they have a round, bulb-like head that are connected to the main body of the dendrite by a thin neck.[45] Other spines are short and stubby or even cup-shaped.[45,46] Dendritic spines play a critical role in the communication between neurons.[47] They are the site at which the postsynaptic neuron receives signals from the axon of the presynaptic neuron.[46] Consequently, NMDA receptors and AMPA receptors can be found on the surface of dendritic spines.[45] Internally, spines contain many proteins that are important for its function. Abundantly present is the cytoskeleton protein actin.[48] Actin provides the necessary framework to maintain the architecture of the dendritic spine.[48]

Dendritic spines are highly plastic; they can assemble and disassemble very rapidly.[46] The highly dynamic nature of actin permits this. Evidence indicates that dendritic spines and their plasticity are closely linked to memory and learning. Both artificial stimulation of hippocampal slices[49,50] and training in animals[51–53] induced the development of dendritic spines.

A decrease in spine density is another pathology seen in AD,[54] as well as other neuropathic disorders such as schizophrenia and autism spectrum disorders.[55] Since there appears to be a relationship between dendritic spines and memory, perhaps modulating the density of dendritic spines may be an effective therapeutic strategy to combat AD and other neuropathic disorders. Aside from BTA-EG$_4$'s ability to induce spinogenesis, little else is known about this phenomenon. This body of work seeks to provide the foundation to understanding the mechanism of BTA-EG$_4$-induced spinogenesis.

1.6 Determining Cellular Targets of Small Molecules

The mechanism behind BTA-EG$_4$-induced spinogenesis is unknown. These unknown details motivate the work in this dissertation. Finding the cellular binding partners of this small molecule provides a first good step towards this goal.

Perhaps the most common way that small molecule targets are identified is through affinity-based methods. Biomolecules are purified based on their affinity to a solid support (Figure 1.5).[56] In practice, the small molecule of interest is immobilized on a resin. This often involves chemically modifying a small molecule so that it contains a chemical group that can attach to the resin. The resin is then added to a mixture of proteins, usually cell lysates. Proteins that bind to the small molecule of

interest should adhere to the resin while proteins that do not bind to the small molecule should be washed away readily. After purification, the isolated proteins can be identified, typically by mass spectrometry methods.[57]

Crew and workers employed an affinity-based approach to discover the target of the natural product didemnin B. Didemnin B is a depsipeptide that contains seven amino acids and exhibits anti-proliferative properties.[58] Chromatography was performed with immobilized didemnin B, and it was demonstrated that the molecule binds to the elongation factor EF-1α.[58]
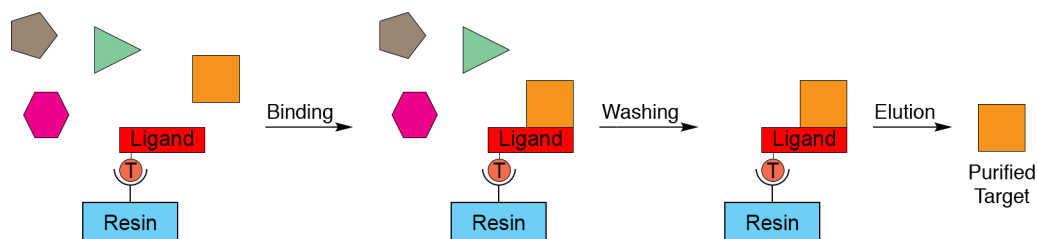
Figure 1.5. **General Scheme of Affinity-Based Target Identification.** The ligand is modified with an affinity tag (T) and is immobilized on resin. A mixture of protein is incubated with the resin. After binding, proteins that do not bind are washed away, leaving proteins bound to the ligand. The purified protein can be eluted and identified.

One of the downsides of this approach is the difficulty of finding weak binding partners. Weak binding targets may be readily lost during wash steps. To address this, photoaffinity labeling has been developed as a modification to typical affinity-based methods.[59,60] A photoreactive group is incorporated into a small molecule of interest. Upon photoactivation, the ligand covalently attaches to its target, and standard affinity chromatography methods can be employed to purify the target. Since the target is covalently attached to the ligand, even targets that are weakly bound to the ligand can be labeled and captured. Photoaffinity labeling can also provide information about the ligand binding site.[59] Mass spectrometry methods

provide a way to determine which amino acids were labeled. This information can be used in conjunction with a known 3D structure of the target to find a probable binding site.

Zhou and colleagues used a photoaffinity labeling strategy to find the target of chalcone.[61] Chalcone is a small molecule whose basic framework is present is several bioactive compounds.[61] It was shown that chalcone binds to β-tubulin, and that chalcone stops a cell's progression through the cell cycle.[61]

1.6 Goals of the Dissertation

Clearly, the BTA class of molecules have interesting activities that are not mechanistically understood. To gain insight into BTA-EG$_4$-induced spinogenesis, I employed photoaffinity labeling to find the cellular binding partners of BTA-EG$_4$. The goals of the dissertation are threefold:

1. Designing and synthesizing a photoaffinity labeling probe based on BTA-EG$_4$

2. Using the photoaffinity labeling probe to label and capture binding partners and using tandem mass spectrometry to identify these potential cellular targets

3. Performing biochemical assays to validate the potential targets

Part 1 of this dissertation will focus on the first two goals. In Chapter 2, I will present the design and synthesis of a BTA-EG$_4$-based photoaffinity labeling probe. In Chapter 3, I will describe photoaffinity labeling experiments in which I capture and subsequently identify candidate binding partners of BTA-EG$_4$. Part II will focus on fascin 1, a protein that was identified by mass spectrometry. Chapter 4 will provide a

brief survey of this protein. In Chapter 5, I will report findings that validate binding between BTA-EG$_4$ and fascin 1 as well as some mechanistic studies that provide clues into how BTA-EG$_4$ and fascin 1 may be involved in spinogenesis.

Chapter 2

The Design and Synthesis of a BTA-EG$_4$-based Photoaffinity Labeling Probe

2.1   Introduction

The overarching goal of this dissertation is to gain insight into the spinogenic properties of BTA-EG$_4$ by finding its protein binding partners in the cell. I have chosen a photoaffinity labeling approach to meet this aim.

The first objective towards this greater goal was to create a photoaffinity labeling probe based on BTA-EG$_4$. In the first part of this chapter, I will describe the rationale behind the design of my probe. Next, I will present the synthesis of the photoaffinity labeling probe, as well as a control compound. Finally, I will report experiments that allowed me to verify that the probe is UV reactive and to characterize the products and kinetics of photodegradation.

2.2   Target Design and Synthetic Overview

There were several considerations that I made when planning the synthesis of the photoaffinity labeling probe. These include the choice and placement of photoreactive group, the choice of an affinity tag, and the choice of BTA derivative (Figure 2.1).

There are many photoreactive group that are used for photoaffinity labeling. I focused on the aryl azide and the trifluoromethyl diazirine (TFMD), two of the smallest photoreactive groups.[59,62] Size was an important factor since I wanted to minimize the potential perturbations that may arise when incorporating a photoreactive group into the structure of BTA-EG$_4$. I ultimately chose the TFMD because of its photochemical properties. TFMDs are unstable when exposed to longwave UV light ($\lambda \sim 365$ nm) and are converted into carbenes.[63] Both

characteristics are advantageous. First, longwave UV light is less likely to cause damage to proteins than more energetic shortwave UV light. In addition, the carbene crosslinks via a bond insertion mechanism and does not need to be proximal to any specific residue.[64] The aryl azide, on the other hand, photoactivates at short wavelengths ($\lambda \sim 250$ nm) and decomposes into the dehydroazepine, which requires a nearby nucleophilic group such as a lysine for crosslinking.[62]
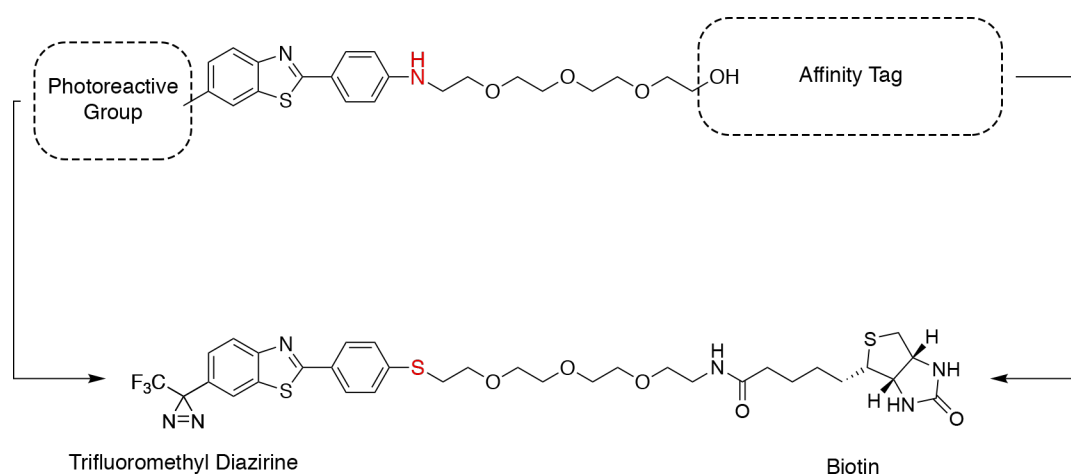
Figure 2.1. **Design of a Photoaffinity Labeling Probe.** The trifluoromethyl diazirine was placed in the same position as the methyl group on the benzothiazole ring. Biotin was added at the end of the tetraethylene glycol tail. In addition, the aniline nitrogen was replaced with a sulfur (shown in red).

Typical photoaffinity labeling probes are often synthesized by incorporating the photoreactive group onto the ligand via a reactive handle. For example, an aryl azide derivative of glucose has been synthesized by reacting 6-aminoglucose with a commercially available aryl azide NHS-ester.[65] I, instead, constructed the TFMD directly on the ligand. BTA-EG$_4$ contains a methyl group at the 6-position of the benzothiazole ring. I decided to place the TMFD there to maintain the steric bulk at that position.

Ultimately, I wanted to crosslink a protein with probe **2.1** (Figure 2.2) and isolate the protein for protein identification via mass spectrometry. Because of this, I also incorporated biotin as an affinity pull-down tag. This allows me to isolate the proteins I label. Biotin is one of the smallest affinity tags available and binds to its partner streptavidin with great avidity ($K_d \sim 10^{-15}$).[66] I placed biotin at the end of the ethylene glycol tail to keep it distal from the 2-arylbenzothiazole core.

Finally, I opted to use a sulfur-containing derivative of BTA-EG$_4$. This version of BTA-EG$_4$ exhibits similar biological activity to the parent compound.[67] However, the sulfur derivative of BTA-EG$_4$ are far easier to synthesize. When making BTA-EG$_4$, the major synthetic bottleneck is coupling the benzothiazole aniline to the polyethylene glycol iodide via a substitution reaction. Accomplishing this requires fairly harsh conditions: either a weeklong reflux in acetone or microwave assistance at high temperatures.[40,68] The sulfur analog of BTA-EG$_4$ can be made under much gentler conditions. In addition, the literature[69] and anecdotal evidence suggests that the amine group of aniline is not compatible with some oxidation reactions required for the synthesis.

2.1

2.2
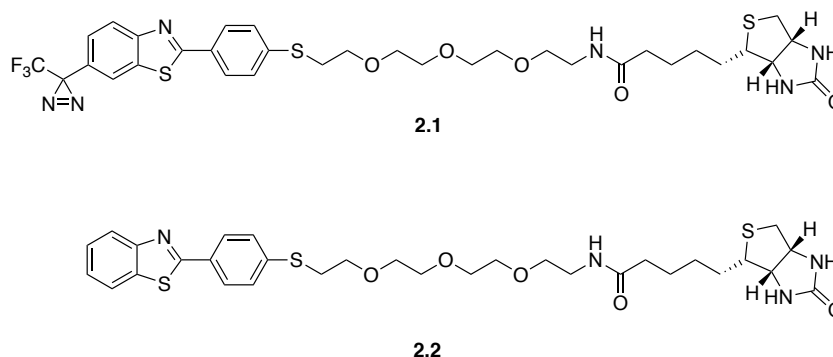
Figure 2.2. **Chemical Structures of Synthetic Targets.** Compound **2.1** is the photoaffinity labeling probe that contains a TFMD and biotin. Compound **2.2** is a non-photoreactive version of compound **2.1**.

Ultimately, I set out to synthesize two compounds (Figure 2.2). Compound **2.1** is the photoaffinity labeling probe containing the TFMD. Compound **2.2**, on the other hand, is a control compound that lacks the TFMD. Retrosynthetically, compound **2.1** can be broken down into two major pieces: a functionalized tetraethylene glycol tail and the 2-arylbenzothiazole (Figure 2.3). These two pieces can be coupled together via a "Pummerer-Methanolysis-Substitution" sequence. From the aldehyde handle, the TFMD can be constructed. Finally, biotinylation provides the final product. Control compound **2.2** is synthesized in a similar fashion except that the diazirine synthesis is omitted and a non-formylated 2-arylbenzothiazole is one of the major building blocks.
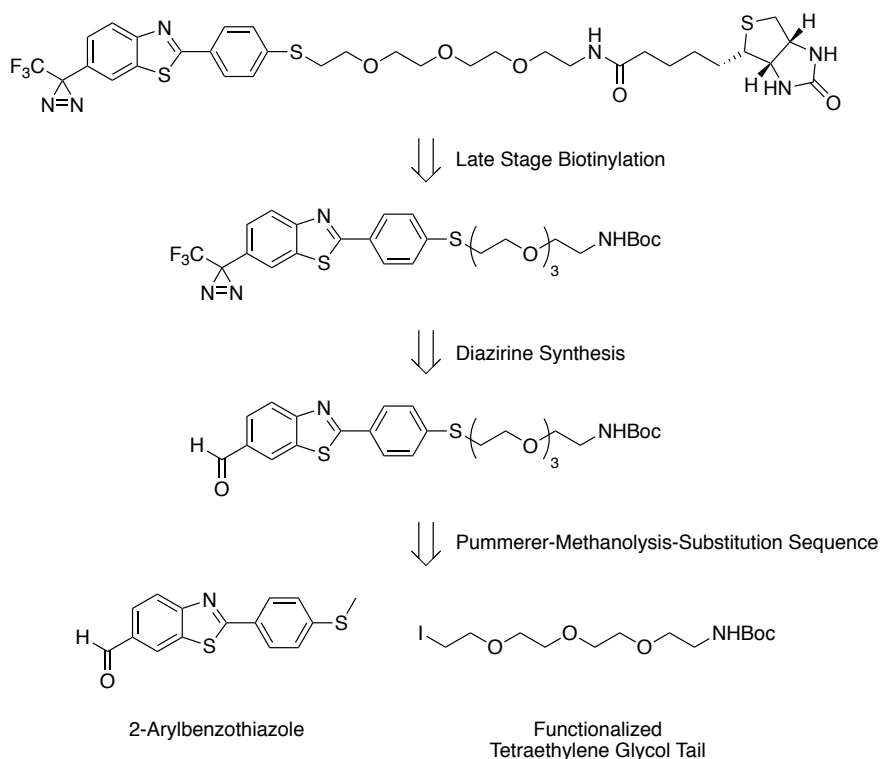
Figure 2.3. **Retrosynthetic Analysis of Compound 2.1.**

2.3 Synthesis of the Functionalized Tetraethylene

Glycol Tail

Synthesis of the functionalized tetraethylene glycol tail involved standard chemistry.
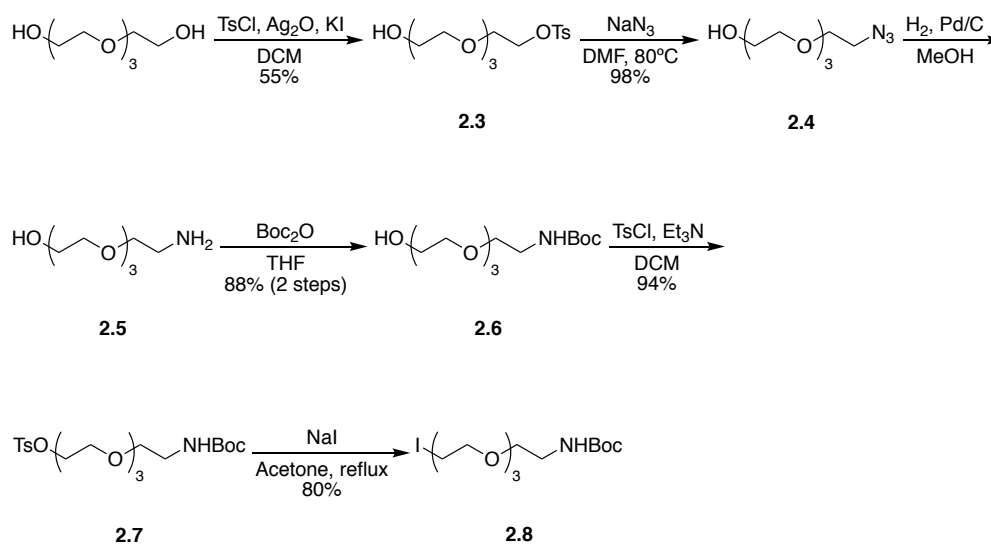
Figure 2.4. **The Synthesis of Functionalized Tetraethylene Glycol Tail 2.8.**

First, I tosylated tetraethylene glycol with Ag_2O and catalytic KI, conditions which preferentially give the monotosylated product **2.3**.[70] After tosylation, I displaced the tosyl group with NaN_3 to give azide **2.4**. Reduction of azide **2.4** with H_2 and Pd/C furnished amine **2.5**. Amine **2.5** was then protected with Boc_2O. After protection, the remaining hydroxyl group was tosylated to give compound **2.7**. Finally, the tosyl group was displaced with the iodide using Finkelstein conditions to yield iodide **2.8**.

2.4   Synthesis of the 2-Arylbenzothiazole Core

The synthesis of the 2-arylbenzothiazole core was perhaps the greatest challenge of this synthesis. Although our lab previously used a microwave-assisted coupling reaction between aryl aldehydes and *o*-aminothiophenols, to general new derivatives of BTA-EG$_4$,[71] I was not able to use this method because of a lack of commercially available *o*-aminothiophenols and a lack of general methods to access this moiety (Figure 2.5A).
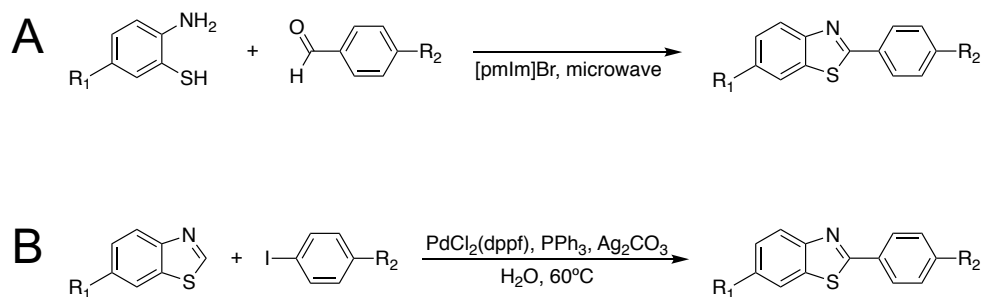
Figure 2.5. **Methods to Synthesize 2-Arylbenzothiazoles.** (A) Synthesis of 2-arylbenzothiazole with *o*-aminothiophenols and aryl aldehydes. The reaction requires an ionic liquid and microwave irradiation. (B) Synthesis of 2-arylbenzothiazole with benzothiazole and aryl iodides. The reaction proceeds via a palladium-catalyzed C-H bond activation.

I spent a great deal of time trying to find a method to synthesize the 2-arylbenzothiazole. The reaction that proved most fruitful was perhaps also the most exotic. Dubbed an "on-water arylation", the reaction is an arylation that occurs through a palladium-catalyzed C-H bond activation (Figure 2.5B).[72] The reaction does not occur in the aqueous phase; neither of the reactants are appreciably soluble in water. Rather, unknown surface effects on water have been implicated to play a role in this transformation.[72] The discovery of these odd reaction conditions

was truly serendipitous. In short, previous work reported an increase in yields after a reflux condenser broke and introduced water into the reaction mixture.[73]

I first needed 4-iodothioanisole for the on-water arylation. The methyl sulfide would ultimately be the handle from which the 2-arylbenzothiaozle core would be coupled to compound **2.8**. I treated 4-bromothioanisole with *tert*-butyllithium to give the corresponding organolithium. Quenching with I_2 yielded iodide **2.9**.
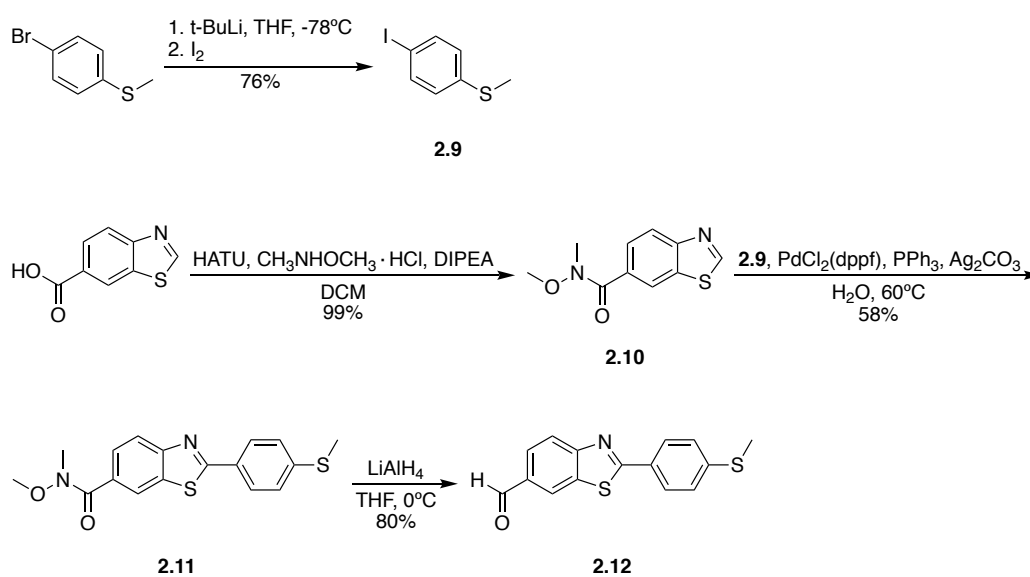
Figure 2.6. **The Synthesis of the 2-Arylbenzothiazole Core.**

Ultimately, I wanted an aldehyde on the 6-position of the benzothiazole ring since I planned on constructing the TFMD from this handle. I tried performing the on-water arylation with methyl ester and aldehyde at the 6-position; yields for these reactions were low due to solubility and purification issues. However, I achieved decent yields when I used the Weinreb amide. Weinreb amide **2.10** was made via an HATU coupling of 6-benzothiazole carboxylic acid with *N,O*-dimethyl hydroxylamine. With benzothiazole **2.10** in hand, I coupled it to iodide **2.9** via the on-

water arylation. Finally, reduction of compound **2.11** with LiAlH$_4$ provided aldehyde **2.12**.

2.5 Coupling the Functionalized Tetraethylene Glycol Tail with the 2-Arylbenzothiazole Core

The next part of the synthesis was to couple functionalized tetraethylene glycol **2.8** to 2-arylbenzothiazole **2.12**. To liberate the free thiolate, I first converted methyl sulfide **2.12** into methyl sulfoxide **2.13** using mCPBA. Conducting the reaction at low temperatures and with a stoichiometric amount of mCPBA prevented any significant conversion to the sulfone. Next, I refluxed sulfoxide **2.13** with trifluoroacetic anhydride, which gave the Pummerer arrangement product. After, I treated the Pummerer product with Et$_3$N and MeOH. Methanolysis of the Pummerer product occurred immediately; the development of a richly red solution indicated the
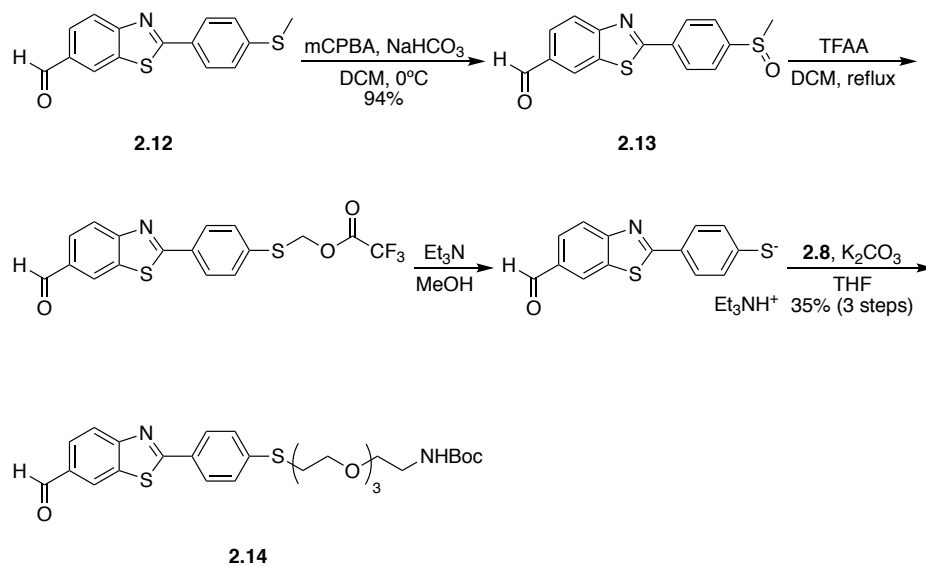
Figure 2.7. **The Pummerer-Methanolysis-Substitution Sequence.**

presence of the thiolate. Finally, I reacted the thiolate with iodide **2.8** in an S_N2

reaction to furnish the coupled product **2.14**.

2.6   Synthesis of the Trifluoromethyl Diazirine

The synthesis of the TFMD has been thoroughly described.[63,74,75] However,

the synthetic challenge I faced was producing a trifluoromethyl ketone (TFMK), the

precursor to the TFMD. Typical syntheses use the reaction of 1-trifluoroacetyl

piperidine with Grignard reagents or organolithium reagents (Figure 2.8A).[74,75]

Unfortunately, Grignard reagents and organolithium reagents are not compatible

with the acidic carbamate proton present on compound **2.14**.
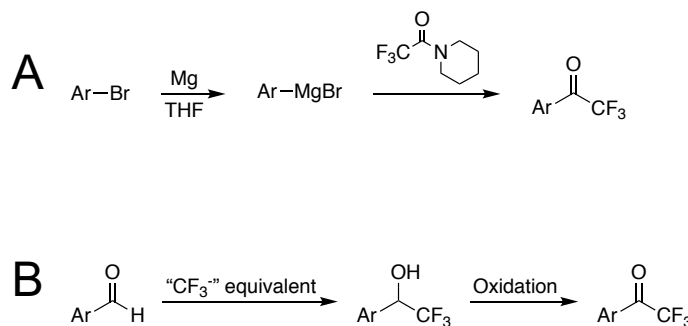
Figure 2.8. **Two Different Standard Routes to an Aryl Trifluoromethyl Ketone.** (A) The typical route to trifluoromethyl ketones used when synthesizing photoaffinity labeling probes. CF_3 is added through an acylation. (B) An alternative route towards the trifluoromethyl ketone. CF_3 is introduced via a nucleophilic trifluoromethylation of an aldehyde.

Because of this, I opted to proceed down a "nucleophilic" route to construct

the TFMK (Figure 2.8B). Rather than performing a trifluoromethylacetylation (the

"electrophilic" route), I decided instead to do a nucleophilic trifluoromethylation of an

aldehyde. This reaction yields a carbinol that can be oxidized to the TFMK.

First, I treated aldehyde **2.14**, with the Ruppert-Prakash reagent, TMS-CF_3,

and a trace amount of K_2CO_3. In this reaction, K_2CO_3 acts as a nucleophilic initiator

for the trifluoromethylation.[76] The product of this reaction is a TMS-protected alcohol. Once the reaction appeared complete, I immediately removed the TMS group with TBAF to furnish carbinol **2.15**. The carbinol was oxidized into the ketone using Dess-Martin periodinane to give TFMK **2.16**.[77]
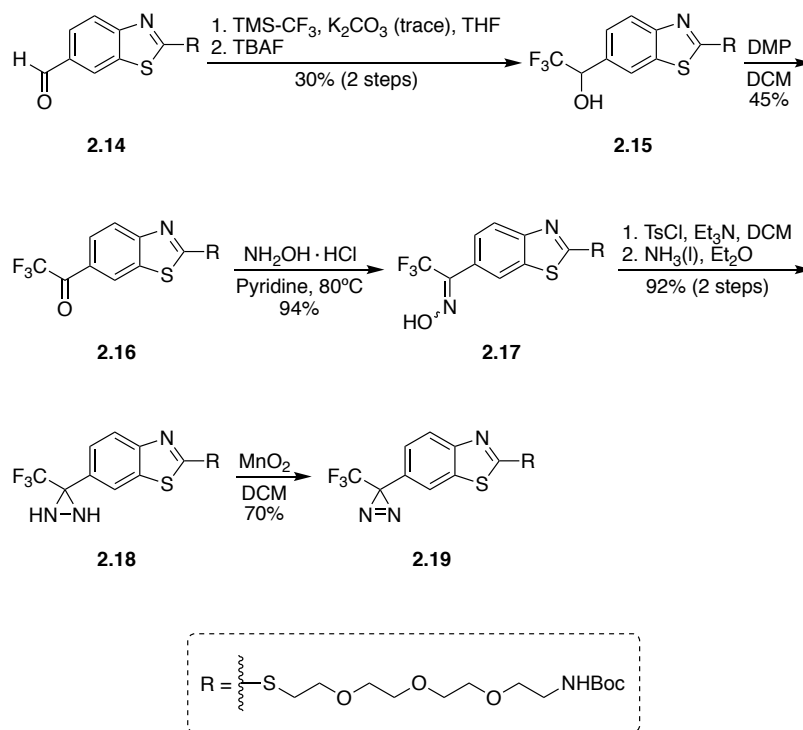
Figure 2.9. **The Synthesis of the Trifluoromethyl Diazirine.**

With TFMK **2.16** in hand, I constructed the TFMD. First, reaction of TFMK **2.16** with hydroxylamine hydrochloride in heated pyridine provided oxime **2.17**.[75] ^{1}H NMR indicated that the product was a mixture of both the *(E)* and the *(Z)* diastereomer in nearly equal amounts. Next, I tosylated the oxime. I did not isolate the tosylated intermediate since it is reported that purification tends to decrease yields.[75] Once I judged the reaction was complete by TLC, the tosylated oxime was

treated with 50% liquid ammonia in ether.[75] This reaction gave in diaziridine **2.18**. Finally, diaziridine **2.18** was oxidized with MnO$_2$ to give diazirine **2.19**.[75]

2.7 Synthetic Endgame

I decided to add biotin at the end of the synthesis since biotin imparts solubility issues to whatever it is conjugated. I used the NHS-ester of biotin, **2.20**, as my biotinylating agent. To make NHS-ester **2.20**, I did a DCC coupling of N-hydrosuccinimide with biotin.
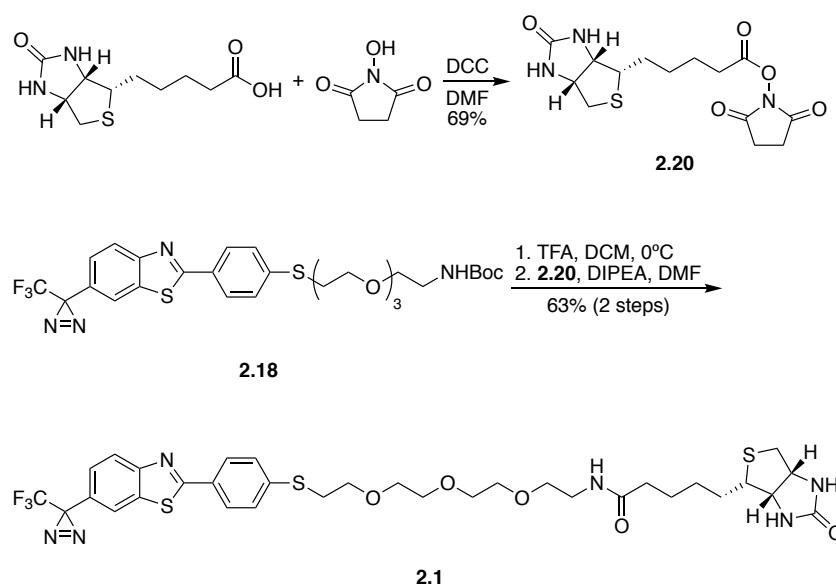
Figure 2.10. **The Synthetic Endgame.**

To finish the synthesis, I removed the Boc group on compound **2.18** using trifluoroacetic acid to furnish the ammonium salt. Finally, I conjugated the biotin group using NHS ester **2.20** to yield the final product **2.1**.

2.8 Synthesis of a Non-Photoreactive Control Compound

I also synthesized a version of **2.1** lacking the TFMD. This served as a control for the photoaffinity labeling experiments. Shown below is the synthesis of the control compound **2.2**.
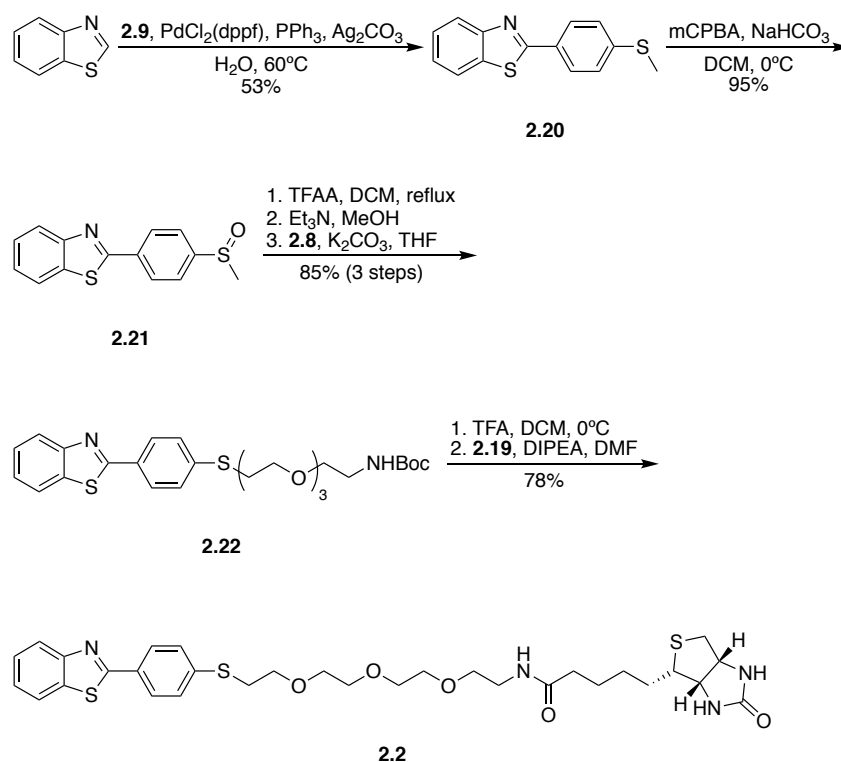
Figure 2.11. **The Synthesis of the Non-Photoreactive Compound 2.2.**

This synthesis recapitulates most of the chemistry used for compound **2.1**. Commercially available benzothiazole was coupled to iodide **2.9** through the on-water arylation to yield coupled product **2.20**. I oxidized sulfide **2.20** into sulfoxide **2.21** with mCPBA. I subjected sulfoxide **2.21** to the Pummerer-Methanolysis-

Substitution sequence with iodide **2.8** to furnish coupled compound **2.22**. Finally, deprotection of the Boc group and biotinylation with **2.20** gave the final product **2.2**.

2.9 Photodecomposition Studies

Since compound **2.1**, to my knowledge, is the first example of a TFMD-containing benzothiazole, I performed a ^{19}F NMR study to characterize the photodegradation of probe **2.1**. Compound **2.1** was dissolved in deuterated methanol, and the solution was transferred to an NMR tube (Figure 2.12A). The solution was irradiated with a handheld UV lamp, and at selected time points, the
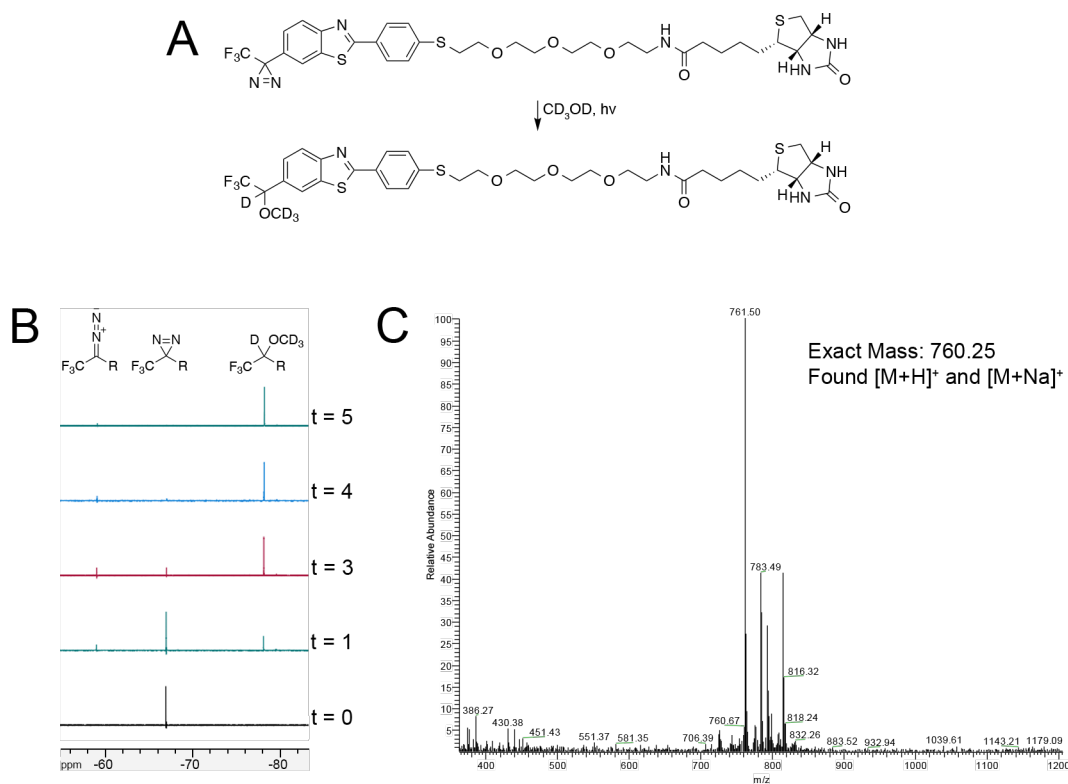
Figure 2.12. **Photodecomposition Study.** (A) The reaction of probe **2.1** when exposed to UV light in deuterated methanol. (B) ^{19}F NMR study. Spectrum of reaction mixture is shown after 1 minute, 3 minutes, 4 minutes, and 5 minutes of irradiation. Proposed corresponding structure shown above each peak. (C) ESI mass spectrum of methanol adduct shown in A.

reaction mixture was analyzed by ^{19}F NMR. I monitored the disappearance of the signal from the trifluoromethyl group in **2.1**.
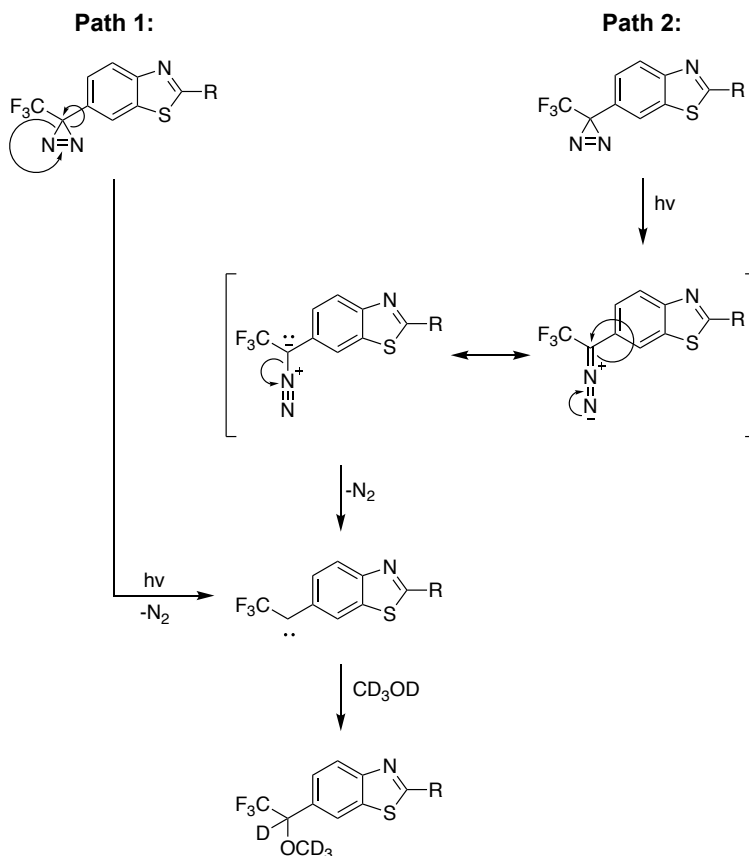
Figure 2.13. **Proposed Mechanism of Photolysis.** In addition to decomposing directly to a carbene (Path 1), compound **2.1** can undergo an alternative pathway (Path 2) in which it isomerizes into a diazo compound. The diazo compound is converted into the carbene upon release of N_2 gas.

Over the course of the reaction, the original peak (δ -66.95) decreased in intensity (Figure 2.12B). Interestingly, two new peaks formed; one peak persisted (δ -78.09) while the other peak was transient (δ -58.98). The literature suggests that the TFMD can isomerize to a linear diazo compound and subsequently lose N_2 to become a carbene.[64] Thus, I attribute the transient peak to the formation of an

unstable trifluoromethyl diazo intermediate and the persistent peak to the formation of the methanol adduct (Figure 2.13). Finally, ESI mass spectrometry confirmed the identity of the product (Figure 2.12C).

The NMR study also allowed me to characterize the kinetics of photodegradation. When the integration data from the NMR spectra is plotted against time, the data fits nicely to the integrated first order rate law (Figure 2.14). Under the conditions I used, photodecomposition occurred with a half-life of approximately 1.2 minutes.
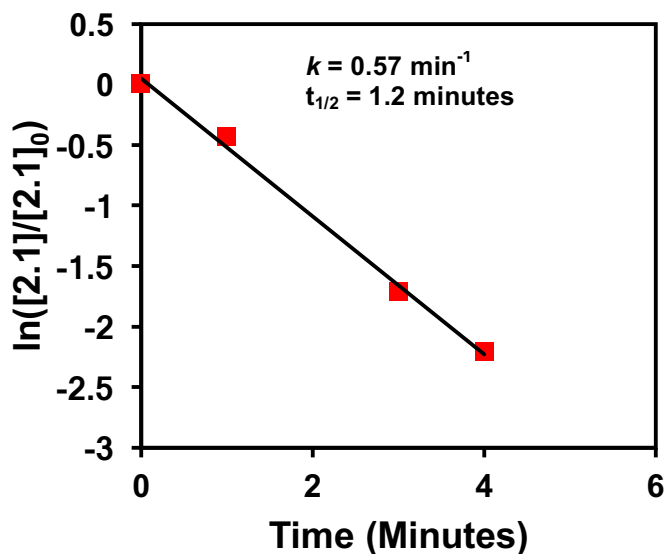
Figure 2.14. **Quantification of ^{19}F NMR Data to Determine Rate of Reaction.** To determine the fraction of **2.1** remaining, the initial integration of the peak of **2.1** was compared to the integration of the same peak at a given time point. The natural logarithm of the fraction of **2.1** remaining was taken and was plotted against time. The data was fitted to the integrated first order rate law to determine kinetic parameters.

Due the amount of material used in this experiment, I only performed the experiment once and because of this, I was not able to establish the precision of the $t_{1/2}$ I observed. However, the key piece of information gleaned from this study was

an evaluation of the order of magnitude of time required for complete photolysis. Knowing the approximate timescale of photolysis guided the design of a photoaffinity labeling protocol.

2.10 Conclusions

I successfully synthesized a photoaffinity labeling probe based on BTA-EG$_4$ as well as a non-photoreactive version of the probe. This probe contained a trifluoromethyl diazirine for crosslinking and biotin for subsequent affinity pulldowns. Furthermore, I demonstrated that probe **2.1** reacts very rapidly under longwave UV light. The half-life of this reaction was approximately 1.2 minutes. ^{19}F NMR also revealed that this decomposition may also involve an isomerization step in which the TFMD rearranges into a diazo compound prior to carbene formation.

In the next chapter, I will describe the development of a photoaffinity labeling protocol using probe **2.1**. I will then use this protocol to label and capture potential molecular targets of BTA-EG$_4$.

2.11 Experimental Methods

All reagents were purchased from Fisher Scientific, Sigma Aldrich, Spectrum Chemicals, or TCI. Reagents were used without further purification. NMR spectra were obtained from a 400 Hz Varian Mercury spectrometer, 500 Hz Jeol ECA spectrometer, or 500 Hz Varian VX 500 spectrometer at the NMR facility in the Department of Chemistry and Biochemistry at the University of California, San Diego. Electrospray ionization mass spectrometry (ESI-MS) and high resolution

mass spectrometry (HR-MS) were performed at the Molecular Mass Spectrometry Facility in the Department of Chemistry and Biochemistry at the University of California, San Diego.

Synthesis of Compound 2.3
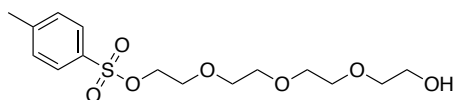
Tetraethylene glycol (2.00 g, 10.3 mmol) was dissolved in DCM (50 mL) with stirring. KI (341 mg, 2.06 mmol) was added, followed by Ag_2O (3.58 g, 15.4 mmol). TsCl (1.96 g, 10.3 mmol) was added in portions. After the addition of TsCl was complete, the reaction was stirred for 2 hours. The reaction mixture was filter over a pad of Celite to remove solids. The flow-through was concentrated under reduced pressure. The resulting oil was purified via silica chromatography (using EtOAc as eluent) to yield product **2.3** as a clear oil (1.96 g, 55%). Characterization of **2.3**: ^{1}H-NMR (400 MHz, $CDCl_3$) δ 7.73 (d, 2H), 7.29 (d, 2H), 4.10 (t, 2H), 3.65-3.52 (m, 16H), 2.33 (s, 3H). ESI-MS (*m/z*) [M+Na][+] 371.1, [M+K][+] 387.1.

Synthesis of Compound 2.4
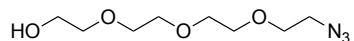
Compound **2.3** (4.36 g, 12.5 mmol) was dissolved in dry DMF (15 mL). NaN_3 (2.44 g, 37.5 mmol) was added, and the mixture was heated to 60°C. The reaction was stirred overnight. The mixture was cooled to room temperature, and a large excess of Et_2O (250 mL) was added. Solids were filtered off over a pad of Celite. The flow-through was concentrated under reduced pressure to yield product **2.4** as

a clear oil and was used without any further purification (2.79 g, 98%).
Characterization of **2.4**: ^{1}H-NMR (400 MHz, CDCl$_3$) δ 3.72-3.58 (m, 14H), 3.38 (t,
2H). ESI-MS (*m/z*) [M+NH$_4$]$^+$ 237.28, [M+Na]$^+$ 242.04.

Synthesis of Compound 2.5

HO$\diagdown\diagup$O$\diagdown\diagup$O$\diagdown\diagup$O$\diagdown$NH$_2$
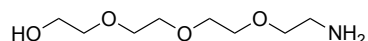
      Compound **2.4** (2.50 g, 11.4 mmol) was dissolved in 10 mL MeOH.
Approximately 625 mg Pd/C was added. The reaction was stirred at room
temperature under an atmosphere of H$_2$ for 3 days. The crude was filtered over a
pad of Celite, and solvent was removed under reduced pressure. Compound **2.5**
was a clear oil and was carried over to the next step without any further purification.

Synthesis of Compound 2.6

HO$\diagdown\diagup$O$\diagdown\diagup$O$\diagdown\diagup$O$\diagdown$N(H)C(=O)O-*t*-Bu
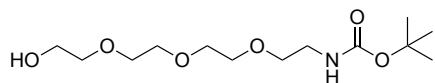
      Compound **2.5** (2.16 g, 11.18 mmol) was dissolved in THF. Boc$_2$O (2.68 g,
12.29 mmol) was added, and the mixture was stirred. The reaction was stirred for 4
hours. Solvent was removed under reduced pressure. The resulting oil was purified
via silica chromatography (using EtOAc as eluent) to yield product **2.6** as a clear oil
(3.28 g, 98% over two steps). Characterization of **2.6**: ^{1}H-NMR (400 MHz, CDCl$_3$) δ
3.73-3.59 (m, 14H), 3.32 (q, 2H), 1.43 (s, 9H). ESI-MS (*m/z*) [M+H]$^+$ 294.92,
[M+Na]$^+$ 316.10.

Synthesis of Compound 2.7
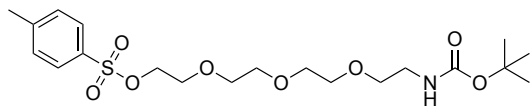
Compound **2.6** (1.50 g, 5.11 mmol) was dissolved in DCM (15 mL). Et₃N

(1.42 mL, 10.22 mmol) was added, and the mixture was cooled to 0°C. Once cooled,

TsCl (1.95 g, 10.22 mmol) was added. The reaction was stirred overnight. A solid

precipitate formed over the course of the reaction. Solvent was removed under

reduced pressure. The product was purified via silica chromatography (using a

gradient from 1:1 hexanes/EtOAc to 1:3 hexanes/EtOAc as eluent) to yield product

2.7 as an oil (2.15 g, 94%). Characterization of **2.7**: ^{1}H-NMR (500 MHz, CDCl₃) δ

7.76 (d, 2H), 7.31 (d, 2H), 4.99 (s, 1H), 4.13 (t, 2H), 3.66 (t, 2H), 3.58-3.55 (m, 8H),

3.49 (t, 2 H), 3.27 (m, 2H), 2.41 (s, 3H), 1.40 (s, 9H). ESI-MS (*m/z*) [M+H]$^+$ 447.85,

[M+Na]$^+$ 470.06.

Synthesis of Compound 2.8
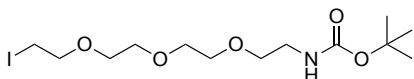
Compound **2.7** (1.00 g, 2.23 mmol) was dissolved in dry acetone. NaI (1.34

g, 8.94 mmol) was added, and the mixture was heated to reflux. The reaction was

stirred overnight. The crude was filtered over a pad of Celite to remove any solids.

The flow-through was concentrated under reduced pressure and was dissolved in

EtOAc (30 mL). The crude was washed with 10% Na₂S₂O₃ (20 mL) and brine (20

mL). The organic layer was separated and dried over Na₂SO₄. The organic layer

was then filtered to remove Na₂SO₄. The solvent was removed under reduced

pressure to yield **2.8** as a clear oil (719 mg, 80%). Characterization of **2.8**: ^{1}H-NMR (500 MHz, CDCl3) δ 3.76 (t, 2H), 3.67-3.61 (m, 8H), 3.26 (t, 2H), 1.44 (s, 9H). ESI-MS (*m/z*) [M+H]$^{+}$ 403.87, [M+Na]$^{+}$ 426.05.

Synthesis of Compound 2.9
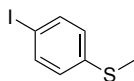
A solution of 4-bromothioanisole (1.50 g, 7.39 mmol) in THF (30 mL) was cooled to -78°C in a dry ice-acetone bath. Once cooled, *tert*-butyllithium (9.56 mL, 1.7 M solution in pentane, 16.26 mmol) was added to the mixture dropwise. Once all the *tert*-butyllithium was added, the solution remained yellow. I_2 (2.06 g, 8.13 mmol) was dissolved in THF and was added dropwise to the solution. Once all the I_2 was added, the solution became dark red. The mixture was warmed to room temperature. After, a saturated solution of $Na_2S_2O_3$ was added until the solution became colorless. Et_2O (50 mL) was added, and the organic layer was separated. The aqueous layer was extracted with Et_2O (2 x 50 mL). The organic layers were combined and dried over Na_2SO_4. Solvent was removed under reduced vacuum. Under vacuum, compound **2.9** became green. When the compound was exposed to air, it became yellow (1.40 g, 76%). Characterization of **2.9**: ^{1}H NMR (CDCl$_3$, 400 MHz) δ 7.56 (d, 2H), 6.97 (d, 2H), 2.44 (s, 3H).

Synthesis of Compound 2.10
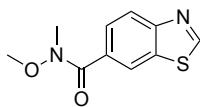
Benzothiazole-6-carboxylic acid (1.50 g, 8.37 mmol) was suspended in dry DCM (40 mL). DIPEA (5.84 mL, 33.48 mmol) was added, and the solution clarified. HATU (3.82 g, 10.04 mmol) was added, and the mixture was stirred for 10 minutes. After, *N,O*-dimethylhydroxylamine (950 mg, 10.04 mmol) was added. The reaction was stirred for 1 hour. The reaction mixture was diluted with DCM, and the organic layer was washed with 1 M HCl (20 mL) and saturated bicarbonate (20 mL). The organic layer was dried over Na_2SO_4, and solvent was removed under reduced pressure. The crude was purified via silica chromatography (using 1:3 Hexanes/EtOAc as eluent) to yield product **2.10** as an oil which crystallized into an off-white solid when kept at -20°C (1.84 g, 99%). Characterization of **2.10**: ^{1}H NMR (CDCl$_3$, 500 MHz) δ 9.10 (s, 1H), 8.35 (s, 1H), 8.13 (d, 1H), 7.84 (dd, 1H), 3.53 (s, 3H), 3.39 (s, 3H). ESI-MS (*m/z*) [M+H]$^+$ 223.16.

Synthesis of Compound 2.11
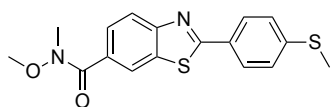
Compound **2.10** (1.00 g, 4.50 mmol), compound **2.9** (1.35 g, 5.40 mmol), PdCl$_2$(dppf) (329 mg, 0.45 mmol), PPh$_3$ (236 mg, 0.90 mmol), and Ag$_2$CO$_3$ (2.48 g, 9.00 mmol) were combined and were ground together with a pestle and mortar. The mixture was placed in a screw cap tube. Water (5 mL) was added to suspend the solid mixture, and the reaction mixture was heated at 60°C overnight. The mixture

became black over the course of the reaction. DCM (10 mL) was added to the reaction mixture, and the solids were filtered over a pad of Celite. The pad of Celite was washed with a large amount of DCM (150 mL). The flow-through was washed with water (50 mL). The organic layer was removed and was dried over Na_2SO_4. The crude was purified via silica chromatography (using a 3:1 to 2:1 to 1:1 hexanes/EtOAc gradient as eluent) to yield product **2.11** as a white solid (891 mg, 58%). Characterization of **2.11**: ^{1}H NMR (CDCl$_3$, 500 MHz) δ 8.26 (s, 1H), 8.03-7.98 (m, 3H), 7.81 (dd, 1H), 7.31 (d, 2H), 3.56 (s, 3H), 3.40 (s, 3H), 2.53 (s, 3H). ^{13}C NMR (CDCl$_3$, 500 MHz) δ 170.12, 169.28, 155.67, 143.68, 134.68, 130.70, 129.89, 128.08, 126.93, 126.06, 122.54, 122.51, 61.41, 34.02, 15.28. ESI-MS (*m/z*) [M+H]$^+$ 345.20.

Synthesis of Compound 2.12
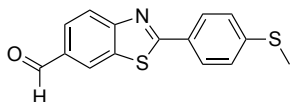
Compound **2.11** (891 mg, 2.59 mmol) was dissolved in dry THF (20 mL). The solution was cooled to 0°C. Once cooled, LAH (2.84 mL, 1 M in THF, 2.84 mmol) was added dropwise. The reaction was stirred for 1 hour. After, EtOAc (20 mL) was added to quench any remaining LAH. A saturated solution of Rochelle salt (30 mL) was added, and the biphasic mixture was stirred vigorously for 1 hour. The organic layer was removed, and the aqueous layer was extracted with DCM (2 x 20 mL). The combined organic layers were collected and were dried over Na_2SO_4. The solvent was removed under reduced pressure. The resulting solid crude was recrystallized from iPrOH to provide product **2.12** as an off-white solid (596 mg,

80%). Characterization of **2.12**: ^{1}H NMR (CDCl$_3$, 500 MHz) δ 10.09 (s, 1H), 8.42 (s, 1H) 8.12 (d, 1H), 8.01 (d, 2H), 7.98 (dd, 1H), 7.32 (d, 2H), 2.54 (s, 3H). ^{13}C NMR (CDCl$_3$, 500 MHz) δ 191.35, 172.33, 158.34, 144.46, 135.63, 133.32, 129.57, 128.24, 127.69, 126.01, 124.51, 123.61, 15.22. ESI-MS (*m/z*) [M+H]$^+$ 286.26, [M+MeOH+H]$^+$ 318.30.

Synthesis of Compound 2.13
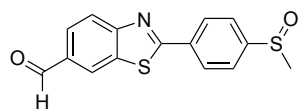
Compound **2.12** (260 mg, 0.91 mmol) and NaHCO$_3$ (306 mg, 3.64 mmol) were suspended in DCM (5 mL). The mixture was cooled to 0°C. mCPBA (204 mg, 0.911 mmol, ~77% purity) was dissolved in DCM (5 mL), and the solution was added dropwise. The reaction was stirred for 1 hour at 0°C. After, the crude was diluted with DCM (20 mL) and was washed with 1 M NaOH (10 mL). The organic layer was collected and was dried over Na$_2$SO$_4$. The solvent was removed under reduced pressure. The crude was purified via silica chromatography (using a gradient of DCM to 2% MeOH in DCM as eluent) to yield product **2.13** as a white solid (258 mg, 94%). Characterization of **2.13**: ^{1}H NMR (CDCl$_3$, 500 MHz) δ 10.12 (s, 1H), 8.46 (d, 1 H), 8.28 (d, 2H), 8.19 (d, 1H), 8.03 (dd, 1H), 7.79 (d, 2H), 2.79 (s, 3H). ^{13}C NMR (CDCl$_3$, 500 MHz) 191.24, 170.88, 158.04, 149.66, 135.91, 135.67, 133.83, 128.83, 127.76, 124.74, 124.57, 124.26, 44.16. ESI-MS (*m/z*) [M+H]$^+$ 302.25, [M+MeOH+H]$^+$ 334.19.

Synthesis of Compound 2.14
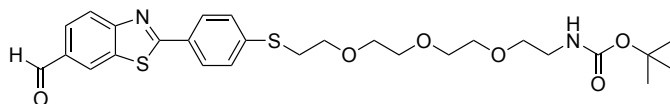
Compound **2.13** (160 mg, 0.531 mmol) was suspended in DCM (~2 mL). TFAA (~2 mL) was added. The mixture was refluxed for 1 hour. The solvents were removed under reduced pressure. The crude was carried over to the next step.

The crude was dissolved in a solution of 50% Et$_3$N in MeOH (~4 mL). The crude became red and was stirred for 10 minutes. Solvents were removed under reduced pressure.

The crude was then dissolved in dry THF (3 mL). K$_2$CO$_3$ (147 mg, 1.06 mmol) was added. Compound **2.8** (107 mg, 0.266 mmol) was dissolved in THF and was added to the mixture. The reaction was stirred overnight. After, solvent was removed under reduced pressure, and the crude was dissolved in EtOAc. The organic layer was washed with 1 M NaOH (~20 mL), water (~20 mL), and brine (~20 mL). The organic layer was then dried over Na$_2$SO$_4$. The crude was purified via silica chromatography (using a gradient of 2:1 Hexanes/EtOAc to 1:2 Hexanes/EtOAc as eluent) to yield product **2.14** as an off-white solid (87.3 mg, 60%). Characterization of **2.14**: ^{1}H NMR (CDCl$_3$, 500 MHz) δ 10.11 (s, 1H), 8.44 (s, 1H), 8.15 (d, 1H), 8.03-8.00 (m, 3H), 7.43 (d, 2H), 3.76 (t, 2H), 3.66-3.62 (m, 8H), 3.54 (t, 2H), 3.32 (q, 2H), 3.25 (t, 2H), 1.43 (s, 9H). ^{13}C NMR (CDCl$_3$, 500 MHz) δ 191.36, 172.13, 158.31, 156.20, 142.34, 135.68, 133.40, 130.33, 128.34, 127.93, 127.69, 124.56, 123.71, 70.81, 70.77, 70.45, 69.86, 40.54, 32.10, 28.63. ESI-MS (*m/z*) [M+H]$^+$ 547.14, [M+Na]$^+$ 569.22.

Synthesis of Compound 2.15
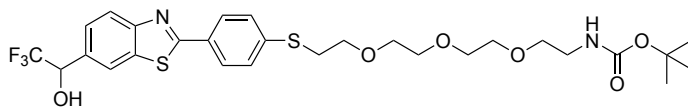
Compound **2.14** (51 mg, 0.093 mmol) was dissolved in dry DMF (~ 2 mL). A trace amount of K_2CO_3 (a few grains) were added the mixture. $TMSCF_3$ was added. The reaction proceeded for 30 minutes. The reaction progress was monitored by TLC. Once the reaction was judged to be complete, TBAF was added to remove the TMS group. The crude was purified via silica chromatography (using a gradient of 1:1 Hexanes/EtOAc as eluent) to yield product **2.15** as a white solid (17.2 mg, 30%). Characterization of **2.15**: ^{1}H NMR ($CDCl_3$, 400 MHz) δ 8.05-8.03 (m, 2H), 7.96 (d, 2H), 7.57 (d, 1H), 7.39 (d, 2H), 5.20-5.15 (m, 1H), 3.74 (t, 2H), 3.66-3.60 (m, 8H), 3.50 (t, 2H), 3.28 (q, 2H), 3.21 (t, 2H), 1.43 (s, 9H). ESI-MS (*m/z*) [M+H]$^+$ 617.14, [M+Na]$^+$ 639.20.

Synthesis of Compound 2.16
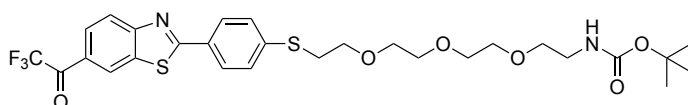
Compound **2.15** (11 mg, 0.018 mmol) was dissolved in dry DCM (2 mL). The mixture was cooled to 0°C in an ice bath. Once cooled, DMP (30 mg, 0.071 mmol) was added, and the mixture was warmed to room temperature. The reaction was stirred for two hours. After, more DCM and saturated $NaHCO_3$ was added. The mixture was stirred until the organic layer became clear. The organic layer was separated from the aqueous layer. The aqueous layer was extracted with DCM (~10 mL). The combined aqueous layers were dried over Na_2SO_4. The crude was purified

via silica chromatography (using a gradient of 3:1 Hexanes/EtOAc to as eluent) to yield product **2.16** as a white solid (5 mg, 42%) Characterization of **2.16**: ^{1}H NMR (CDCl$_3$, 500 MHz) δ 8.65 (s, 1H), 8.20-8.02 (m, 2H), 8.03 (d, 2H), 7.43 (d, 2H), 3.76 (t, 2H), 3.69-3.61 (m, 8H), 3.54 (t, 2H), 3.32 (q, 2H), 3.25 (t, 2H), 1.43 (s, 9H). ESI-MS (*m/z*) [M+Na+H$_2$O]$^+$ 655.26, [M+Na+MeOH]$^+$ 669.26.

Synthesis of Compound 2.17
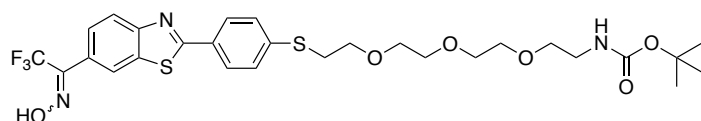
Compound **2.16** (16 mg, 0.027 mmol) was dissolved in pyridine (2 mL). NH$_2$OH·HCl (6 mg, 0.08 mmol) was added. The mixture was heated to 80°C and was stirred for 6 hours. After, the solvent was removed under reduced pressure. The crude was purified via silica chromatography (using 1:2 Hexanes/EtOAc as eluent) to yield product **2.17** as a white solid (15.4 mg, 92%). NMR indicated that the product was a mixture of diasteromers. Characterization of **2.17**: ^{1}H NMR (CDCl$_3$, 500 MHz) δ 8.11-8.07 (m, 1H), 8.04-8.00 (m, 1H), 7.94-7.90 (m, 2H), 7.62 (t, 1H), 7.35 (t, 2H), 3.73 (t, 2H), 3.67-3.65 (m, 8H), 3.55 (t, 2H), 3.33 (q, 2H), 3.20 (t, 2H), 1.41 (s, 9H). ESI-MS (*m/z*) [M+H]$^+$ 630.08, [M+Na]$^+$ 652.21.

Synthesis of Compound 2.18
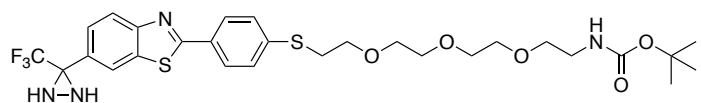
Compound **2.17** (15.4 mg, 0.025 mmol) was dissolved in DCM (~2 mL). Et$_3$N (~7 μL, 0.05 mmol) was added, and the solution was cooled to 0°C. TsCl (9.5 mg,

0.05 mmol) was added. The mixture was stirred for 1 hour. Solvent was removed under reduced pressure. The crude was carried over to the next step.

The crude was dissolved in Et$_2$O (2 mL) and was transferred to a thick-walled screw cap tube. The solution was cooled to -78°C. Once cooled, liquid ammonia (~2 mL) was transferred to the solution by cannula. The tube was sealed and was stirred vigorously. The solution was warmed to room temperature. The reaction was stirred for 4 hours. After, the tube was carefully opened, and excess ammonia was evaporated. The crude was purified via silica chromatography (using 1:2 Hexanes/EtOAc as eluent) to yield product **2.16** as a white solid (10.0 mg, 92%). Characterization of **2.17**: ^{1}H-NMR (500 MHz, CDCl$_3$) δ 8.18 (s, 1H), 78.07 (d, 1H), 8.00 (d, 2H), 7.73 (d, 1H), 7.43 (d, 2H), 3.74 (t, 2H), 3.66-3.61 (m, 8H), 3.53 (t, 2H), 3.31 (q, 2H), 3.23 (t, 2H), 2.90 (d, 1H), 2.35 (d, 1H), 1.43 (s, 9H). ESI-MS (*m/z*) [M+Na]$^+$ 371.1, [M+K]$^+$ 387.1.

Synthesis of Compound 2.19
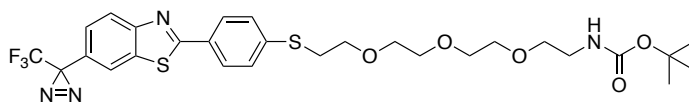
Compound **2.18** (10 mg, 0.016 mmol) was dissolved in dry DCM (~ 2 mL). MnO$_2$ was added (~14 mg, 0.16 mmol), and the suspension was stirred for 1 hour. The crude was filtered over a pad of Celite to remove the solids. The crude was purified via silica chromatography (using 1:1 Hexanes/EtOAc as eluent) to yield product **2.19** as a white solid (7.0 mg, 70%). Characterization of **2.19**: ^{1}H-NMR (400 MHz, CDCl$_3$) δ 8.04 (d, 1H), 7.98 (d, 2H), 7.75 (s, 1H), 7.42 (d, 2H), 7.32 (d, 1H),

3.74 (t, 2H), 3.67-3.60 (m, 8H), 3.53 (t, 2H), 3.32 (q, 2H), 3.23 (t, 2H), 1.43 (s, 9H).

ESI-MS (*m/z*) [M-N$_2$+Na]$^+$ 621.20, [M+Na]$^+$ 649.10.

Synthesis of Compound 2.20
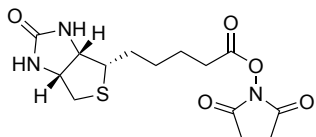
Biotin (1.00 g, 4.09 mmol) and N-hydrosuccinimide (471 mg, 4.09 mmol) were suspended in DMF. The suspension was heated until it became clear. DCC (928 mg, 4.50 mmol) was added, and the mixture was cooled to room temperature. The reaction proceeded overnight. The precipitate was filtered off, and the solvent was removed under reduced vacuum. The crude suspended in ether and was filtered. The leftover solids were recrystallized from iPrOH to yield a flakey white solid (970 mg, 69%). Characterization of **2.20**: ^{1}H-NMR (400 MHz, DMSO) δ 6.44 (s, 1H), 6.38 (s, 1H), 4.31 (t, 1H), 4.14 (t, 1H), 3.10 (m, 1H), 2.85-2.81 (m, 5H), 2.67 (t, 2H), 2.58 (d, 1), 1.68-1.61 (m, 3H), 1.53-1.40 (m, 3H).

Synthesis of Compound 2.1
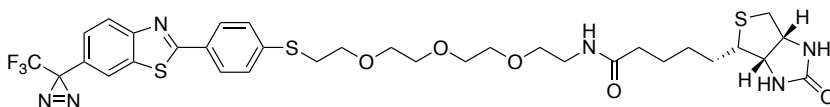
Compound **2.18** (2.4 mg, 0.0038 mmol) was dissolved in DCM (1 mL). The solution was cooled to 0°C. TFA (1 mL) was added dropwise. Solution became bright yellow upon addition of the TFA. The solution was warmed to room temperature, and the reaction was stirred for 2 hours. After, solvent was removed

under reduced vacuum. The crude was carried over to the next step without further purification

The crude was dissolved in DMF (1 mL). DIPEA (3 µL, 0.015 mmol) was added, followed by compound **2.20** (2 mg, 0.0057 mmol). The mixture was stirred for 4 hours. After, the solvent was removed under reduced pressure. The crude was dissolved in DCM (6 mL) and was washed with 1 M NaOH (4 mL). The aqueous layer was extracted with DCM (6 mL). The combined organic layers were dried over Na_2SO_4. The crude was purified by silica chromatography (using a gradient of DCM to 10% MeOH in DCM as eluent) to yield product **2.1** as a white, slightly tacky solid (1.8 mg, 63%). Characterization of **2.1**: ^{1}H NMR (CDCl$_3$, 500 MHz) δ 8.01 (d, 1H), 7.96 (d, 2H), 7.73 (s, 1H), 7.39 (d, 2H), 7.29 (d, 1H), 6.65 (s, 1H), 6.31 (s, 1H), 5.31 (s, 1H), 4.46 (t, 1H), 4.27 (t, 1H), 3.71 (t, 2H), 3.63-3.60 (m, 8H), 3.54 (t, 2H), 3.45-3.37 (m, 2H), 3.20 (t, 2H), 3.10-3.06 (m, 1H), 2.86 (dd, 1H), 2.70 (d, 1H), 2.22-2.15 (m, 2H), 1.72-1.58 (m, 4H), 1.41-1.37 (m, 2H). ESI-MS (*m/z*) [M-N$_2$+Na]$^+$ 747.37, [M+H]$^+$ 753.22, [M+Na]$^+$ 775.19. HR-MS (m/z) calculated for [M+Na]$^+$ 775.1988; found [M+Na]$^+$ 775.1986.

Synthesis of Compound 2.21
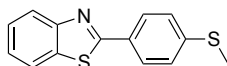
Benzothiazole (0.5 g, 3.70 mmol), compound **2.9** (1.1 g, 4.44 mmol), PdCl$_2$(dppf) (270 mg, 0.370 mmol), PPh$_3$ (194 mg, 0.739 mmol), and Ag$_2$CO$_3$ (2.04 g, 7.39 mmol) were combined and were ground together with a pestle and mortar. The mixture was placed in a screw cap tube. Water (5 mL) was added to suspend the solid mixture, and the reaction mixture was heated to 60°C. The reaction was

stirred overnight. The mixture became black over the course of the reaction. DCM (10 mL) was added to the reaction mixture, and the solids were filtered over a pad of Celite. The pad of Celite was washed with a large amount of DCM (150 mL). The flow-through was washed with water (50 mL). The organic layer was removed and was dried over Na_2SO_4. The crude was purified via silica chromatography (using a 9:1 to 4:1 hexanes/EtOAc gradient as eluent). After silica chromatography, the crude was further purified by recrystallization from iPrOH to yield product **2.21** as a white solid (506 mg, 53%). Characterization of **2.21**: ^{1}H NMR (CDCl₃, 500 MHz) δ 8.05 (s, 1H), 8.01 (d, 2H), 7.90 (s, 1H), 7.49 (t, 1H), 7.38 (t, 1H), 7.33 (d, 2H), 2.55 (s, 1H). ^{13}C NMR (CDCl₃, 500 MHz) δ 167.81, 154.32, 142.97, 135.04, 130.25, 127.96, 126.54, 126.11, 125.29, 123.21, 121.79, 15.36. ESI-MS (*m/z*) [M+H][+] 258.32.

Synthesis of Compound 2.22
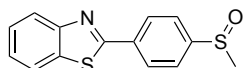
Compound **2.21** (75 mg, 0.29 mmol) and $NaHCO_3$ (98 mg, 1.17 mmol) were suspended in DCM (2 mL). The mixture was cooled to 0°C. mCPBA (65.4 mg, 0.29 mmol, ~77% purity) was dissolved in DCM (2 mL), and the solution was added dropwise. The reaction was stirred for 2 hour at 0°C. After, the crude was diluted with DCM (15 mL) and was washed with 1 M NaOH (10 mL). The organic layer was collected and was dried over Na_2SO_4. The solvent was removed under reduced pressure. The crude was purified via silica chromatography (using EtOAc followed by a gradient of DCM to 2% MeOH in DCM as eluent) to yield product **2.22** as a white solid (76 mg, 95%). Characterization of **2.22**: ^{1}H NMR (CDCl₃, 500 MHz) δ

8.26 (d, 2H), 8.11 (d, 1H), 7.95 (d, 1H), 7.78 (d, 1H), 7.53 (t, 1H), 7.44 (t, 1H), 2.79 (s, 3H). ^{13}C NMR (CDCl$_3$, 500 MHz) 166.46, 154.23, 148.58, 136.33, 135.34, 128.55, 126.88, 125.97, 124.42, 123.75, 121.99, 44.19. ESI-MS (*m/z*) [M+H]$^+$ 274.15.

Synthesis of Compound 2.23
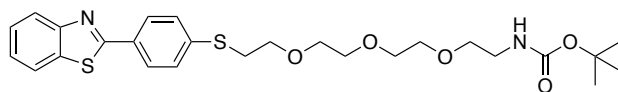
Compound **2.22** (20 mg, 0.073 mmol) was suspended in DCM (~2 mL). TFAA (~2 mL) was added. The mixture was refluxed for 1.5 hours. The solvents were removed under reduced pressure. The crude was carried over to the next step.

The crude was dissolved in a solution of 50% Et$_3$N in MeOH (~4 mL). The crude became red and was stirred for 10 minutes. Solvents were removed under reduced pressure.

The crude was then dissolved in dry THF (3 mL). K$_2$CO$_3$ (20 mg, 0.148 mmol) was added. Compound **2.8** (14.8 mg, 0.037 mmol) was dissolved in THF and was added to the mixture. The reaction was stirred proceed overnight. After, solvent was removed under reduced pressure, and the crude was dissolved in EtOAc. The organic layer was washed with 1 M NaOH (~10 mL), water (~10 mL), and brine (~10 mL). The organic layer was then dried over Na$_2$SO$_4$. The crude was purified via silica chromatography (using a gradient of 1:1 Hexanes/EtOAc) to yield product **2.23** as an off-white solid (16.3 mg, 85%). Characterization of **2.23**: ^{1}H NMR (CDCl$_3$, 500 MHz) δ 8.05 (d, 1H), 8.00 (d, 2H), 7.90 (d, 1H), 7.49 (t, 1H), 7.43-7.37 (m, 3H), 3.74 (t, 2H), 3.66-3.60 (m, 9H), 3.53 (t, 2H), 3.32 (q, 2H), 3.22 (t, 2H), 1.43 (s, 9H). ^{13}C NMR (CDCl$_3$, 500 MHz) δ 167.60, 156.21, 154.31, 140.71, 135.09, 131.09, 128.27,

128.07, 126.59, 125.39, 123.29, 121.83, 79.40, 76.66, 70.79, 70.72, 70.43, 69.93, 40.53, 32.30, 28.63. ESI-MS (*m/z*) [M+H]$^+$ 519.07, [M+Na]$^+$ 541.13.

Synthesis of Compound 2.2
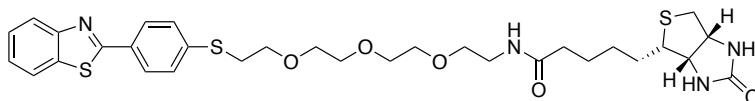
Compound **2.23** (16.3 mg, 0.0314 mmol) was dissolved in DCM (2 mL). The solution was cooled to 0°C. TFA (2 mL) was added dropwise. Solution became bright yellow upon addition of the TFA. The solution was warmed to room temperature, and the reaction was stirred for 1 hour. After, solvent was removed under reduced vacuum. The crude was carried over to the next step.

The crude was dissolved in DMF (2 mL). DIPEA (16 μL, 0.0442 mmol) was added, followed by compound **2.20** (12.8 mg, 0.0377 mmol). The mixture was stirred for 5 hours. After, the solvent was removed under reduced pressure. The crude was dissolved in DCM (6 mL) and was washed with 1 M NaOH (4 mL). The aqueous layer was extracted with DCM (6 mL). The combined organic layers were dried over Na$_2$SO$_4$. The crude was purified by silica chromatography (using 8% MeOH in DCM as eluent) to yield product **2.2** as a white, slightly tacky solid (15.8 mg, 78%). Characterization of **2.2**: ^{1}H NMR (CDCl$_3$, 500 MHz) δ 8.04 (d, 1H), 7.99 (d, 2H), 7.89 (d, 1H), 7.48 (t, 1H), 7.42-7.36 (m, 3H), 6.84 (s, 1H), 6.70 (s, 1H), 5.66 (s, 1H), 4.46 (t, 1H), 4.26 (t, 1H), 3.72 (t, 2H), 3.65-3.59 (m, 8H), 3.55 (t, 2H), 3.47-3.36 (m, 2H), 3.21 (t, 2H), 3.10-3.06 (m, 1H), 2.87-2.83 (dd, 1H), 2.71 (d, 1H), 2.19 (t, 2H), 1.75-1.59 (m, 4H), 1.42-1.37 (m, 2H). ^{13}C NMR (CDCl$_3$, 500 MHz) δ 173.56, 167.54, 164.28, 154.24, 140.68, 135.04, 131.05, 128.23, 128.06, 126.60, 125.41,

123.24, 121.84, 70.64, 70.59, 70.23, 70.15, 69.84, 61.87, 60.36, 55.81, 40.72, 39.31, 36.18, 32.37, 29.89, 28.39, 28.26, 25.82. ESI-MS (*m/z*) [M+H]$^+$ 645.38, [M+Na]$^+$ 667.40. HR-MS (m/z) calculated for [M+Na]$^+$ 667.2053; found [M+Na]$^+$ 667.2052.

Photodegradation Study

Compound **2.1** (0.6 mg) was dissolved in 1.5 mL deuterated methanol. The mixture was transferred to a quartz NMR tube. The tube was attached the surface of a handheld UV lamp (UVP-28 EL Series UV lamp, 8 W, λ=365 nm), and the lamp and mixture were placed at 4°C. The UV light was turned on. After one minute intervals, the light was turned off, and the mixture was analyzed by ^{19}F NMR on a 500 Hz Jeol ECA 500 spectrometer. This was done for a total of 4 minutes at which point the reaction appeared to be complete. The relative intensities of the peaks were measured to calculate the fraction of unreacted compound **2.1** remained in the mixture. The data was fit to the integrated first order rate law to determine the rate constant and half-life of the photolysis reaction. The crude reaction mixture was also submitted for ESI mass spectrometry analysis.

2.12 Acknowledgements

Chapter 3

Target Discovery Using a BTA-EG$_4$-Based

Photoaffinity Labeling Probe

3.1 Introduction

The first goal of this dissertation was to design and synthesize a photoreactive version of BTA-EG$_4$. Having accomplished this, I proceeded towards the second goal—labeling, isolating, and identifying potential targets of BTA-EG$_4$ using probe **2.1** (Figure 3.1).
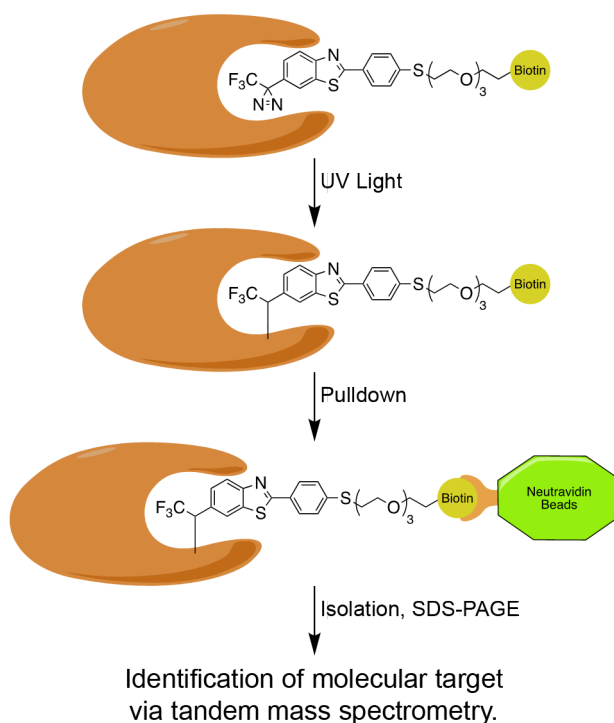
Figure 3.1. **Scheme for the Labeling, Isolation, and Identification of BTA-EG$_4$ Binding Partners.** After binding, irradiation causes probe **2.1** and its binding partner to be crosslinked. Once cross-linked, the protein can be immobilized onto Neutravidin beads. The protein can then be isolated, separated by SDS-PAGE, and submitted for tandem mass spectrometry analysis to identify the protein.

In this chapter, I will describe the development and optimization of a photoaffinity labeling protocol. Once established, I will then use this protocol to capture potential binding partners. Subsequently, these captured proteins will be identified via tandem mass spectrometry.

3.2   Photoaffinity Labeling in Cell Lysates

I first wanted to establish that probe **2.1** could label proteins in a cell lysate. I was fortunate enough to have access to human cortex, allowing me to perform my labeling studies in an extremely relevant tissue type. I decided to do the labeling in detergent-free conditions since I was concerned that detergent may interfere with the binding of the probe to its target. Because of this, I used a mechanical cell lysis method as opposed to a chemical one. To extract the proteins, I homogenized the tissue in a Dounce homogenizer, centrifuged the homogenate, and isolated the supernatant. Although I could perform my experiments without detergent, my extraction method limited me to probing soluble proteins.

To demonstrate that any labeling was caused by the photoactivation of probe **2.1**, I tested several reaction conditions (Figure 3.2A). Samples were treated with either probe **2.1** or compound **2.2**, and the mixtures were incubated in the dark. After equilibration, the samples were incubated in the presence or absence of UV light. Guided by my previous photodegredation study, I irradiated the samples for 20 minutes, a length of time that corresponds to greater than 16 half-lives.

After, I analyzed the samples to see if any labeling occurred. I performed a Western blot using a streptavidin-HRP conjugate to probe for the presence of biotin. It was important to differentiate proteins that were biotinylated *de novo* and proteins that were natively biotinylated. To distinguish between the two, I ran untreated samples along the treated samples as a control.

Two strong bands at 80 kDa and 170 kDa and one faint band at 237 kDa appear in all samples—including the untreated lysates (Figure 3.2A). This result suggests that these bands are endogenously biotinylated proteins. Carboxylases, a

class of enzymes that are involved in metabolic processes such as gluconeogenesis and fatty acid synthesis, are natively biotinylated.[78] Based on the apparent molecular weight, the band at 80 kDa may correspond to propionyl-CoA carboxylase[79] and the band at 237 kDa may correspond to acetyl-CoA carboxylase[80]. The band at 170 kDa does not appear to match the molecular weight of any carboxylases.

Perhaps more interesting are bands that only appear in the lane that corresponds to cell lysates that were treated with probe **2.1** and were irradiated with UV light. These bands correspond to proteins that are labeled by the probe. Surprisingly, the only prominent band is seen at 55 kDa. Overall, these results demonstrate that probe **2.1** binds to and crosslinks proteins in a light-dependent manner.
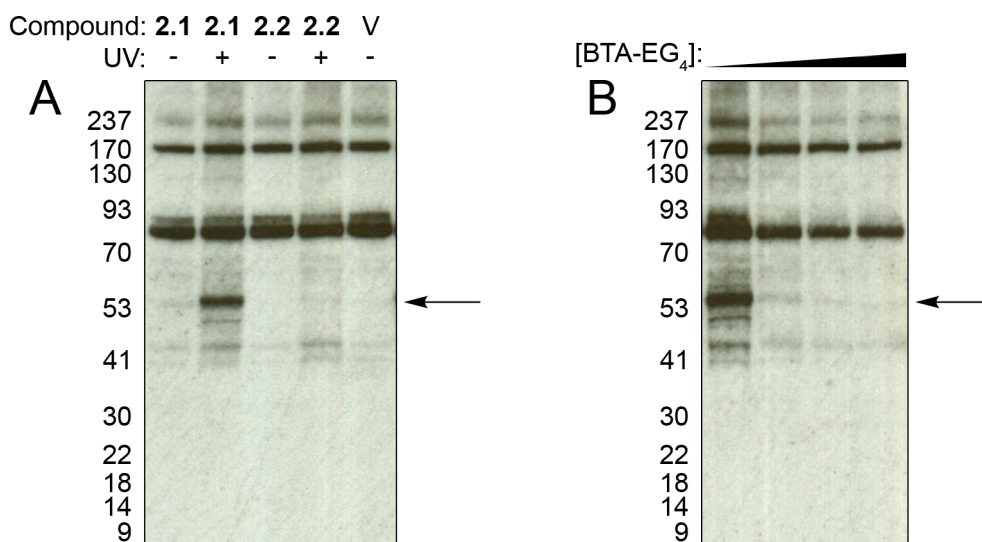
Figure 3.2. **Photoaffinity Labeling in Human Cortex Lysate.** (A) Western blot of photoaffinity labeling reactions. V corresponds to the untreated vehicle control. The arrow points to the band seen at 55 kDa. (B) Western blot of competition assay. **2.1** and increasing concentrations of BTA-EG$_4$ (0 – 500 µM with 1% DMSO) are used. The arrow points to the band previously seen at 55 kDa when the photoaffinity labeling experiment is carried out in the absence of BTA-EG$_4$.

Although probe **2.1** labels a 55-kDa protein, this does not necessary mean that BTA-EG$_4$ binds to it. To show that BTA-EG$_4$ specifically targets the 55-kDa protein, I performed a competition assay with the **2.1** and BTA-EG$_4$. I set up labeling reactions just as previously described, but I added increasing amounts of BTA-EG$_4$ to the mixtures. If BTA-EG$_4$ and **2.1** bind to the same site, excess BTA-EG$_4$ should displace **2.1** and inhibit labeling.

BTA-EG$_4$ does appear to inhibit labeling (Figure 3.2B). When BTA-EG$_4$ is added, the intensity of the band decreases dramatically. This result suggests that BTA-EG$_4$ is on-target to the 55-kDa protein.

3.3   Affinity Pull-downs of Labeled Targets

Next, I performed affinity pull-down experiments with a Neutravidin-agarose resin to isolate the labeled proteins—namely the 55-kDa protein. Ultimately, proteins that are captured on the beads will be separated by SDS-PAGE and will be visualized by silver staining. I needed to ensure that I had enough labeled protein to meet the detection limit of silver staining. Because of this, I used lysates from an immortalized cell line rather than human cortex. Using cultured cells provided me with a virtually unlimited source of protein. I chose SH-SY5Y cells since they are derived from human neuroblastoma and are often used as a model system for neurons.[81]

One complication that can arise in affinity pull-down purifications is that proteins can non-specifically bind to the resin. This can lead to high background and false positives. To control for this, I incubated untreated lysates with the Neutravidin

beads. This allowed me to distinguish between proteins that bind to the resin non-specifically and proteins that bind to the resin due to labeling by probe **2.1**.

      To further reduce background, I optimized the wash conditions. After incubating the beads with lysates, it was necessary to wash the beads to remove proteins that are bound to the resin non-specifically. If wash conditions are too gentle, significant background may persist. However, if wash conditions are too harsh, labeled proteins may be lost as well. I tested two wash buffers: TBS with 0.1% Tween 20 (TBST) and TBS with 2% SDS. The former uses the gentler Tween 20 as detergent while the latter uses the harsher SDS. Although binding between biotin and Neutravidin is extremely strong, I wanted to ensure that SDS at a relatively high concentration did not disturb the interaction.
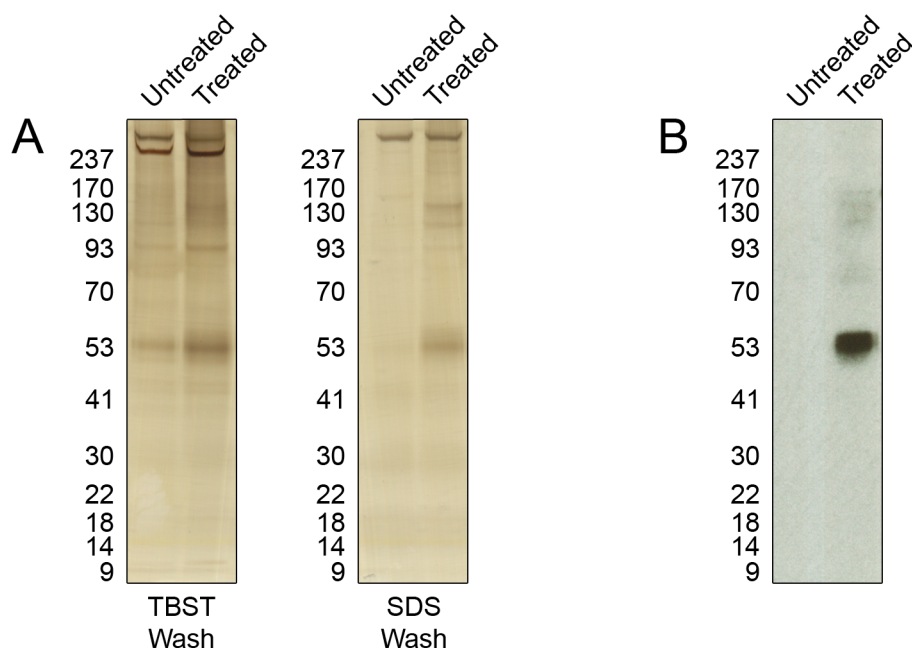
Figure 3.3. **Wash Optimization.** (A) Silver stains of proteins eluted from Neutravidin-agarose beads after washes with either TBST or SDS. Treated samples were incubated with compound **2.1** and were irradiated. Proteins were eluted by boiling beads in LDS sample buffer. (B) Western blot of proteins eluted from Neutravidin-agarose beads after SDS wash. Streptavidin-HRP was used to probe for biotinylation.

As expected, silver stains and the Western blots of proteins eluted from SDS-washed beads produced cleaner lanes than those of proteins eluted from TBST-washed beads (Figure 3.3A). Fortunately, 2% SDS did not appear to dissociate biotin from Neutravidin. This is evident since the 55-kDa band and some minor bands are absent in the untreated lane (vehicle and no irradiation) but are present in the treated lane (compound 2.1 and irradiation) even after harsh washing.

To further demonstrate that the immobilized proteins were labeled with **2.1** and that wash conditions did not dissociate biotin from the resin, I performed a Western blot on the proteins from the SDS-washed beads and probed the blot with Streptavidin-HRP (Figure 3.3B). The bands seen by Western blot reiterate the result from silver staining. Streptavidin-HRP detects labeled proteins, demonstrating that SDS did not interfere with biotin binding to Neutravidin. In addition, the major band at 55-kDa was seen, as well as some higher molecular weight minor bands.

3.4 Tandem Mass Spectrometry Analysis of Isolated Proteins

To determine the identity of the proteins I capture, I employed tandem mass spectrometry. As the name of the technique implies, tandem mass spectrometry involves two subsequent mass spectrometry steps (Figure 3.4). In short, proteins are digested with a protease—often trypsin—into much smaller peptides.[82] These smaller peptides are often separated by liquid chromatography prior to mass spectrometry.[82] In the first round of mass spectrometry, these peptides are ionized, and the mass-to-charge ratio (m/z) of these fragments are determined.[82] After this

step, the fragments are further broken into smaller pieces and are processed through a second round of mass spectrometry.[82] The mass spectrum of the peptide can then be compared to theoretical spectra from a sequence database to determine the sequence of the peptide.[82] Ultimately, the collection of peptide sequences can be compared to a database of protein sequences to deduce the identity of the protein of interest.
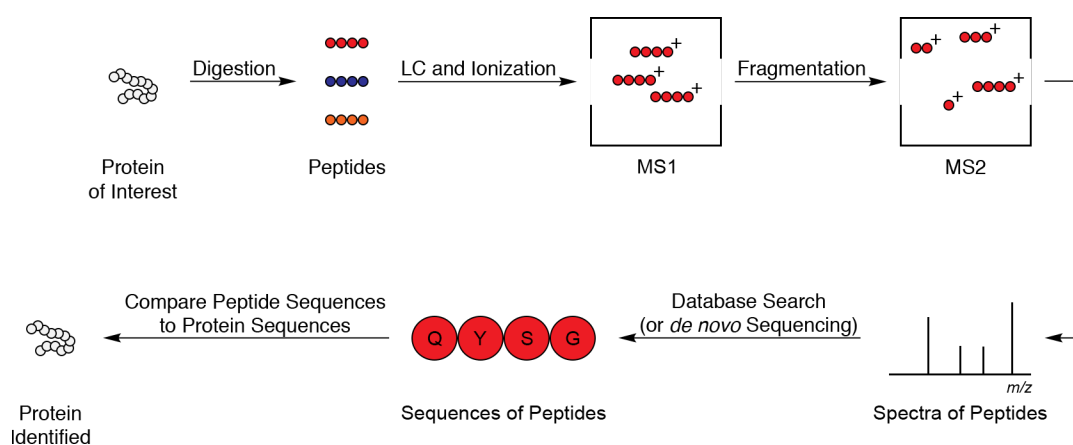
Figure 3.4. **Tandem Mass Spectrometry Protein Identification Scheme.** A protein of unknown identity is digested into small peptides. The peptides are separated by liquid chromatography, and each peptide is ionized and subjected to the first round of mass spectrometry. After, the peptide-ions are fragmented and subjected to the second round of mass spectrometry. The spectra generated can be used to obtain the sequence of the peptides. Finally, the collection of peptide sequence data can be compared to known protein sequences to identify the protein.

After optimizing my photoaffinity-labeling and protein capture protocol, I submitted samples for tandem mass spectrometry analysis. I performed SDS-PAGE to separate the proteins and silver stained the gels. By my eye, I saw three bands that appear only in the treated lane: the band at 55-kDa and two higher molecular weight bands (Figure 3.5). I excised these bands from the gel and submitted them for protein identification at the UCSD Biomolecular Mass Spectrometry Facility.

The list of hits was extremely long. Because of this, I needed to winnow out false positives from actual positives. I established three criteria that each protein on the list must follow in order not to be discarded.

First, I took advantage of the fact that I submitted multiple bands. I checked to see if any proteins were present on all three lists. If a protein appeared in all three lists, this would suggest that this protein is part of the background. These include proteins that are ubiquitous in the environment like keratin and albumin.[83]
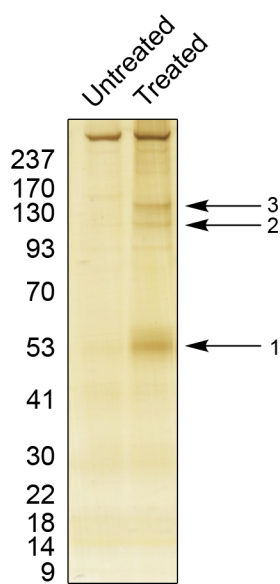
Figure 3.5. **Bands submitted for mass spectrometry.** Silver stain of proteins eluted from beads using optimized conditions. Bands in the treated lanes were compared to bands in the untreated lanes. Bands that only appear in the treated lanes were excised and submitted for tandem mass spectrometry analysis. Submitted bands are labeled "1", "2", and "3" respectively.

Next, I looked at the Unused ProtScore. The Unused score can be thought of a measure of the percent confidence that the protein was in the sample.[84] The peptides fragments that are detected and sequenced by mass spectrometry are compared to a database of protein sequences.[84] If the sequence of a fragment

matches the sequence of a protein, then that fragment is "assigned" to that protein.[84] Any fragment is used only once as evidence to support the presence of a protein.[84] The Unused score is determined by how many fragments are used as evidence to support a protein.[84] An Unused score of 1.3 corresponds to a percent confidence of 95%. If a protein had an Unused score less than 1.3, I considered it a false positive and discarded it.

Finally, I took into consideration the actual mass of remaining hits and the mass I would expect to see by SDS-PAGE. If these two values were inconsistent, I considered the hit a false positive.

Table 3.1. **Results from tandem mass spectrometry.** List of proteins found in the three bands submitted for tandem mass spectrometry analysis. This list does not include false positives. A protein was considered a false positive if it fit at least one of the following criteria: (1) It is present in multiple bands. (2) Its Unused score is less than 1.3. (3) Its actual mass and apparent mass according to SDS-PAGE are inconsistent.

Mass Spectrometry Results			
Band	Protein	Unused	Mass
1	fascin 1	41.47	54.4
	phosphoglycerate dehydrogenase	12	56.5
	vimentin	6	55.5
	enolase 1	4.84	47
	eukaryotic translation elongation factor 1 alpha 2	4	50.3
	eukaryotic translation elongation factor 1 alpha 1	0	50
2	CSE1 chromosome segregation 1-like protein	28.02	110.2
3	importin 7	12.76	119.3
	RAN binding protein 5	3.72	125.4
	RAN binding protein 6	0	124.6

Table 3.1 summarizes the proteins that were identified by mass spectrometry. Of all the hits, the one that caught my attention the most was fascin 1. Fascin 1 was found in band 1, and its Unused score was very high. Interestingly, fascin 1 is a protein that is involved in actin dynamics. Considering that

spinogenesis involves changes to the shape of a neuron and that these changes are associated with actin remodeling, fascin 1 appeared to be a promising lead for further investigation.

3.5 Verifying the Results from Tandem Mass Spectrometry

To confirm the result from tandem mass spectrometry, I performed a Western blot on the proteins isolated on the Neutravidin beads. I probed both the untreated samples and the treated samples with Streptavidin-HRP and a fascin 1 antibody. In addition, I did small-scale pulldowns with human cortex and mouse
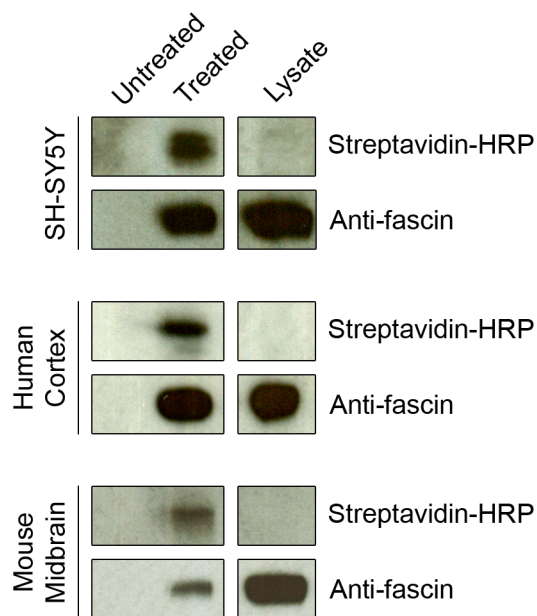
Figure 3.6. **Western Blot of Protein on Neutravidin Beads.** Proteins isolated on Neutravidin beads were probed for biotin and fascin 1 in SH-SY5Y, human cortex, and mouse midbrain. Fascin 1 is only pulled-down in the treated samples and is not isolated in the absence of probe **2.1** and UV light.

midbrain tissue to demonstrate that the results in SH-SY5Y cells translates to different tissue types.

Fascin 1 should only be immobilized onto the beads if it is labeled since probe **2.1** introduces a biotin group into the protein. When cell lysates are treated with probe **2.1** and UV light, fascin is pulled-down from the lysates. A band appears at 55 kDa that is positive for biotin and positive for fascin. If cell lysates are not treated with **2.1** and UV light, fascin is not pulled-down. No bands are seen at 55 kDa when probed with either anti-fascin or Streptavidin-HRP These results demonstrate that **2.1** does in fact label fascin and confirms that 55-kDa band is fascin 1.

3.6 Conclusions

In this chapter, I reported the development of a photoaffinity labeling protocol using probe **2.1**. Probe **2.1** labeled a 55-kDa protein. In the presence of BTA-EG$_4$, labeling was inhibited. This observation suggests that BTA-EG$_4$ is on-target to this protein.

This band, as well as two other minor bands, were submitted for protein identification. Tandem mass spectrometry revealed that several proteins were present in all three bands. However, the most prominent protein detected was fascin 1. Subsequent western blot analysis of the isolated proteins confirmed that fascin was present.

The remainder of this dissertation will focus on fascin 1. I will characterize the protein-ligand interaction between fascin 1 and BTA-EG$_4$. Furthermore, I will investigate the effects of BTA-EG$_4$ on fascin 1 activity.

3.7 Experimental Methods

Lysate Preparation

Lysates for photoaffinity-labeling were made from either SH-SY5Y cells, frozen human cortex, or frozen mouse midbrain. SY-SY5Y cells (ATCC) were cultured in a 1:1 mixture of MEM and Ham's F12 media supplemented with 10% FBS. Cells were grown at 37°C in a humidified atmosphere with 5% CO_2. Once the cells reached ~80% confluence, they were trypsinized and pelleted. Human brain tissue was a given generously by the Eliezer Masliah lab at UCSD Department of Pathology

Cells or tissue was incubated in a hypotonic lysis buffer (20 mM Tris, pH 7.4, cOmplete Protease Inhibitor Cocktail (Roche)) for 30 minutes on ice. After incubation, the cells or tissue was transferred to a Dounce homogenizer and was homogenized. The homogenate was centrifuged (15 minutes, 15,000 xg), and the pellet was discarded. The concentration of protein in the supernatant was determined by the BCA assay (ThermoFisher). The lysate was diluted with hypotonic lysis buffer to a final concentration of 1.25 mg/mL (for cells) or 1 mg/mL (for tissue).

Photoaffinity Labeling

Lysates were treated with compound (either probe or control compound) to a final concentration of 5 µM with 1% DMSO. The treated lysates were incubated at 4°C for 30 minutes in the dark. After incubation, the lysates were transferred to a 96-well plate (~170 µL sample/well). A handheld UV lamp (UVP-28 EL Series UV lamp,

8W, λ=365 nm) was placed on top of the plate, and the samples were irradiated for 20 minutes at 4°C.

General SDS-PAGE and Western Blotting Protocol

Samples were treated with 4X LDS sample buffer and were heated at 70°C for 10 minutes. Twenty-microliters of sample were loaded onto a NuPAGE Novex 4-12% Bis-tris gel (ThermoFisher). The gel was run at 200V in NuPAGE MOPS SDS running buffer (ThermoFisher) for approximately 45 minutes. If required, the proteins were transferred onto a 0.45 μm nitrocellulose blot (ThermoFisher). Transfer occurred at 10V in a tris-glycine buffer (25 mM Tris, 20 mM glycine) for 1 hour. The blot was blocked in blocking buffer (20 mM Tris, 125 mM NaCl, 0.1% Tween 20, 5% BSA) for 1 hour. Blots were incubated with either a primary antibody diluted in blocking buffer or Streptavidin-HRP diluted in PBS buffer (Corning) with 0.1% Tween 20 and 1% BSA. Blots were washed 5 times in wash buffer (TBS + 0.1% Tween 20). If necessary, blots were incubated with a secondary antibody diluted in blocking buffer and were washed just as previously mentioned. Blots were developed with Amersham ECL Western Blotting Detection Reagent (GE Healthcare Life Sciences).

Affinity pull-downs

Neutravidin-agarose beads (Pierce) were washed in lysis buffer. Samples were mixed with neutravidin-agarose slurry (9 parts sample to 1 part neutravidin-agarose slurry) and were shaken for 1 hour at room temperature. After agitation, the mixture was collected and spun down. The supernatant was removed and wash

buffer (20 mM Tris, pH 7.4, 2% SDS) was added. The beads were incubated in the wash buffer for 3 minutes with occasional vortexing. The slurry was centrifuged, and the supernatant was removed. The beads were washed twice more. After the washes, the bead slurry was treated with 2X LDS sample buffer (Novex) and was heated at 70°C for 10 minutes to elute bound proteins.

Sample Preparation for Tandem Mass Spectrometry Analysis

Proteins that were eluted from Neutravidin-agarose were separated by SDS-PAGE. The gels were stained with the SilverQuest Silver Staining Kit (ThermoFisher) according to the manufacturer's instructions. Bands that appear in the lane with treated sample but not in the lane with untreated sample were excised. The bands were treated the destainer provided in the SilverQuest kit. Samples were stored in MilliQ water and were submitted for mass spectrometry analysis.

3.8   Acknowledgements

PART 2

Validating Fascin 1 as a Target of BTA-EG$_4$

Chapter 4

Fascin 1: A Brief Survey

4.1 Fascin: Structure and Function

Fascin refers to a class of proteins that bind and bundle filamentous actin (Figure 4.1). Fascin was first discovered in the 1970s by Robert Kane when he was observed that sea urchin egg extracts would form a gel during a procedure to isolate filamentous actin (F-actin).[85] When the gel was analyzed, Kane observed that in addition to actin, the gel also contained an abundance of two other proteins, one of which had a mass of 58 kDa.[85] Subsequent experiments demonstrated that mixing the isolated components of the gel resulted in the formation of the gel.[86] The 58-kDa protein was eventually named "fascin" due to its ability group F-actin into fascicles.[87]
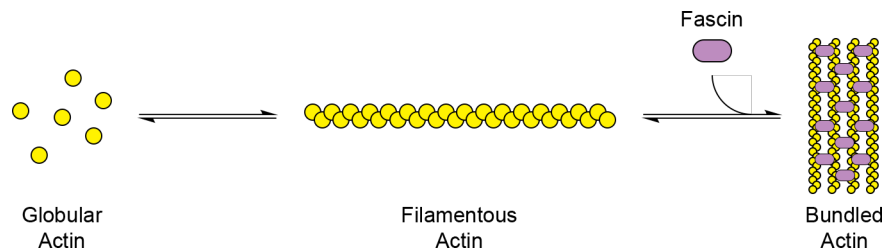
Figure 4.1. **Actin and fascin.** Actin exists as a globular monomer that can polymerize into filamentous actin. These actin filaments can be grouped into bundles by fascin.

After the discovery of fascin in sea urchin eggs, proteins exhibiting similar activity were also found. In 1985, Yamashiro-Matsumura and coworkers discovered that soluble cell extracts from HeLa cells could induce gelation of F-actin.[88] They were able to isolate a 55 kDa protein from the gel.[88] Later, Bryan and colleagues sequenced the cDNA sequence for echinoid fascin and expressed it.[89] Comparisons of the peptide sequence of this fascin to the sequence of the *singed* gene product from *Drosophila melanogaster* and the sequence of Yamashiro-Matsumura 55 kDa protein showed high levels of similarity.[89] From these findings, it was concluded that

these proteins should be grouped together as "fascin" proteins.[89] Homologs of fascin were found in other organisms such as mouse[90] and xenopus[91].

In mammals, there are three isoforms of fascin, each labeled 1, 2, and 3 respectively. Fascin 2 is expressed in the retina[92], and fascin 3 is expressed in the testes[93]. Fascin 1, however, can be found in many tissue types. For example, it can be found in low abundance in the spleen and small intestine and in high abundance in the brain.[90] Fascin 1 was the isoform found in my photoaffinity labeling experiments and will be the focus of the second part of this dissertation. From here on forward, fascin 1 will be referred to simply as "fascin".

Fascin's actin-bundling activity is critical for the development of filopodia. Filopodia are slender cell membrane projections that are important for a variety of cellular functions such as motility and adhesion.[94] Fascin-crosslinked actin bundles are highly abundant in filopodia and provide the necessary structural support to maintain their architecture.[94] RNAi experiments demonstrate that fascin is necessary for filopodia to form properly.[95] In studies performed in mouse melanoma B16F1 cells, knockdown of fascin resulted in the development of filopodia that lacked bundled actin as well as an overall decrease in the number of filopodia.[95]

Structurally, fascin is a globular, monomeric protein that binds actin at a 1:4 stoichiometry.[88] Over the past two decades, fascin crystal structures have been reported. The crystal structure of Sedeh and colleagues revealed that fascin folds into four β-trefoil domains that are grouped into two pairs.[96] These two pairs act semi-independently from each other and are related by pseudo 2-fold symmetry.[96] Through a combination of crystallographic data and mutagenesis experiments, Jansen and coworkers elucidated some mechanistic aspects of fascin's actin-
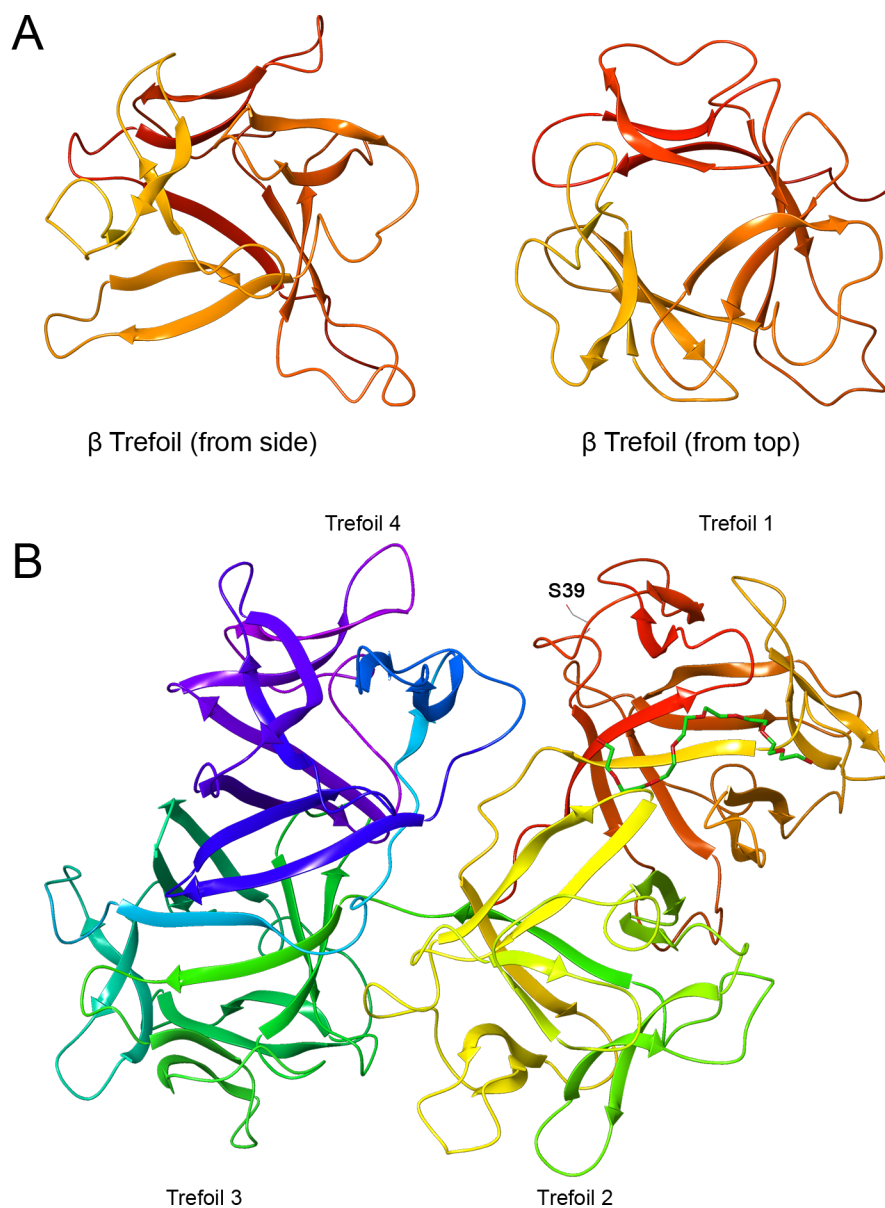
Figure 4.2. **Fascin Crystal Structure.** (A) Trefoil 1 as a representative example of a β-trefoil.[97,98] View from top shows that β-sheets creates a barrel-like structure. (B) Crystal structure of fascin (PDB ID: 3P53).[97,98] Fascin contains four trefoil domains. Trefoils 1 and 2 make up one domain and trefoils 3 and 4 make up the other domain. These two domains are related by pseudo 2-fold symmetry. Location of regulatory site Ser39 is shown explicitly.

bundling activity.[97] They employed amino acid conservation analysis to find parts of

the surface of fascin that do not change much throughout evolution.[97] From their

analysis, they observed that domains 1 and 3 contained highly conserved sites.[97]

They investigated further by generating fascin with mutations at these sites and determined how these mutations affected fascin's actin-bundling activity and the cell's ability to develop filopodia.[97] Their findings demonstrated that fascin has two actin-binding sites, a site in domain 1 and a site in domain 3.[97]

Fascin also contains a regulatory site. Upon phosphorylation at Ser39 by Protein Kinase C (PKC), fascin's ability to bind, and thus bundle, actin is greatly diminished.[99] Ser39 coincides with one of fascin's actin-bundling sites[97], and this observation suggests a mechanism for the inhibition of actin binding[99]. The binding site contains several lysine residues that are thought to be critical for actin binding.[97,99] When Ser39 is phosphorylated, interaction between the negatively charged phosphoryl group and the positively charged actin binding site may interfere with actin binding.[99]

4.2 Fascin Binding Partners Other Than Actin

In addition to phosphorylation by PKC, several proteins are known to bind directly with fascin and affect its activity or localization.

β-Catenin

β-Catenin is a multifaceted protein. It participates in Wnt signaling, a signaling pathway that is involved in regulating cellular proliferation and differentiation.[100] Activation of the Wnt signaling pathway by a Wnt ligand causes the buildup of β-catenin, and this eventually leads to the expression of downstream genes.[100] β-catenin is also part of the cadherin complex, an ensemble of proteins that facilitate cell-cell adhesion.[101] Cadherin are proteins that span the cell

membrane and can mediate adhesion by interacting other cadherin proteins on other cells[102]. β-catenin associates with the intracellular portion of cadherins and, in coordination with α-catenin, links cadherins to the actin network.[102] The extent that β-catenin's structural function and role in gene regulation are linked is still not clearly known.

β-Catenin has been found to bind with fascin. Tao and colleagues, through a yeast two-hybrid screen and immunoprecipitation, demonstrated that β-catenin associates with fascin.[103] It was also observed that β-catenin and fascin colocalize at the leading edge of cells.[103] The function of the fascin-β-catenin complex has not been well characterized.

LIM Kinase 1

LIM kinase (LIMK) 1 is a member of the LIM kinase family of protein that also includes one other member, LIMK2.[104] These kinases are a downstream target of the Rho signaling pathway.[104] The Rho signaling pathway can be conceptualized as a relay of messengers (Figure 4.3). The protein Rho receives signals from membrane proteins, and in turn, Rho activates its downstream effectors, which can send the signal to another downstream protein.[105] The message is relayed until it reaches its destination. With respect to LIMK1, the kinase ROCK, a Rho effector protein, activates LIMK1 by phosphorylating it at T505.[106] Active LIMK1 is known to affect actin dynamics and architecture within the cell. One of most well-known downstream target of LIMK1 is the actin-severing protein cofilin.[106] Upon phosphorylation by LIMK1, cofilin's ability to depolymerize actin is hindered.[106]
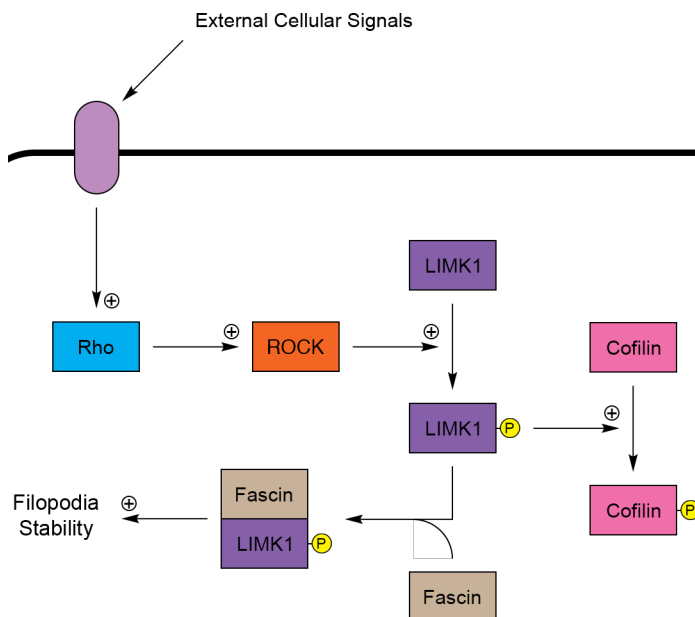
Figure 4.3. **Rho Signaling, LIMK1, and Fascin.** Rho signaling relays signals from outside the cell to the appropriate receiver inside the cell. Rho can activate the kinase ROCK, which in turn can activate LIMK1 by phosphorylating it. LIMK1 has several targets. It can inactivate cofilin's actin depolymerization activity by phosphorylating it. Binding with fascin causes increased filopodia stability.

Jayo and coworkers discovered that LIMK1 binds to fascin and affects the interaction between fascin and actin.[107] Upon inhibition of Rho signaling with the endotoxin C3, it was observed that the binding between fascin and actin is disturbed.[107] To discover which part of the Rho signaling pathway is involved, the authors performed FRET studies and affinity pull-downs to show that there is a direct interaction between LIMK1 (as well as LIMK2) and fascin.[107] Subsequent in vitro experiments revealed that the LIMK1-fascin interaction appears to promote filopodia stability.[107]

Rab35

Rab35 is a member of the Rab family of proteins, which itself is part of the Ras superfamily of proteins.[108] Biochemically, members of the Ras superfamily have

two common properties; they bind to GTP and can hydrolyze their bound GTP into GDP.[109] The phosphorylation state of the bound guanosine nucleotide regulates the activity of these proteins (Figure 4.4). When the protein is bound to GTP, it is in the active state. When the protein is bound to GDP, the protein is in the inactive state. GTPase activating proteins (GAPs) cause Ras proteins to hydrolyze its GTP into GDP; conversely, guanine exchange factors (GEFs), swap out the GDP with GTP.[109]
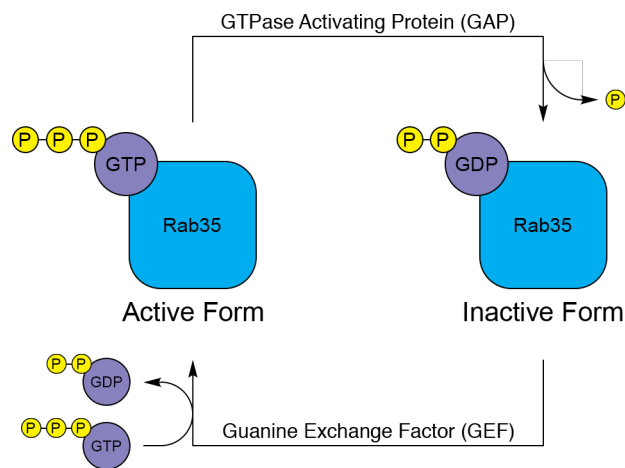
Figure 4.4. **Rab35 and its GTPase Activity.** When Rab35 is bound to GTP, it is active. Rab35 can hydrolyze its bound GTP into GDP upon GTPase activation by a GAP. When Rab35 is bound to GDP, it is inactive. It can become reactivated if a GEF exchanges the GDP with GTP.

Recent studies have demonstrated that Rab35 is involved with the regulation of cell shape in an actin dependent manner.[110,111] Chavellier and colleagues have shown that Rab35 associates with actin and that overexpression of Rab35 results in development of outgrowths on the surface of cells.[111] In one instance, they observed an increase in neurite outgrowth in N1E-115 neuroblastoma cells that expressed

constitutively active Rab35 mutant and a decrease in neurite outgrown when Rab35 was silenced.[111]

Furthermore, Zhang and coworkers demonstrated that fascin is an effector protein of Rab35 and that Rab35 affects the localization of fascin.[110] They showed that functional Rab35 is important for fascin localization to the cell membrane.[110] Specifically, it was observed that less fascin can be found at the membrane when cells express a dominant negative Rab35 mutant.[110] To further validate this point, it was demonstrated that directing Rab35 to other parts of the cell where it is not normally found, such as the mitochondria, also directs fascin and its associated actin to the same place.[110]

4.3 Fascin in Neurons

In neurons, fascin is found abundantly in the growth cone.[112] Growth cones are found at the tips of axons and are critical for the development of the nervous system since growth cones are able to sense and move towards certain chemotropic cues.[113] Fascin is involved with the development of filopodia that are needed for growth cone motility.

Surprisingly, fascin is not found in dendritic spines.[114] Considering that filopodia and dendritic spines are both cell protrusions, it may be tempting to assume they are similar and to conclude that fascin may be present in dendritic spines. However, the work of Korobova and coworkers demonstrate that these two structures have several distinguishing characteristics.[114] While filopodia contain tightly bound parallel bundles of actin filaments, dendritic spines contain shorter filaments that are branched.[114] Even though dendritic spines do contain some long

actin filaments, especially inside of the neck, these filaments are loosely bound.[114] These structural differences can be attributed to the different actin binding proteins found in these structures. Filopodia are fascin-positive while dendritic spines are fascin-negative.[114] The Arp2/3, a protein complex that is responsible for actin branching, is found in dendritic spines but is not found in filopodia. This observation may be important to understanding the mechanism of BTA-EG$_4$ induced spinogenesis.

4.4 Fascin and Disease

Metastasis and its associated complications are the most common cause of death from cancer.[115] Fascin appears to have a close association with metastatic cancers. In a meta-analysis of numerous histoimmunochemical studies, Tan and coworkers demonstrated that there is a connection between fascin and the metastasis of colorectal and gastric cancers.[116] Fascin serve as a biomarker for the early diagnosis of potentially aggressive cancers.

Fascin can also be linked to the mechanism behind cancer metastasis. A hallmark of metastatic cancer is the ability of cancer cells to move and to invade surrounding healthy tissue.[115] Cancer cells accomplish this by developing invadopodia. Invadopodia are protrusions that allow cancer break down the surrounding extracellular matrix that would normally block the cancer's migration.[117] As with filopodia, fascin is important for the structure and function of invadopodia.[118] Machesky and coworkers demonstrated that knockdown of fascin results in fewer, shorter, and less persistent invadopodia.[118] Fascin may be a potential therapeutic target that can be exploited to slow or halt the progression of metastatic cancer.

4.5 Fascin and Drug Discovery

Because of its relevance to metastatic cancer, fascin has been the focus of much drug discovery work. Migrastatin, a 14-membered macrolactone isolated from a stain of *Streptomyces*, has been shown to inhibit the migration of human esophageal cancer EC17 cells and mouse melanoma B16 cells.[119] In a later study by the Chen and colleagues, it was demonstrated that macroketone, a derivative of migrastatin, targets fascin and is able to inhibit its actin-bundling activity.[120]
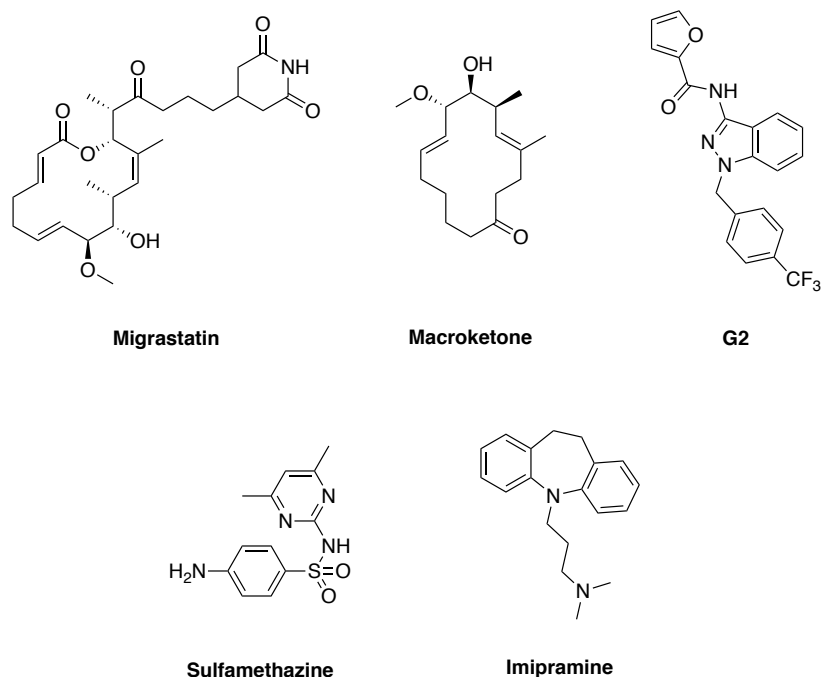
Figure 4.5. **Chemical structures of Migrastatin, Macroketone, G2, Sulfamethazine, and Imipramine.** Sulfamethazine and imipramine were part of the cell-based bioassay screen. Sulfamethazine was an example of a fascin-pathway enhancer, and imipramine was an example of a fascin-pathway blocker.

Compounds that target fascin have also been found in chemical libraries. As a follow-up to the previously mentioned work with migrastatin, macroketone, and

fascin, Huang and coworkers investigated a library of 165,000 compounds to find small molecule inhibitors of fascin's actin-bundling activity.[121] They developed a high-throughput imaging-based assay in which actin filaments and fascin were incubated with compounds and were subsequently stained and visualized.[121] Since, under the microscope, bundled actin look dramatically different than unbundled actin, the appearance of the actin filaments could be used to determine if a small molecule was an inhibitor of fascin's ability to bundle actin.[121] Overall, they discovered 15 compounds that were deemed to be fascin inhibitors of fascin's bundling-activity. Their work focused on one of these compound, G2.[121] It was demonstrated that G2 stops cancer migration. In addition, the authors generated fascin mutants and assayed the mutants' ability to bundle actin. These studies indicated that G2 may bind to an actin binding site on fascin.[121]

Kraft and colleagues developed a cell-based bioassay to screen for small molecules that target fascin-related biological pathways.[122] Specifically, they took advantage of the "filigree" phenotype seen in cultured Drosophila neurons with a mutated *singed* gene (Drosophila version of fascin).[122] The neurons with mutant *singed* develop curved offshoots that are very distinguishable from normal neurons.[122] What was notable about their screen was that it not only identified compounds that inhibited fascin-associated pathways, but also compound that enhanced them.[122] This was accomplished by using a mutant that expressed a phenotype that was midway between the wild-type and a *singed*-null and by determining if a particular compound rescued or exacerbated the filigree phenotype.[122] Also noteworthy was that the library of compounds included many drugs that are already FDA-approved.[122]

4.6   A Hypothesis for BTA-EG$_4$-Induced

Spinogenesis

Little has been reported about fascin's role in dendritic spines and spinogenesis since fascin in not found in dendritic spines.[114] This suggests fascin may not directly control the formation of dendritic spines. By extension, BTA-EG$_4$ also should not directly affect this process. Fascin, however, is found abundantly in filopodia.[114] With these conclusions in mind, I focused on the idea that dendritic spines are distinct from filopodia to develop a hypothesis for BTA-EG$_4$ induced spinogenesis.
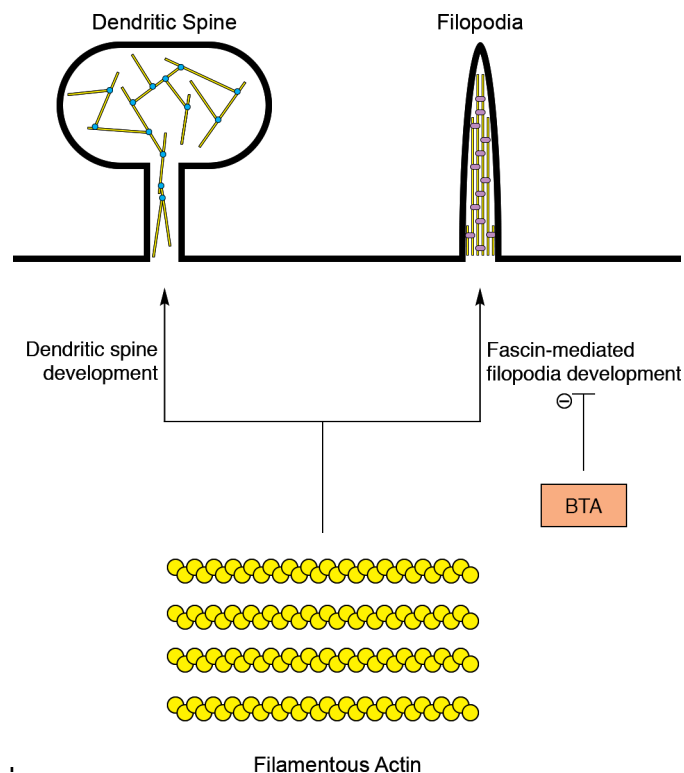
Figure 4.6. **A Model for BTA-EG$_4$-Induced Spinogenesis.** Actin can be used to build filopodia or dendritic spines. The actin-binding proteins found in either structure are different. BTA-EG$_4$ may inhibit fascin and cause actin to be directed towards dendritic spine formation.

I propose that actin can be destined to be part of a filopodium or a dendritic spine and that the relative abundance of these two structures are in some sort of equilibrium. BTA-EG$_4$, by modulating fascin activity, affects how a neuron's pool of actin is used up and changes the position of this equilibrium. In short, BTA-EG$_4$ acts like a shunt that moves actin away from filopodia development and thus indirectly funnels it towards dendritic spine formation. The simplest mechanism to account for this would be that BTA-EG$_4$ is an inhibitor of fascin's ability to bind or bundle to actin—in a similar vein to macroketone and G2.

This hypothesis guided the rest of my work. In the remainder of this dissertation, I will characterize the interaction between fascin and BTA-EG$_4$. Finally, I will report mechanistic work that provide further details about BTA-EG$_4$'s ability to affect fascin activity.

Chapter 5

Characterizing the Interaction Between

BTA-EG$_4$ and Fascin

5.1 Introduction

Photoaffinity labeling and tandem mass spectrometry revealed that fascin is a potential target of BTA-EG$_4$. The remainder of this thesis will be dedicated to validating and characterizing this protein-ligand interaction and gaining preliminary mechanistic insight into how BTA-EG$_4$ acts on fascin.

5.2 Expressing Recombinant Fascin

Performing biochemical assays to investigate the fascin-BTA-EG$_4$ interaction requires a steady source of purified fascin. Because of this, I constructed a plasmid for the inducible expression of fascin in bacteria.
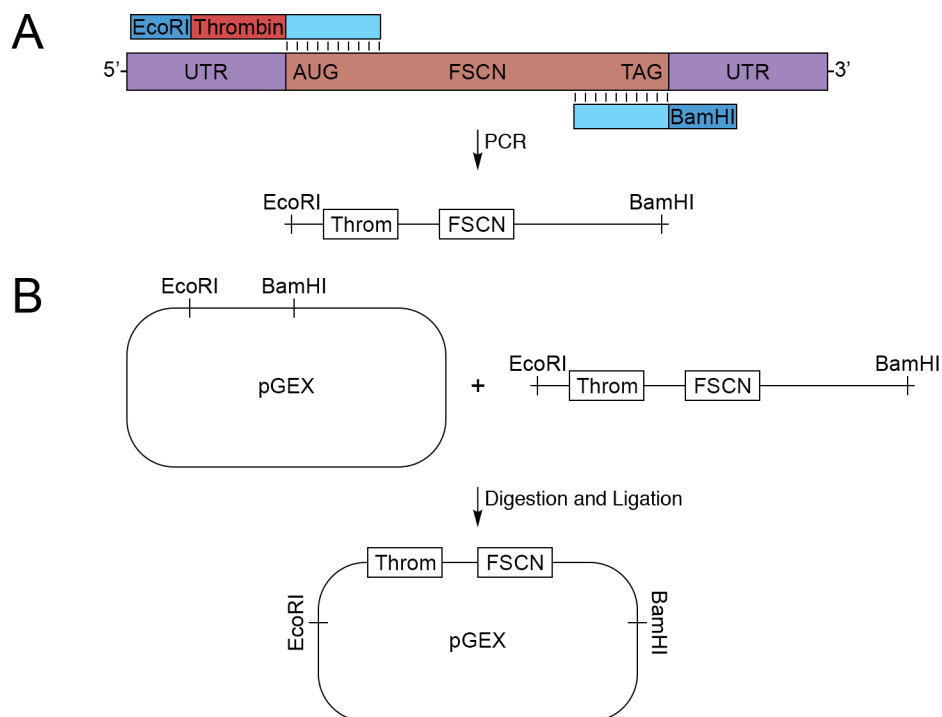
Figure 5.1. **Summary of Cloning Strategy.** (A) Amplification of fascin cDNA and incorporation of restriction site and cleavage sequence by overhang PCR. (B) Digestion and ligation of the amplicon into the pGEX vector.

My strategy was to create a GST-fascin fusion protein containing a thrombin cleavage site between GST and fascin. The GST serves two purposes. First, the GST group aids in the purification process since the fusion protein can be immobilized onto glutathione-agarose beads. After extensive washing, free fascin can be cleaved off the resin. Second, the GST group provides a convenient affinity tag for GST pull-down assays.
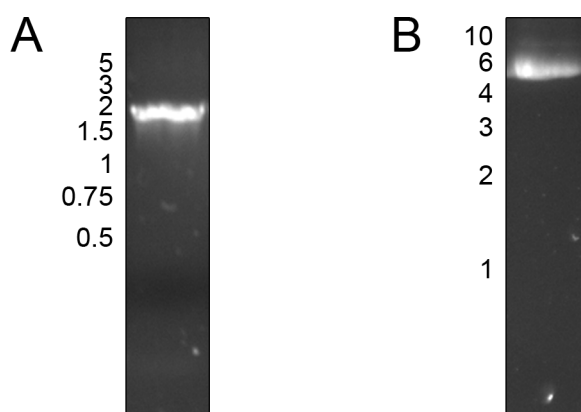
Figure 5.2. **PCR Product and Purified Plasmid.** (A) PCR product using primers with overhangs. The expected mass of the amplicon is approximately 1.8 kb. (B) Purified plasmid after digestion, ligation, and miniprep. The expected mass of the plasmid is 6.7 kb. The plasmid was sequenced to confirm the presence of the insert.

To create the plasmid, I needed an appropriate vector and fascin cDNA. Fortunately, both are commercially available. I used a pGEX plasmid as the vector, and I used a fascin-containing plasmid as the source of the fascin cDNA. Since I needed to incorporate the thrombin sequence and flank the fascin sequence with restriction sites, I turned to overhang PCR (Figure 5.1A). Overhang PCR is a technique that allows for the addition of nucleotides to the 5' and the 3' ends of an amplicon. Primers are made with an overhang segment and a segment that can hybridize with the target DNA. The final PCR product ultimately contains this

overhang sequence. I designed a forward primer with an EcoRI restriction site and the thrombin sequence and a reverse primer with a BamHI restriction site. PCR with these primers and the fascin cDNA-containing plasmid was successful (Figure 5.2A).

After purifying the PCR product, I inserted the amplicon into the pGEX-5X-2 plasmid. I digested and ligated my PCR product and the vector (Figure 5.1B). Then, I transformed the plasmid into TOP10 E. coli and selected for colonies on ampicillin plates. Subsequently, I cultured one of the colonies and purified the plasmid (Figure 5.2B). The plasmid was sequenced to confirm that it contained the insert.
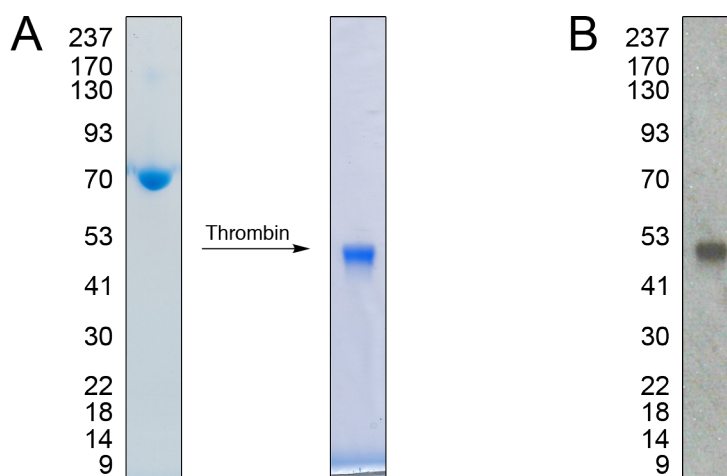
Figure 5.3. **SDS-PAGE of Purified Fascin.** (A) Coomassie stain of GST-fascin and free fascin after thrombin cleavage. (B) Western blot of fascin using an anti-fascin antibody.

Having confirmed that the plasmid contained the insert, I proceeded to express fascin. I transformed the plasmid into BL21(DE3) E. coli. Then, I cultured the bacteria and induced expression of fascin with IPTG. To purify the expressed protein, I lysed the cells and incubated the lysates with glutathione beads. After extensive washing, I treated the mixture with thrombin to release free fascin from the beads. Alternatively, I eluted the GST-fascin fusion protein by incubating the

beads in excess glutathione. SDS-PAGE revealed that the protein was pure, and the apparent molecular weight was consistent with the known molecular weight of fascin and GST-fascin (Figure 5.3A). In addition, I performed a Western blot with an anti-fascin antibody to confirm that the purified protein was fascin (Figure 5.3B).
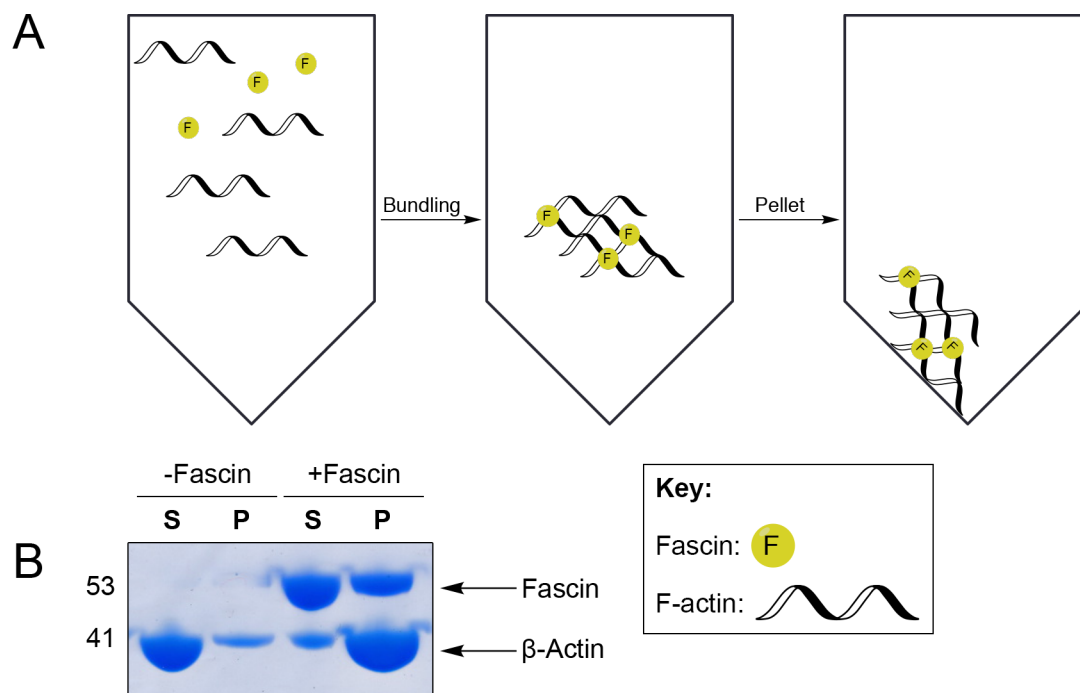
Figure 5.4. **The Slow-speed Actin Pelleting Assay.** (A) Diagraming showing how the actin polymerization works. Free fascin bundles free F-actin. If bundles are formed, the actin-fascin complex can be pelleted. (B) Coomassie stain of the supernatants (**S**) and pellets (**P**) of F-actin incubated with and without fascin.

To test if the recombinant fascin retains its actin-bundling activity, I turned to an actin-bundling assay (Figure 5.4A).[88,121] When fascin bundles actin, a gel-like material forms. Upon centrifugation, the gel-like material will pellet. Unbundled actin, however, remains in the supernatant.

F-actin was incubated in either the presence or absence of recombinant fascin. When fascin was not present, most of the actin remained in the supernatant

(Figure 5.4B). However, when actin and fascin were incubated together, most of the actin sedimented. This demonstrates that the recombinant fascin can bundle actin filaments.

5.3   Photoaffinity Labeling with Recombinant Fascin

With recombinant fascin in hand, I performed assays to probe the fascin-BTA-EG$_4$ interaction. First, I performed photoaffinity labeling experiments with probe **2.1** and recombinant fascin. The results were consistent with the results from photoaffinity labeling studies with cell lysates. When recombinant fascin was incubated with probe **2.1**, fascin was labeled and became streptavidin-HRP reactive (Figure 5.5A). However, when BTA-EG$_4$ was added to the reaction mixture with probe **2.1**, photo-induced labeling was inhibited in a concentration dependent manner.
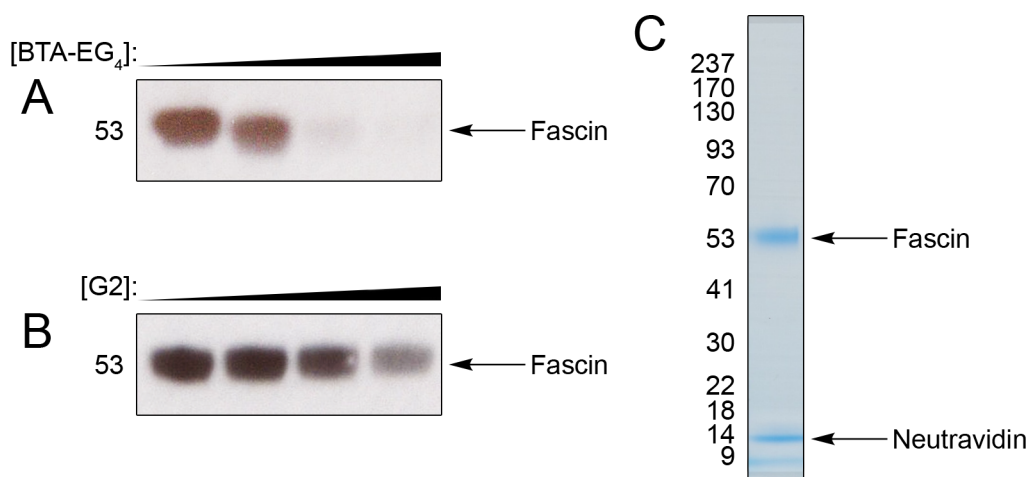
Figure 5.5. **Photoaffinity Labeling on Recombinant Fascin.** (A) Competition assay with probe **2.1** and BTA-EG$_4$. Labeling was inhibited with increasing concentrations of BTA-EG$_4$ (0 – 200 µM). (B) Competition assay with probe **2.1** and G2. G2 did not inhibit labeling as efficiently as BTA-EG$_4$. (C) Coomassie stain of labeled fascin. Labeled fascin was immobilized on Neutravidin beads and were analyzed by SDS-PAGE.

I also performed the competition assay with G2, the compound discovered by Huang and colleagues that inhibits fascin's actin-bundling activity.[121] Interestingly, BTA-EG$_4$ inhibited labeling by probe **2.1** more robustly than G2. While BTA-EG$_4$ completely inhibited labeling at concentrations below than 200 µM, labeling still occured at G2 concentrations greater than 200 µM (Figure 5.5B). These data suggest that although BTA-EG$_4$ and G2 target fascin, the two compounds may be mechanistically distinct. BTA-EG$_4$ and G2 may bind to different sites on fascin.

Finally, I performed a pull-down of labeled recombinant fascin. I performed the photoaffinity labeling experiments and incubated the reaction mixture with Neutravidin beads. After extensive washings, I analyzed the beads by SDS-PAGE and saw that fascin was captured (Figure 5.5C). In addition, I submitted the band for tandem mass spectrometry. Fascin was the primary protein detected.

5.4   Isothermal Titration Calorimetry

Photoaffinity labeling experiments provided qualitative evidence that BTA-EG$_4$ binds to fascin. I turned to isothermal titration calorimetry (ITC) to gauge this binding quantitatively.

BTA-EG$_4$ has poor solubility in water. Even when using 5% DMSO as cosolvent, BTA-EG$_4$'s solubility in water is in the submillimolar range. This limited solubility posed an issue for ITC experiments since high concentrations of ligand are usually required. Because of this, I used BTA-EG$_6$ for ITC instead. Surprisingly, the extra two ethylene glycol units dramatically increases the solubility of the compound. Previous work has demonstrated that BTA-EG$_6$ exhibits similar spinogenic properties as BTA-EG$_4$.[123]
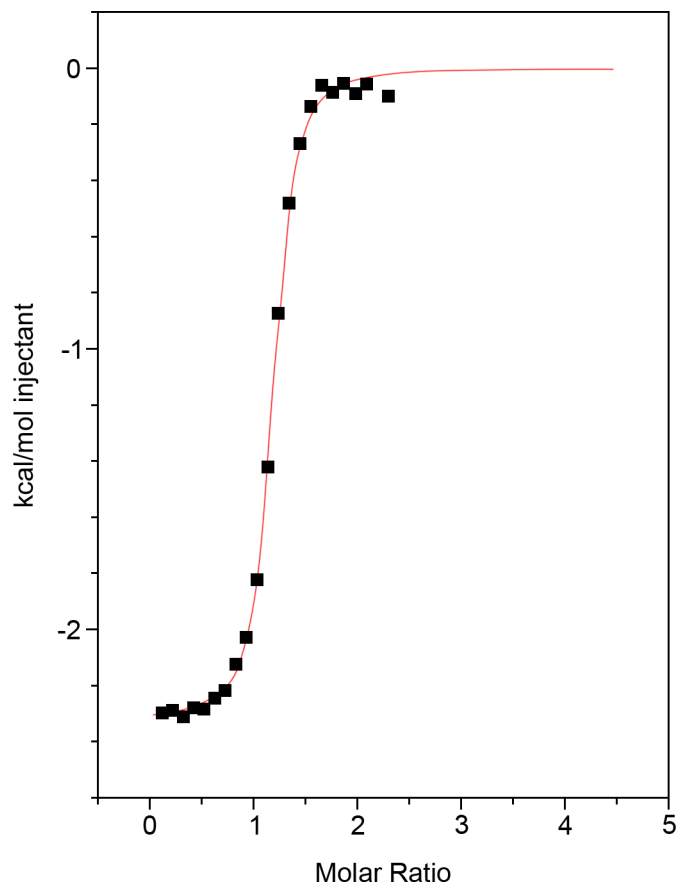
Figure 5.6. **Isothermal Titration Calorimetry.** Binding isotherm of a titration of 2 mM BTA-EG_6 into 100 µM fascin.

I prepared a 100 µM solution of fascin and a 2 mM solution of BTA-EG_6 and sent samples to Creative Biolabs for ITC analysis. ITC confirms the physical binding between fascin and BTA-EG_6. ITC revealed that BTA-EG_6 binds to fascin at a 1:1 ratio with a K_d of 0.97 ± 0.06 µM. The binding was found to be exothermic ($\Delta H = -2.3 \pm 0.012$ kcal/mol) and to involve an increase in entropy ($\Delta S = 19.7$ cal/(mol·K)).

5.5 BTA-EG_4 and Actin-Bundling

I first hypothesized that BTA-EG_4 may inhibit fascin's actin-bundling activity. To test this, I performed the slow-speed actin sedimentation assay in the presence

of BTA-EG$_4$. I also performed this assay with G2, the known inhibitor of fascin's

actin-bundling activity,[121] as a positive control.

	-Fascin +DMSO		+Fascin +DMSO		+Fascin +G2		+Fascin +BTA	
	P	S	P	S	P	S	P	S

A
41 ←— Actin

[BTA-EG$_4$] (µM): 0 5 10 25 50

	0		5		10		25		50	
	P	S	P	S	P	S	P	S	P	S

B
41 ←— Actin
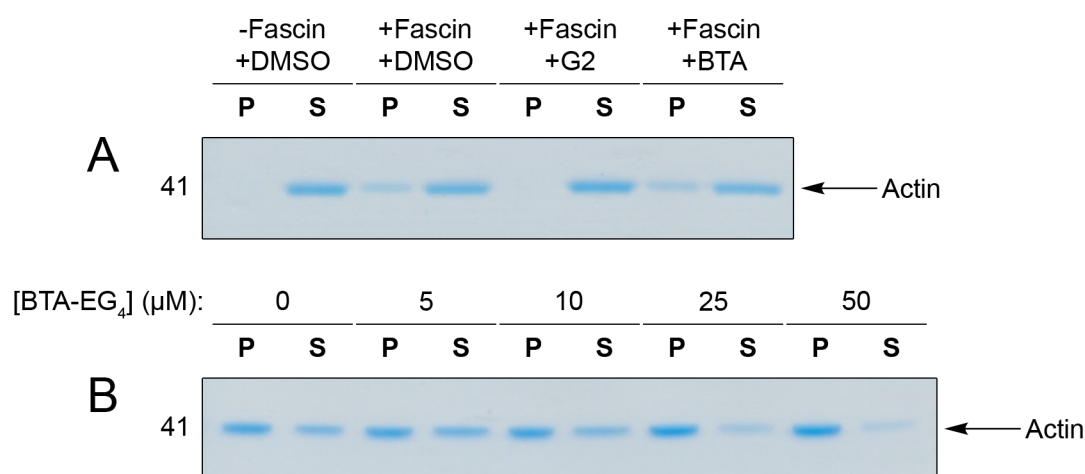
Figure 5.7. **Slow-speed Actin Sedimentation Assay with BTA-EG$_4$.** (A) Slow-speed actin sedimentation assay with 10 µM BTA-EG$_4$, 10 µM G2, or 1% DMSO vehicle. When fascin is omitted or when G2 is included, no actin is pelleted. BTA-EG$_4$ appears to have no effect on bundling since actin is still seen in the pellet. (B) Slow-speed actin sedimentation assay with increasing concentrations of BTA-EG$_4$. Even at high concentrations of BTA-EG$_4$, actin remains in the pellet.

These results demonstrate that BTA-EG$_4$ does not inhibit fascin's actin-

bundling activity (Fig. 5.7A). When fascin was treated with G2, bundling was clearly

inhibited. No actin was found in the pellet; this result looks comparable to actin that

was not incubated with fascin. However, when fascin was incubated with BTA-EG$_4$,

bundling appeared to be unaffected. Actin pelleted similar to the fascin samples that

were not treated with any compound. These data provide further evidence that BTA-

EG$_4$ and G2 are mechanistically distinct.

I considered the possibility that BTA-EG$_4$ does not inhibit fascin-promoted

bundling of actin at the concentration originally used. To test whether higher

concentrations of BTA-EG$_4$ could inhibit actin-bundling activity, I performed the

bundling assay with increasing concentrations of BTA-EG$_4$ (0 – 50 µM) to determine

if inhibition has a concentration dependence (Fig. 5.7B). Again, it does not appear

that BTA-EG$_4$ affects fascin's actin-bundling activity at concentrations up to 50 µM.

5.6   GST Pull-downs

The actin sedimentary assay demonstrated that BTA-EG$_4$ does not inhibit

fascin's bundling activity. Next, I wanted to explore if BTA-EG$_4$ affects the binding of

fascin to any of its other known protein binding partners. I decided to test if BTA-EG$_4$

affects fascin's binding to actin, β-catenin, LIMK1, or Rab35.
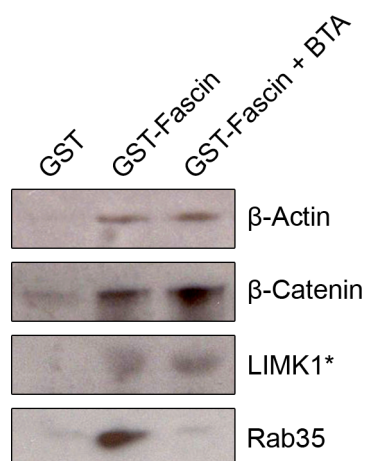
Figure 5.8. **GST Pull-downs.** Immobilized GST or GST-fascin was incubated with human cortex lysates. The GST-fascin pulldown was also performed in the presence of 100 µM BTA-EG$_4$. β-Actin and β-Catenin were captured in the presence of BTA-EG$_4$. However, Rab35 did not pull-down in the presence of BTA-EG$_4$. *Due to overlap of GST-fascin and LIMK1 bands, results regarding LIMK1 are inconclusive.

I immobilized GST-fascin onto magnetic glutathione beads and quantified

the protein content on the beads. I also did this with free GST to control for non-

specific binding to the resin and for binding to GST. Human brain lysates were

prepared and were incubated with the resin-bound fascin. After incubation, the beads were extensively washed and were heated under denaturing conditions. I then performed a Western blot to probe for each of the four proteins.

As expected, actin still was captured, even in the presence of BTA-EG$_4$ (Figure 5.8). This result is in accord with the results from the actin-bundling assay. The assay also demonstrated that BTA-EG$_4$ does not affect the binding between fascin and β-catenin. However, Rab35 was not pulled-down when lysates were treated with BTA-EG$_4$. This suggests that BTA-EG$_4$ inhibits fascin binding to Rab35.

The results from pull-down of LIMK1 were inconclusive. Because of the high concentration of GST-fascin used, the LIMK1 antibody bound non-specifically to the fusion protein. Unfortunately, GST-fascin and LIMK1 have similar molecular weights, and their corresponding bands overlap. Because of this, I was not able to draw any conclusions regarding the binding of LIMK1 and fascin in the presence of BTA-EG$_4$ from these data.

5.7   Conclusions

In this chapter, I characterized the binding interaction between BTA-EG$_4$ and fascin. I expressed recombinant fascin for subsequent experiments. First, I repeated photoaffinity labeling and competition experiments to confirm the results from the previous studies with cell lysates. These results provided further qualitative evidence that BTA-EG$_4$ binds to fascin. To characterize the binding quantitatively, I turned to isothermal titration calorimetry. ITC revealed that the BTA-EG$_4$ analog BTA-EG$_6$ binds to fascin with a 1:1 stoichiometry. In addition, this binding is in the micromolar range and is exothermic.

After, I sought to gain some mechanistic insight into this protein-ligand interaction. My initial hypothesis was that BTA-EG$_4$ may inhibit fascin's ability to bundle actin. This, however, was disproven since slow speed sedimentation assays demonstrated that BTA-EG$_4$ did not affect bundling. Next, I investigated other fascin binding partners by performing GST-pulldown assays. This assay revealed that BTA-EG$_4$ inhibits fascin binding to Rab35 but not β-actin or β-catenin. I was not able to arrive at a conclusion regarding LIMK1.
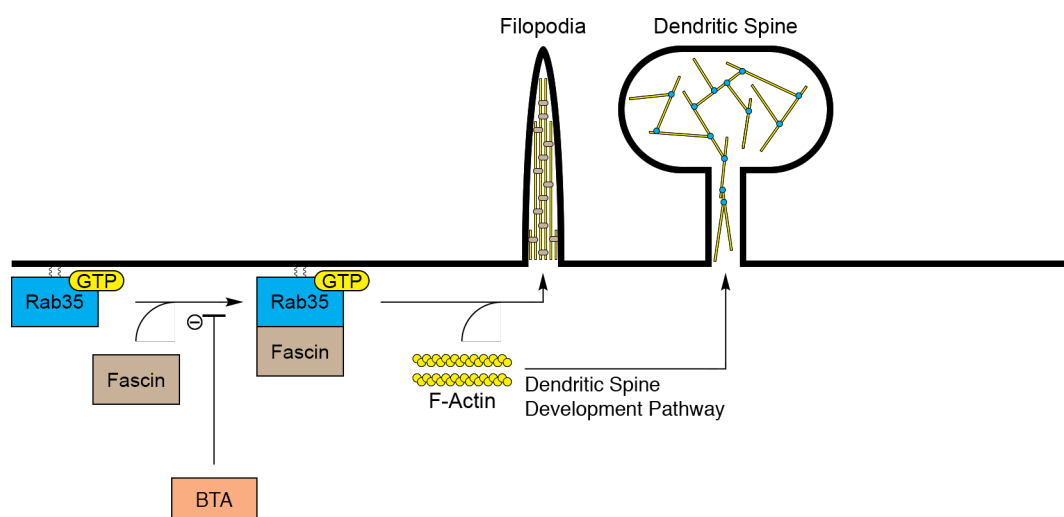
Figure 5.9. **A Revised Model for BTA-EG$_4$-Induced Spinogenesis.** BTA-EG$_4$ was shown to inhibit the binding of fascin to Rab35. Rab35 has been shown to recruit fascin to the cell membrane. Inhibition of this interaction may prevent fascin from being recruited to the membrane.[110] This may hinder filopodia development. Increased dendritic spine density may be a consequence of this.

Rab35 is thought to regulate actin dynamics by localizing fascin to the cell membrane.[110] This observation provides insight into how BTA-EG$_4$ may cause spinogenesis. BTA-EG$_4$ may prevent fascin from binding to membrane-anchored Rab35 (Figure 5.9). With less fascin at the membrane, less filopodia should develop.

This may allow for more actin to be dedicated to dendritic spine formation and thus result in increased spine density.

5.8   Future Directions

Although the mechanism of BTA-EG$_4$-promoted spinogenesis remains elusive, this work represents a good first step towards this goal. Photoaffinity labeling and subsequent biochemical assays reveal properties of BTA-EG$_4$ that were previously unknown. BTA-EG$_4$ binds to the actin-bundling protein fascin and inhibits fascin binding to the GTPase Rab35.

The studies presented in this dissertation were performed using either cell lysates or recombinant proteins. Future work should attempt to replicate these results in intact cells. BTA-EG$_4$'s inhibitory effect on the interaction between fascin and Rab35 can be studied via microscopy. FRET is a method often used to confirm interactions between molecules in the cell.[124] Fascin and Rab35 can be expressed with fluorescent tags. Binding of fascin and Rab35 should result in a FRET signal. If BTA-EG$_4$ abolishes this interaction, the FRET signal should disappear.

Determining if this fascin-related pathway is involved in spinogenesis will be a challenging feat. To investigate this, I propose that a series of fascin mutants be generated via alanine scanning. These mutants can then be assayed for activity. If a mutant that bundles actin but cannot bind Rab35 can be generated, it can be expressed in primary neurons to see what effect inhibiting the fascin-Rab35 interaction has on dendritic spine density. If the proposed hypothesis is correct, expression of this fascin mutant should phenocopy the effect of BTA-EG$_4$.

5.9 Experimental Methods

Cloning Procedure

Overhang PCR was used create a fascin amplicon containing an EcoRI restriction site and the thrombin cleavage sequence at the 5' end and a BamHI restriction site at the 3' end. Oligonucleotides were synthesized by Eton Bioscience, Inc (San Diego). The sequences of the primers are given below.

Forward Primer:

5'-CGCGAATTCTGGTTCCGCGTGGATCCACTGCCACCATGACCGCCA-3'

Reverse Primer:

5'- CGCGGATCCCTACTGCCACCATGACCGCCAA-3'

PCR was performed using Phusion Flash High Fidelity PCR Master Mix (ThermoFisher). The PCR product was run on an agarose gel in TAE buffer containing 1X SYBR Safe DNA Gel Stain (Invitrogen). The DNA was visualized under blue light, and the band containing the amplicon was excised from the gel. The DNA was purified using the Wizard SV Gel and PCR Clean-Up System (Promega), and the amount of purified DNA was quantified by gel.

PCR product and the pGEX-5X-2 vector (GE Life Sciences) were separately digested using BamHI and EcoRI in 1X CutSmart buffer (New England BioLabs) for 1.5 hours at 37°C. After, CIAP was added to both digestion reactions, and the mixture was incubated 37°C for 1 hour (New England BioLabs). The DNA was purified, and the amount of DNA purified was quantified by gel.

The digested vector and insert were mixed together in a 4:1 reaction by mass. DNA ligase (New England BioLabs) was added, and the ligation reaction was

incubated for 10 minutes at room temperature. Subsequently, the mixture was heated at 65°C for 10 minutes to inactivate the DNA ligase.

The mixture was then transformed into TOP10 competent cells (ThermoFisher) according to the manufacturer's instructions. After transformation, the TOP10 cells were plated on LB Amp-100 agar plates (Biomyx), and the plates were incubated at 37°C overnight. The next day, six colonies were chosen and were used to inoculate 12 mL LB Amp-100. The cultures were incubated overnight at 37°C with shaking. The next day, the TOP10 cells were pelleted, and the plasmid was purified using a QIAprep Spin Miniprep Kit (Qiagen). The amount of purified DNA was quantified by gel. The plasmid was submitted to Eton Biosciences for sequencing to confirm the presence and sequence of the insert.

Fascin Expression and Purification

The pGEX-fascin vector was transformed into competent BL-21(DE3) cells. The transformed bacteria were plated onto LB Amp-100 agar plates, and the plates were incubated overnight at 37°C. The next day, a freshly grown colony was used to inoculate ~50 mL 2XYT Amp-100 broth. The overnight culture was incubated overnight at 37°C with stirring.

The next day, 1 L 2XYT Amp-100 broth was inoculated with approximately 40 mL overnight culture. The culture was grown at 37°C until it reached an OD_{600} reading of ~0.8. Fascin expression was induced with 0.5 mM isopropyl β-D-thiogalactoside (Teknova). Induction occurred overnight at room temperature.

After induction, the bacteria were pelleted (15 minutes, 4000 xg). The pellet was treated with B-PER Bacterial Protein Extraction Reagent (ThermoFisher)

according to the manufacturer's instructions. PMSF (Sigma-Aldrich) was added to the extraction reagent to a final concentration of 0.2 mM. After, the lysate was centrifuged (15 minutes, 15,000 xg), and the pellet was discarded. The supernatant was incubated with 4 mL of settled Glutathione Sepharose 4B (GE Healthcare Life Sciences) at 4°C for 2 hours with mixing. The beads were washed with copious amounts of TBS (20 mM Tris, 150 mM NaCl, pH 8.0) and were resuspended in thrombin cleavage buffer (20 mM Tris, 150 mM NaCl, 2 mM $CaCl_2$, 1 mM DTT, pH 8.0). One hundred units of thrombin (GE Healthcare Life Sciences) were added to the mixture, and the mixture was incubated overnight with stirring at 4°C. The beads were removed, and PMSF was added to a final concentration of 0.2 mM. The purified fascin was concentrated using an Amicon 10 MWCO protein concentrator (Millipore). Purity of the recombinant fascin was determined by SDS-PAGE.

Photoaffinity Labeling on Recombinant Fascin

Recombinant fascin was dissolved in hypotonic lysis buffer (20 mM Tris, pH 7.4, cOmplete Protease Inhibitor Cocktail (Roche)) to a final concentration of 5 µM. BTA-EG_4 was added to the protein at varying concentration (0 – 200 µM). Probe **2.1** was then added to a final concentration of 5 µM. The concentration of DMSO used as cosolvent did not exceed 1%. The mixtures were incubated at 4°C for 30 minutes in the dark. After incubation, the mixtures were transferred to a 96-well plate (~170 µL sample/well). A handheld UV lamp (UVP-28 EL Series UV lamp, 8W, λ=365 nm) was placed on top of the plate, and the samples were irradiated for 20 minutes at 4°C. Samples were analyzed by SDS-PAGE and Western blot.

Actin Polymerization Assay

This actin polymerization assay was adapted from the work of Huang and coworkers.[121] Monomeric rabbit G-actin (Cytoskeleton, Inc) was dissolved in polymerization buffer (2 mM Tris, 1 mM ATP, 1 mM DTT, 2 mM $MgCl_2$, 100 mM KCl, pH 8.0) to a final concentration of 2 µM. To polymerize G-actin into F-actin, the mixture was incubated for 1 hour at room temperature. Fascin was dissolved in polymerization buffer to a final concentration of 0.5 µM. BTA-EG_4 or G2 (Xcessbio Biosciences) were dissolved in polymerization buffer to a final concentration of 10 µM (with 1% DMSO). For the dose dependence experiments, BTA-EG_4 was added at various concentrations (0 – 100 µM with 1% DMSO). Equal volumes of the F-actin solution and the fascin solution were gently mixed together and were incubated at room temperature for 1 hour. Then, the samples were centrifuged at 12000 xg for 45 minutes. After, the supernatant was removed, and the pellet was dissolved in a volume of buffer equal to the volume of the supernatant. 4X LDS sample buffer (Novex) was added, and the samples were heated at 70°C for 10 minutes. Actin and fascin were separated by SDS-PAGE, and the gel was stained with SimplyBlue SafeStain (ThermoFisher).

Isothermal Titration Calorimetry

Recombinant fascin was dissolved in TBS buffer (20 mM Tris, 100 mM NaCl, pH 8.0) and was filtered through a .45 µm syringe filter. The concentration of protein was determined by the BCA assay and the protein solution was diluted to 100 µM. BTA-EG_6 was dissolved in the same TBS buffer to a final concentration of 2 mM. The samples were sent to Creative Biolabs (Shirley, NY) for ITC analysis.

GST Pull-down Assays

Recombinant GST-fascin or GST were immobilized on magnetic glutathione-agarose beads (Pierce). Human cortex lysate was prepared as previously mentioned, and the concentration of protein was determined with the BCA Assay. Each sample contained 1 mg total protein and 20 µg GST-fascin (or the equimolar equivalent of GST). Samples containing GST-fascin were treated with either BTA-EG$_4$ to a final concentration of 100 µM (with 1% DMSO) or DMSO. Samples containing GST were treated with DMSO. The samples were shaken at 4ºC for 2 hours.

After incubation, the beads were suspended in 1 mL cold wash buffer (PBS, 0.1% Triton X-100). The beads were inverted several times, and the buffer was removed. This was repeated twice more. After washing, the beads were suspended in 60 µL 1X LDS sample buffer, and were heated at 70ºC for 10 minutes. The beads were removed, and the samples were immunoblotted using anti-β-actin, anti-β-catenin, anti-LIMK1, and anti-Rab35 antibodies.

5.10 Acknowledgements

Appendix

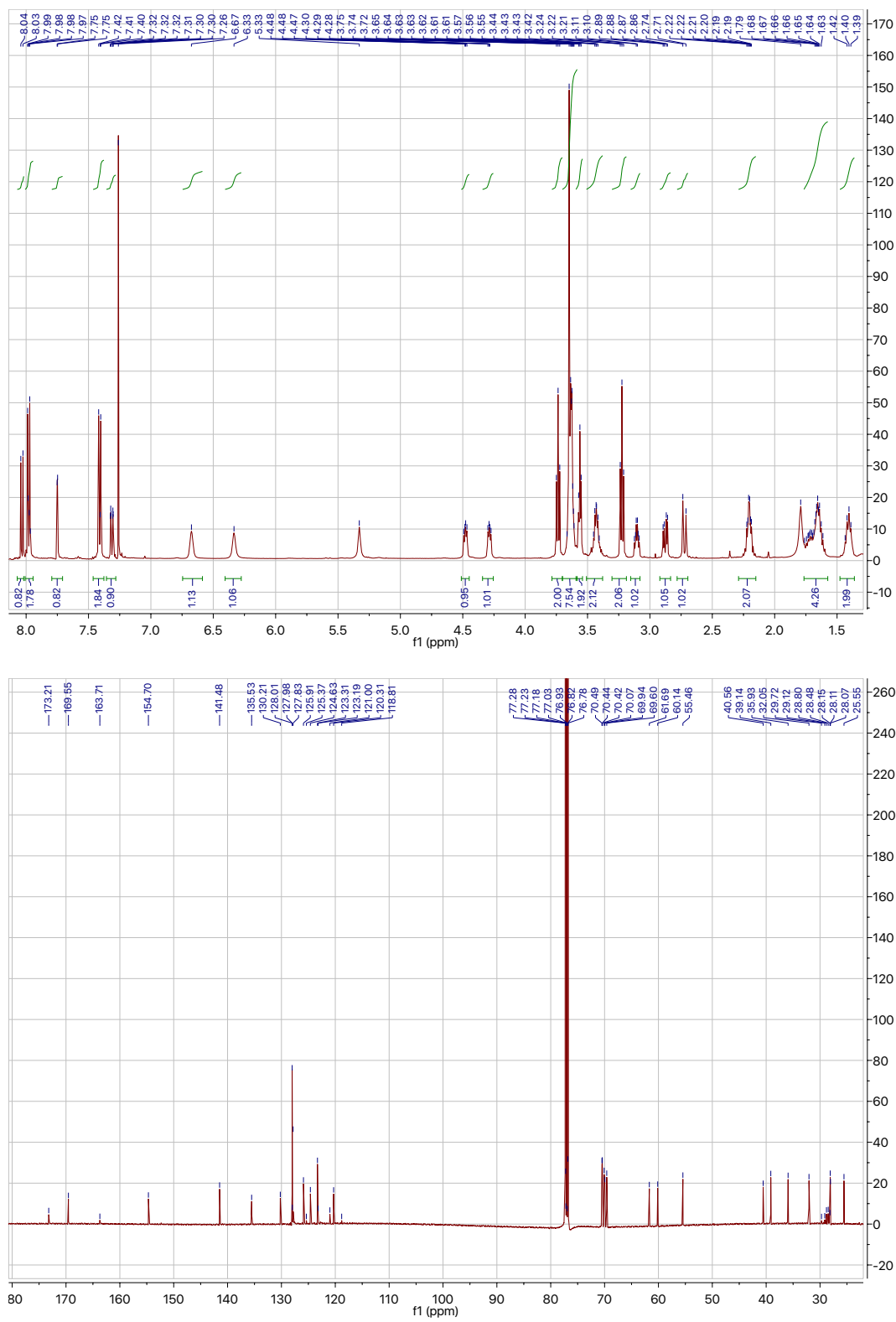Figure A.1. **^{1}H and ^{13}C Spectra of Compound 2.1.**

Figure A.2. **¹H and ¹³C Spectra of Compound 2.2.**

REFERENCES

(1)   Alzheimer's Association. *2016 Alzheimer's Disease Facts and Figures*; 2016; Vol. 12.

(2)   Brunnström, H. R.; Englund, E. M. *Eur. J. Neurol.* **2009**, *16* (4), 488–492.

(3)   Thies, W.; Bleiler, L. *Alzheimer's Dement.* **2013**, *9* (2), 208–245.

(4)   National Institute on Aging. *Preventing Alzheimer's Disease What Do We Know?*; 2012; pp 1–23.

(5)   Huang, Y.; Mucke, L. *Cell* **2012**, *148* (6), 1204–1222.

(6)   Hasselmo, M. E. *Curr. Opin. Neurobiol.* **2006**, *16* (6), 710–715.

(7)   Francis, P. T.; Palmer, A. M.; Snape, M.; Wilcock, G. K. *J Neurol Neurosurg Psychiatry* **1999**, *66*, 137–147.

(8)   Colovic, M. B.; Krstic, D. Z.; Lazarevic-Pasti, T. D.; Bondzic, A. M.; Vasic, V. M. *Curr. Neuropharmacol.* **2013**, *11* (3), 315–335.

(9)   Scott, L. J.; Goa, K. L.; Giacobini, E.; Medical, G.; Mcdowell, F. H.; Masterton, W.; Rehabilitation, B.; Plains, W.; York, N.; Maelicke, A.; Nordberg, A. *Adis Drug Eval.* **2000**, *60* (5), 1095–1122.

(10)   Figiel, G.; Sadowsky, C. *Curr. Med. Res. Opin.* **2008**, *24* (1), 157–166.

(11)   Seltzer, B. *Expert Opin. Drug Metab. Toxicol.* **2005**, *1* (3), 527–536.

(12)   Alberts, B.; Johnson, A.; Lewis, J.; Raff, M.; Roberts, K.; Walter, P. *Molecular Biology of the Cell*; 2008.

(13)   Mark, L. P.; Prost, R. W.; Ulmer, J. L.; Smith, M. M.; Daniels, D. L.; Strottmann, J. M.; Brown, W. D.; Hacein-Bey, L. *Am. J. Neuroradiol.* **2001**, *22* (10), 1813–1824.

(14)   Walton, H. S.; Dodd, P. R. *Neurochem. Int.* **2007**, *50* (7–8), 1052–1066.

(15)   Danysz, W.; Parsons, C. G. *Br. J. Pharmacol.* **2012**, *167* (2), 324–352.

(16)   Danysz, W.; Parsons, C. G. *Int. J. Geriatr. Psychiatry* **2003**, *18* (SUPPL. 1).

(17)   Casey, D. a; Antimisiaris, D.; O'Brien, J. *P T* **2010**, *35* (4), 208–211.

(18)   Qaseem, A.; Snow, V.; Cross Jr, J. T.; Forciea, M. A.; Hopkins Jr, R. *Ann. Intern. Med.* **2008**, No. 148, 370–378.

(19)   Small, D. H.; Cappai, R. *J. Neurochem.* **2006**, *99* (3), 708–710.

(20)   Perl, D. P. *Mt Sinai J Med* **2010**, *77* (1), 32–42.

(21)   O'Brien, R. J.; Wong, P. C. *Annu Rev Neurosci* **2011**, *34*, 185–204.

(22)   Murphy, M. P.; Levine III, H. *J. Alzheimers. Dis.* **2010**, *19*, 311–323.

(23)   Stine, W. B.; Jungbauer, L.; Yu, C.; LaDu, M. J. In *Alzheimer's Disease and Frontotemporal Dementia: Methods and Protocols*; Roberson, E. D., Ed.; Humana Press: Totowa, NJ, 2011; pp 13–32.

(24)   Citron, M.; Oltersdorf, T.; Haass, C.; McConlogue, L.; Hung, A. Y.; Seubert, P.; Vigo-Pelfrey, C.; Lieberburg, I.; Selkoe, D. J. *Lett. to Nat.* **1992**, *360* (6405), 672–674.

(25)   Baranello, R. J.; Bharani, K. L.; Padmaraju, V.; Chopra, N.; Lahiri, D. K.; Greig, N. H.; Pappolla, M. A.; Sambamurti, K. *Curr. Alzheimer Res.* **2015**, *12* (1), 32–46.

(26)   Carson, J. A.; Turner, A. J. *J. Neurochem.* **2002**, *81* (1), 1–8.

(27)   Hamazaki, H. *FEBS Lett.* **1996**, *396* (2–3), 139–142.

(28)   Deane, R.; Bell, R. D.; Sagare, A.; Zlokovic, B. V. *CNS Neurol. Disord. Drug Targets* **2009**, *8* (1), 16–30.

(29)   Kanekiyo, T.; Xu, H.; Bu, G. *Neuron* **2014**, *81* (4), 740–754.

(30)   Kim, J.; Basak, J. M.; Holtzman, D. M. *Neuron* **2009**, *63* (3), 287–303.

(31)   Deane, R.; Sagare, A.; Hamm, K.; Parisi, M.; Lane, S.; Finn, M. B.; Holtzman, D. M.; Zlokovic, B. V. *J. Clin. Invest.* **2008**, *118* (12), 4002–4013.

(32)   Verghese, P. B.; Castellano, J. M.; Garai, K.; Wang, Y.; Jiang, H.; Shah, A.; Bu, G.; Frieden, C.; Holtzman, D. M. *Proc. Natl. Acad. Sci. U. S. A.* **2013**, *110* (19), E1807-16.

(33)   Lorenzo, A.; Yankner, B. A. *Proc. Natl. Acad. Sci.* **1994**, *91* (25), 12243–12247.

(34)   Perry, G.; Cash, A. D.; Smith, M. a. *J. Biomed. Biotechnol.* **2002**, *2* (3), 120–123.

(35)   Ansari, M. A.; Scheff, S. W. *J. Neuropathol. Exp. Neurol.* **2010**, *69* (2), 155–167.

(36) Smith, D. G.; Cappai, R.; Barnham, K. J. *Biochim. Biophys. Acta - Biomembr.* **2007**, *1768* (8), 1976–1990.

(37) Butterfield, D. A.; Swomley, A. M.; Sultana, R. *Antioxid. Redox Signal.* **2013**, *19* (8), 823–835.

(38) Biancalana, M.; Koide, S. *Biochim. Biophys. Acta - Proteins Proteomics* **2010**, *1804* (7), 1405–1412.

(39) Inbar, P.; Yang, J. *Bioorg. Med. Chem. Lett.* **2006**, *16* (4), 1076–1079.

(40) Inbar, P.; Li, C. Q.; Takayama, S. A.; Bautista, M. R.; Yang, J. *ChemBioChem* **2006**, *7* (10), 1563–1566.

(41) Klunk, W. E.; Wang, Y.; Huang, G.; Debnath, M. L.; Holt, D. P.; Mathis, C. A. *Life Sci.* **2001**, *69*, 1471–1484.

(42) Habib, L. K.; Lee, M. T. C.; Yang, J. *J. Biol. Chem.* **2010**, *285* (50), 38933–38943.

(43) Song, J. M.; DiBattista, A. M.; Sung, Y. M.; Ahn, J. M.; Turner, R. S.; Yang, J.; Pak, D. T. S.; Lee, H. K.; Hoe, H. S. *Exp. Neurol.* **2014**, *252*, 105–113.

(44) Megill, A.; Lee, T.; DiBattista, A. M.; Song, J. M.; Spitzer, M. H.; Rubinshtein, M.; Habib, L. K.; Capule, C. C.; Mayer, M.; Turner, R. S.; Kirkwood, A.; Yang, J.; Pak, D. T.; Lee, H. K.; Hoe, H. S. *J Neurosci* **2013**, *33* (22), 9306–9318.

(45) Rochefort, N. L.; Konnerth, A. *EMBO Rep.* **2012**, *13* (8), 699–708.

(46) Heike, H.; Morgan, S. *Nat. Rev. Neurosci.* **2001**, *2* (December), 880–888.

(47) Segal, M. *Nat Rev Neurosci* **2005**, *6* (4), 277–284.

(48) Hotulainen, P.; Hoogenraad, C. C. *J. Cell Biol.* **2010**, *189* (4), 619–629.

(49) Collin, C.; Miyaguchi, K.; Segal, M. *J. Neurophysiol.* **1997**, *77* (3), 1614–1623.

(50) Engert, F.; Bonhoeffer, T. *Nature* **1999**, *399* (May), 66–70.

(51) Xu, T.; Yu, X.; Perlik, A. J.; Tobin, W. F.; Zweig, J. A.; Tennant, K.; Jones, T.; Zuo, Y. *Nature* **2009**, *462* (7275), 915–919.

(52) Airey, D. C.; Kroodsma, D. E.; DeVoogd, T. J. *Neurobiol. Learn. Mem.* **2000**, *73* (3), 274–281.

(53) Leuner Benedetta; Falduto Jacqueline; Shors Tracey J. *J. Neurosci.* **2003**, *23* (2), 659–665.

(54)   Knobloch, M.; Mansuy, I. M. *Mol. Neurobiol.* **2008**, *37* (1), 73–82.

(55)   Penzes, P.; Cahill, M. E.; Jones, K. a; VanLeeuwen, J.-E.; Woolfrey, K. M. *Nat. Neurosci.* **2011**, *14* (3), 285–293.

(56)   Lomenick, B.; Olsen, R. W.; Huang, J. *ACS Chem. Biol.* **2011**, *6* (1), 34–46.

(57)   Dunham, W. H.; Mullin, M.; Gingras, A. C. *Proteomics* **2012**, *12* (10), 1576–1590.

(58)   Crews, C. M.; Collins, J. L.; Lane, W. S.; Snapper, M. L.; Schreiber, S. L. *J. Biol. Chem.* **1994**, *269* (22), 15411–15414.

(59)   Smith, E.; Collins, I. *Future Med. Chem.* **2015**, *7* (2), 159–183.

(60)   Robinette, D.; Neamati, N.; Tomer, K. B.; Borchers, C. H. *Expert Rev. Proteomics* **2006**, *3* (4), 399–408.

(61)   Zhou, B.; Yu, X.; Zhuang, C.; Villalta, P.; Lin, Y.; Lu, J.; Xing, C. *ChemMedChem* **2016**, *11* (13), 1436–1445.

(62)   Hermanson, G. T. *Bioconjugate Techniques*; 2013.

(63)   Hashimoto, M.; Hatanaka, Y. *European J. Org. Chem.* **2008**, No. 15, 2513–2523.

(64)   Brunner, J.; Senn, H.; Richards, F. M. *J. Biol. Chem.* **1980**, *255* (8), 3313–3318.

(65)   Shanahan, M. F.; Wadzinski, B. E.; Lowndes, J. M.; Ruoho, A. E. *J. Biol. Chem.* **1985**, *260* (20), 10897–10900.

(66)   Kimple, M. E.; Brill, A. L.; Pasker, R. L. *Curr. Protoc. Protein Sci.* **2013**, No. SUPPL.73, 1–23.

(67)   Cifelli, J. L.; Dozier, L.; Chung, T. S.; Patrick, G. N.; Yang, J. *J. Biol. Chem.* **2016**, *291* (23), 11981–11992.

(68)   Rubinshtein, M. Synthesis and Applications of Development of Side Chain-Functionalized Polylactic Acid-based Polymers and Studies Toward a Chemical Method to Degrade Alzheimer's Disease-Related beta-Amyloid Peptides., University of California, San Diego, 2011.

(69)   Heng, C. M.; Xuan, Z. J. *Synlett* **2007**, No. 11, 1679–1682.

(70)   Bouzide, A.; Sauve, G. *Org. Lett.* **2002**, No. I, 8781–8783.

(71)   Ranu, B. C.; Jana, R.; Dey, S. S. *Chem. Lett.* **2004**, *33* (3), 274–275.

(72)   Turner, G. L.; Morris, J. A.; Greaney, M. F. *Angew. Chemie - Int. Ed.* **2007**, *46* (42), 7996–8000.

(73)   Turner, G. L. Direct Arylation of Thiazoles, The University of Edinburgh, 2009.

(74)   Hatanaka, Y.; Hashimoto, M.; Kurihara, H.; Nakayama, H.; Kanaoka, Y. *J. Org. Chem.* **1994**, *59* (2), 383–387.

(75)   Murai, Y.; Masuda, K.; Sakihama, Y.; Hashidoko, Y.; Hatanaka, Y.; Hashimoto, M. *J. Org. Chem.* **2012**, *77* (19), 8581–8587.

(76)   Prakash, G. K. S.; Panja, C.; Vaghoo, H.; Surampudi, V.; Kultyshev, R.; Mandal, M.; Rasul, G.; Mathew, T.; Olah, G. A. *J. Org. Chem.* **2006**, *71* (18), 6806–6813.

(77)   Kelly, C. B.; Mercadante, M. A.; Leadbeater, N. E. *Chem. Commun.* **2013**, *49* (95), 11133.

(78)   Nelson, D. L. *Lehninger Principles of Biochemistry*, 4th ed.; W.H. Freeman: New York, 2005.

(79)   Kalousek, F.; François, B.; Rosenberg, L. E. *J. Biol. Chem.* **1980**, *255* (1), 60–65.

(80)   Abu-Elheiga, L.; Jayakumar, A.; Baldini, A.; Chirala, S. S.; Wakil, S. J. *Proc. Natl. Acad. Sci. U. S. A.* **1995**, *92* (9), 4011–4015.

(81)   Kovalevich, J.; Langford, D. In *Neuronal Cell Culture: Methods and Protocols*; 2013; Vol. 1078, pp 9–21.

(82)   Nesvizhskii, A. I. 2007; Vol. 367, pp 87–121.

(83)   Hodge, K.; Have, S. Ten; Hutton, L.; Lamond, A. I. *J. Proteomics* **2013**, *88*, 92–103.

(84)   Seymour, S. L.; Hunter, C. *ProteinPilot ^{TM} Software Overview*.

(85)   Kane, R. E. *J. Cell Biol.* **1975**, *66*, 305–315.

(86)   Kane, R. E. *J. Cell Biol.* **1976**, *71*, 704–714.

(87)   Otto, J. J.; Kane, R. E.; Bryan, J. *Cell* **1979**, *17* (2), 285–293.

(88)   Yamashiro-Matsumura, S.; Matsumura, F. *J. Biol. Chem.* **1985**, *260* (8), 5087–5097.

(89)   Bryan, J.; Edwards, R.; Matsudaira, P.; Otto, J.; Wulfkuhle, J. *Proc. Natl. Acad. Sci. U. S. A.* **1993**, *90* (19), 9115–9119.

(90) Edwards, R. A.; Herrera-Sosa, H.; Otto, J.; Bryan, J. *Journal of Biological Chemistry*. 1995, pp 10764–10770.

(91) Holthuis, J.; Schoonderwoert, V.; Martens, G. *Biochim. Biophys. Acta* **1994**, *1219*, 184–188.

(92) Wada, Y.; Abe, T.; Takeshita, T.; Sato, H.; Yanashima, K.; Tamai, M. *Investig. Ophthalmol. Vis. Sci.* **2001**, *42* (10), 2395–2400.

(93) Tubb, B.; Mulholland, D. J.; Vogl, W.; Lan, Z.-J.; Niederberger, C.; Cooney, A.; Bryan, J. *Exp. Cell Res.* **2002**, *275* (1), 92–109.

(94) Mattila, P. K.; Lappalainen, P. *Nat. Rev. Mol. Cell Biol.* **2008**, *9* (6), 446–454.

(95) Vignjevic, D.; Kojima, S. I.; Aratyn, Y.; Danciu, O.; Svitkina, T.; Borisy, G. G. *J. Cell Biol.* **2006**, *174* (6), 863–875.

(96) Sedeh, R. S.; Fedorov, A. A.; Fedorov, E. V.; Ono, S.; Matsumura, F.; Almo, S. C.; Bathe, M. *J. Mol. Biol.* **2010**, *400* (3), 589–604.

(97) Jansen, S.; Collins, A.; Yang, C.; Rebowski, G.; Svitkina, T.; Dominguez, R. *J. Biol. Chem.* **2011**, *286* (34), 30087–30096.

(98) Schrödinger Release, 2017-2. *Maestro, Schrödinger, LLC, New York, NY*. 2017.

(99) Ono, S.; Yamakita, Y.; Yamashiro, S.; Matsudaira, P. T.; Gnarra, J. R.; Obinata, T.; Matsumura, F. *J. Biol. Chem.* **1997**, *272* (4), 2527–2533.

(100) MacDonald, B. T.; Tamai, K.; He, X. *Dev. Cell* **2009**, *17* (1), 9–26.

(101) Clevers, H.; Nusse, R. *Cell* **2012**, *149* (6), 1192–1205.

(102) Valenta, T.; Hausmann, G.; Basler, K. *EMBO J.* **2012**, *31* (12), 2714–2736.

(103) Tao, Y. S.; Edwards, R. A.; Tubb, B.; Wang, S.; Bryan, J.; McCrea, P. D. *J. Cell Biol.* **1996**, *134* (5), 1271–1281.

(104) Scott, R. W.; Olson, M. F. *J. Mol. Med.* **2007**, *85* (6), 555–568.

(105) Schwartz, M. *J. Cell Sci.* **2004**, *117* (23), 5457–5458.

(106) Yang, N.; Higuchi, O.; Ohashi, K.; Nagata, K.; Wada, A.; Kangawa, K.; Nishida, E.; Mizuno, K. *Nature* **1998**, *393* (6687), 809–812.

(107) Jayo, A.; Parsons, M.; Adams, J. C. *BMC Biol.* **2012**, *10*, 72.

(108) Chua, C. E. L.; Lim, Y. S.; Tang, B. L. *FEBS Lett.* **2010**, *584* (1), 1–6.

(109) Bos, J.; Rehmann, H.; Wittinghofer, A. *Cell* **2007**, 865–877.

(110) Zhang, J.; Fonovic, M.; Suyama, K.; Bogyo, M.; Scott, M. P. *Science (80-.).* **2009**, *325* (5945), 1250–1254.

(111) Chevallier, J.; Koop, C.; Srivastava, A.; Petrie, R. J.; Lamarche-Vane, N.; Presley, J. F. *FEBS Lett.* **2009**, *583* (7), 1096–1101.

(112) Cohan, C. S.; Welnhofer, E. A.; Zhao, L.; Matsumura, F.; Yamashiro, S. *Cell Motil. Cytoskeleton* **2001**, *48* (2), 109–120.

(113) Lowery, L. A.; Vactor, D. Van. *Nat. Rev. Mol. Cell Biol.* **2009**, *10* (5), 332–343.

(114) Korobova, F.; Svitkina, T. *Mol. Biol. Cell* **2010**, *21* (1), 165–176.

(115) Talmadge, J. E.; Fidler, I. J. *Cancer Res.* **2010**, *70* (14), 5649–5669.

(116) Tan, V. Y.; Lewis, S. J.; Adams, J. C.; Martin, R. M. *BMC Med.* **2013**, *11* (1), 52.

(117) Yamaguchi, H. *Eur. J. Cell Biol.* **2012**, *91* (11–12), 902–907.

(118) Machesky, L. M.; Lia., A. *Commun. Integr. Biol.* **2010**, *3* (3), 263–270.

(119) Nakae, K.; Yoshimoto, Y.; Sawa, T.; Homma, Y.; Hamada, M.; Takeuchi, T.; Imoto, M. *J. Antibiot. (Tokyo).* **2000**, *53* (10), 1130–1136.

(120) Chen, L.; Yang, S.; Jakoncic, J.; Zhang, J. J.; Huang, X.-Y. *Nature* **2010**, *464* (7291), 1062–1066.

(121) Huang, F.; Han, S.; Xing, B.; Huang, J.; Liu, B.; Bordeleau, F.; Reinhart-king, C. A.; Zhang, J. J.; Huang, X. *Nat. Commun.* **2015**, *6* (May), 1–14.

(122) Kraft, R.; Kahn, A.; Medina-Franco, J. L.; Orlowski, M. L.; Baynes, C.; Lopez-Vallejo, F.; Barnard, K.; Maggiora, G. M.; Restifo, L. L. *Dis Model Mech* **2013**, *6* (1), 217–235.

(123) Lee, N. J.; Song, J. M.; Cho, H. J.; Sung, Y. M.; Lee, T.; Chung, A.; Hong, S. H.; Cifelli, J. L.; Rubinshtein, M.; Habib, L. K.; Capule, C. C.; Turner, R. S.; Pak, D. T. S.; Yang, J.; Hoe, H. S. *Biochim. Biophys. Acta - Mol. Basis Dis.* **2016**, *1862* (2), 284–295.

(124) Kenworthy, A. K. *Methods* **2001**, *24* (3), 289–296.